Titre: Title:	Initial Tool Wear Mechanisms in Turning of Titanium Metal Matrix Composites
Auteur: Author:	Saeid Kamali Zadeh
Date:	2016
Type:	Mémoire ou thèse / Dissertation or Thesis
Référence: Citation:	Kamali Zadeh, S. (2016). Initial Tool Wear Mechanisms in Turning of Titanium Metal Matrix Composites [Mémoire de maîtrise, École Polytechnique de Montréal]. PolyPublie. https://publications.polymtl.ca/2235/

Document en libre accès dans PolyPublie
Open Access document in PolyPublie

URL de PolyPublie: PolyPublie URL:	https://publications.polymtl.ca/2235/
Directeurs de recherche: Advisors:	Marek Balazinski, & J. R. René Mayer
Programme: Program:	Génie mécanique

UNIVERSITÉ DE MONTRÉAL

INITIAL TOOL WEAR MECHANISMS IN TURNING OF TITANIUM METAL MATRIX COMPOSITES

SAEID KAMALI ZADEH

DÉPARTEMENT DE GÉNIE MÉCANIQUE

ÉCOLE POLYTECHNIQUE DE MONTRÉAL

MÉMOIRE PRÉSENTÉ EN VUE DE L'OBTENTION

DU DIPLÔME DE MAÎTRISE ÈS SCIENCES APPLIQUÉES
(GÉNIE MÉCANIQUE)

AOÛT 2016

UNIVERSITÉ DE MONTRÉAL

ÉCOLE POLYTECHNIQUE DE MONTRÉAL

Ce mémoire intitulé :

INITIAL TOOL WEAR MECHANISMS IN TURNING OF TITANIUM METAL MATRIX
COMPOSITES

présenté par : KAMALI ZADEH Saeid

en vue de l'obtention du diplôme de : Maîtrise ès sciences appliquées

a été dûment accepté par le jury d'examen constitué de :

M. MUREITHI Njuki William, Ph. D., président

M. BALAZINSKI Marek, Docteur ès sciences, membre et directeur de recherche

M. MAYER René, Ph. D., membre et codirecteur de recherche

Mme BROCHU Myriam, Ph. D., membre

DEDICATION

To my Family and my Friends

ACKNOWLEDGEMENTS

RÉSUMÉ

Cette étude porte sur les mécanismes d'usure initiale de l'outil en tournage mécanique des composites à matrice métallique de titane (Ti-MMCs). Comparés à d'autres matériaux, les MMCs présentent de nombreux avantages, par exemple : une grande rigidité, une haute résistance à la corrosion et une très bonne résistance à l'usure même aux hautes températures.

Toutefois, ces propriétés avantageuses peuvent être à l'origine de certains problèmes lors de l'usinage, comme une usure sévère des outils de coupe ainsi qu'une durée de vie très limitée.

L'usure initiale de l'outil et son effet sur la durée de vie n'ont pas été étudiés en détail et la plupart des études se sont focalisées sur la période d'usure à taux d'usure constant.

Dans cette recherche des outils en carbure de tungstène (WC/Co) avec un liant cobalt, revêtu de TiN/TiAlN ont été utilisés pour tous les tests expérimentaux. L'usure des outils pendant les premières secondes de l'usinage et ses influences sur la durée de vie de l'outil ont été analysées et discutées.

Les forces de coupe ont été mesurées à l'aide d'un dynamomètre. Après l'usinage, les mécanismes d'usure initiale des outils ont été étudiés par la microscopie électronique à balayage (MEB) et l'analyse dispersive en énergie (EDS). Afin de déterminer la variabilité de la composition chimique de surface d'un outil brut et d'une pièce à usiner, une spectrométrie de photoélectrons induits par rayons X (SPX) a été utilisée. La méthode de sonde ionique focalisée (FIB) a été choisie pour découper et déterminer les éléments ou sous-couches qui se développent lors de l'usinage.

Les diagrammes d'usure obtenus par les essais expérimentaux montrent que la première période de transition de l'usure de l'outil se produit dans la première seconde d'usinage. La comparaison de temps de transition de ces diagrammes aux diagrammes de force a dévoilé une bonne corrélation.

L'analyse des mécanismes d'usure a révélé que l'usure commence par une phase préliminaire dite "abrasive" suivie par une phase dominante dite "adhésion".

ABSTRACT

This research focused on the initial tool wear mechanisms in turning of titanium metal matrix composites (Ti-MMCs). Compared to other materials, MMCs have many advantages, such as: high stiffness, high corrosion resistance, and very good wear resistance even at high temperatures.

On the other hand, these advantages cause a lot of problems during the machining process, including severe tool wear and short tool life.

The initial tool wear and its effects on the entire tool life has not been investigated in detail and most studies have been performed in the steady-state wear period. Thus, in this research the first seconds of machining and its effects on tool life was discussed. WC/Co inserts with the coating TiN/TiAlN were used for all the experimental tests.

Machining forces were registered by a dynamometer. After machining, the initial tool wear mechanisms were investigated using Scanning Electron Microscope (SEM) and Energy Dispersive Spectroscopy (EDS).

In order to study the surface chemical compositions of an unused insert and a raw work-piece material, X-ray Photoelectron Spectroscopy (XPS) was used.

Also, to find out what elements or sub-layers are under the layer that develops during the machining, a Focused Ion Beam (FIB) technique was applied to an insert.

Based on the results of the experimental tests and tool wear progression charts, the first transition time of tool wear occurs in the first second of machining. Also, there are good correlations between the transition time in tool wear progression charts and the cutting force diagrams.

Finally, mapping the wear mechanisms in different tools during the initial moments of machining Ti-MMC revealed that the preliminary wear mechanism is abrasion and the dominant wear mechanism is adhesion.

TABLE OF CONTENTS

LIST OF TABLES

LIST OF FIGURES

LIST OF SYMBOLS AND ABBREVIATIONS

ASB   Adiabatic Shear Band

BUE   Built-Up-Edge

BE   Binding Energy

CBN   Cubic Boron Nitride

CNC   Computer-Aided Manufacturing

EDS   Energy Dispersive Spectroscopy

EDX   Energy Dispersive X-ray

F_c Cutting Force

F_f Feed Force

F_t Thrust Force

FEG   Field emission guns

FIB   Focused ion beam

HRC   Rockwell C hardness

HSS   High Speed Steel

KT   Krater Tiefe (Crater wear)

MMCs   Metal matrix composites

PCD   Polycrystalline Diamond

PVD   Physical Vapor Deposition

SEM   Scanning Electron Microscope

SiC   Silicon carbide

t   Time

T   Temperature

TFCD   Thick-Film Diamond

TiB	Titanium boride
TiC	Titanium carbide
Ti-MMCs	Titanium metal matrix composites
VB	Verschleissmarken Breite (Flank wear)
XPS	X-ray Photoelectron Spectroscopy
XRD	X-ray diffraction

CHAPTER 1   INTRODUCTION

Metal matrix composites (MMCs) mostly consist of a low density alloy of aluminium, magnesium, or titanium as matrix and as reinforcement fibers, ceramic particulate, or whiskers. These groups of alloys are suitable for a large number of functional and structural applications. To reach a desired function, some materials are added as reinforcement to metallic matrices through physical or chemical processes. The results are incredible materials with high mechanical and thermal properties, high wear resistance and lots of other advantages (Kainer, 2006).

Ti-MMCs with the advantages of both TiC particles and titanium alloys have excellent features, such as high stiffness, high-performance mechanical properties, fairly high elastic modulus, high wear resistance, increased strength and low density (Pramanik & Littlefair, 2015).

1.1 Problem definition

The most important issues in the machining of Ti-MMCs are poor surface quality, severe tool wear and short tool life. Reinforcing particles are enormously abrasive and have a prominent role in tool wear by surface scratching and crack or hole generating. Poor surface finish could be caused by de-bonding and cracking particles (Hosseini & Kishawy, 2014).

It has been measured that in a very small zone near the cutting edge, during the machining, due to the low thermal conductivity of the titanium alloy (6.7 W/m-K) as matrix, high local temperature is generated results in high tool wear. Additionally, wear mechanisms such as abrasion, adhesion, diffusion, and other chemical reactions reduce the tool life (Davim, 2008; Davim, 2014). Ti-MMCs are hard-to-cut materials and have all the problems related to machining titanium alloys and MMCs (Davim, 2014). Ti-MMCs and CermeTi® MMCs are developed by Dynamet Technology, Inc. They contain a non-metallic phase TiC (10% in weight) dispersed in titanium alloy (Ti-6Al-4V).

Some investigations and analyses were done on aluminum MMCs, but there is a gap in the research for the machining of titanium, especially for initial tool wear.

1.2 Motivation

The effects of the first moment of machining on the entire tool life and initial tool wear mechanism have not been determined clearly and need more investigation. Usually, in a machining process,

the tool life is identified based on a wear curve evolution versus cutting time; this curve shows the variation of tool wear over cutting time and normally contains three individual regions: the primary or initial or running-in, the steady-state, and accelerated wear period.

There is a lot of research in the field of the steady-state wear period but initial tool wear and its important effect on tool life has not been studied enough. Thus, investigating the tool wear mechanisms during the first seconds of machining due to its possible effects on tool life is very important.

The initial wear period occurs fast at a very high wear rate and has an important influence on system performance. Therefore, better understanding of tool wear mechanism to control and optimize the process can extend the tool life (Davim, 2014).

This study focuses on the different initial conditions and their influences on tool life in the turning of Ti-MMCs.

1.3 Research Objectives

1.3.1 Main objective

Research into the machining of Ti-MMCs has not been completed yet. In particular, only a few articles on initial tool wear have been published (Troung et al., 2015& Bejjani et al., 2016).

Due to the direct influences of tool wear on tool life and machining costs, the main aim of this study is to carry out some experimental tests and deep analysis on initial tool wear mechanisms.

This important role of initial tool wear opens some basic questions that require further investigation, such as:

- What is the initial tool wear mechanism?

- How long is the initial stage of tool wear?

- Why is the wear rate so rapid during the first second and decreases in the steady-state period?

1.3.2 Specific objectives

- To provide a comprehensive study of the initial tool wear mechanisms during the turning of Ti-MMCs, using Carbide TiAlN/TiN coated inserts.

- To perform the experimental studies in order to find the possible correlation between the cutting force components and the initial tool wear progression.

- To figure out what happens in the transition time.

1.4 Hypotheses

- All the inserts were ordered from the same production batch.

- The geometry and microstructure of each brand new insert is similar.

- Average flank wear length (VB_B) is an accepted criterion to quantify tool wear. Most researchers use this criterion to measure the tool wear (ISO 3685, 1993).

- The initial cutting conditions are considered to have some influences on the entire tool life in the machining of hard to cut materials (Troung et al., 2015).

1.5 Research approach

In this study, the first step is to find the best cutting speed for machining of Ti-MMCs with carbide tools in order to achieve and draw the principal tool wear curve over time. Then, to investigate experimentally what initial cutting conditions have the most influences on the tool wear. Then after, some tests with a scanning electron microscope (SEM, energy dispersive spectroscopy (EDS), and Focused Ion Beam (FIB) technique are conducted to see the effect of tool wear on the microstructure during the initial moments of machining, especially at the first transition period.

1.6 Outline of the thesis

Chapter 1 provides the research plan for this study. The research questions, motivations, goals, objectives, hypothesis statements and, finally, approaches of the study are presented.

Chapter 2 provides a literature review related to the machinability of the metal matrix composites, titanium metal matrix composites and the initial wear issues.

Chapter 3 provides the study of initial tool wear mechanisms at the first moments of cutting. Furthermore, the first transition period in the tool wear curve between running-in and steady-state wear zones is determined.

Chapter 4 presents an experimental study and analysis of the tool wear progressing versus time.

Chapter 5 provides a deep discussion about the results of experiments, described in the previous chapter.

Chapter 6 presents the conclusions and recommendations for future work.

CHAPTER 2   LITERATURE REVIEW

This chapter presents some research and study results relating to the most important aspects of the machinability of metal matrix composites (MMCs), including the tool wear, cutting forces, and chip formation.

2.1 Introduction

Brun et al. (1985) were the pioneers in doing some research on wear mechanisms during the machining of aluminum metal matrix composites. Davim et al. (2008) were the other researchers who worked on the machining of MMCs, mostly in the machinability of the aluminum MMCs

Ti-MMCs are still new for researchers and there are a lot of unsolved issues in their production, forming and machining (Davim, 2008). In the upcoming sections some basic and essential parameters of machinability of MMCs are introduced.

2.2 Tool Materials

The most important properties of a tool material are:

- **Hardness:** The ability to resist against the indenter penetration and linked to the strength of the material.

  - **Hot hardness**: It is defined as the ability to keep high hardness at elevated temperatures.

  Figure 2-1 shows the hardness of typical tool materials over temperature. It can be seen that PCD tools have the highest hardness among the various tools.

- **Toughness:** It is defined as the way a material reacts against a sudden impact or the ability to resist of a sudden crack propagation.

  When a tool material has high fracture toughness, then it has better shock-load resistance and less vibration, chipping, misalignments and other failures in the machining process. One of the most important research objectives in this domain is to increase tool toughness while keeping hardness (Astakhov & Davim, 2006).
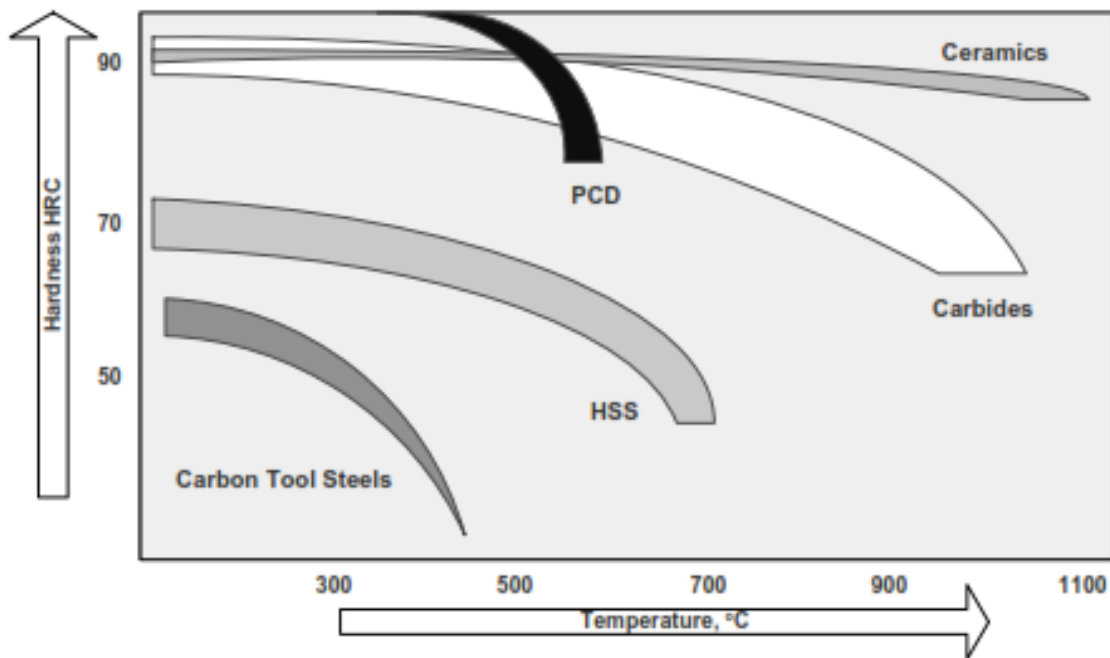
Figure 2-1 : Hardness of tool materials over temperature. Polycrystalline Diamond (PCD) is the hardest, then Ceramics, Carbides, High Speed Steel (HSS), and eventually Carbon Tool Steel (CTS) has the lowest hardness among the tool materials (Astakhov & Davim, 2006)

2.3 Carbides

As a replacement of other tools, like diamonds or high speed steels (HSS), researchers in Germany for the first time presented a new tool named (Widia N – WC-6Co) in 1927.

Nowadays, there are different categories of carbides, such as cermets, tungsten carbides, and titanium carbides.

Normally, a carbide insert contains carbide particles with different sizes bounded in a cobalt matrix by sintering process. In Table 2-1, a guide for primary selection of carbide grade for a given application is offered. In The first column the favourable conditions related to the tool code (second column) and tool color (third column) are suggested. As an example for the first row, CT5005 (HT) with the code P01 is an uncoated titanium-based cemented carbide. This grade has maximum performance in super-finishing of steel and cast-iron when a very exceptional surface finish is needed (Sandvik Coromant, 2014).

Table 2-1 : Guides to select carbide grade (Astakhov & Davim, 2006)

Cutting conditions	Code	Colour
Finishing steels, high cutting speeds, light cutting feeds, favourable work conditions	P01	Blue
Finishing and light roughing of steels and castings with no coolant	P10	
Medium roughing of steels, less favourable conditions. Moderate cutting speeds and feeds.	P20	
General-purpose turning of steels and castings, medium roughing	P30	
Heavy roughing of steels and castings, intermittent cutting, low cutting speeds and feeds	P40	
Difficult conditions, heavy roughing/intermittent cutting, low cutting speeds and feeds	P50	
Finishing stainless steels at high cutting speeds	M10	Yellow
Finishing and medium roughing of alloy steels	M20	
Light to heavy roughing of stainless steel and difficult-to-cut materials	M30	
Roughing tough skinned materials at low cutting speeds	M40	
Finishing plastics and cast irons	K01	Red
Finishing brass and bronze at high cutting speeds and feeds	K10	
Roughing cast irons, intermittent cutting, low speeds and high feeds	K20	
Roughing and finishing cast irons and non-ferrous materials.	K30	

Usually, the amount of cobalt (varies between 3 to 20% of the carbide tools composition depending on the chosen combination of toughness and hardness) has an important role in the properties of carbide inserts. This amount has direct influence on toughness and reverse influence on the hardness and strength. If some parameters such as: the grade of carbide inserts, layer deposition

sequence, coating materials, and the coating technology are selected correctly, the result is a tool with high wear resistance (Torres et al., 2014).

Selecting the optimum grade of carbides due to their direct effects on desired machining productivity, efficiency and quality is too important for manufacturers.

2.4 Coating

For 40 years, thermal diffusion processes and thin-film hard coatings have had a revolutionary role in the machining of hard metals. This thin layer greatly improves tool life and performance in the machining hard-to-cut materials. It increases machining speed or feed rate, wear or corrosion or oxidation resistance, and hardness and reduces friction and cutting forces, among so many other improvements. Nowadays, 85% of carbides, 40% of super-hard tools and 50% of HSS which are used in machining are coated (Smith, 2008).

Coatings are applied to gain the desired functions such as: abrasion or oxidation resistance, increased hardness, and protecting the substrate against high temperatures.

Oakham found that all wear mechanisms in machining could be optimized by applying an appropriate coating. (Oakham, 2007)

Some of the most common methods of coating are: Physical Vapor deposition (PVD), Chemical Vapor Deposition (CVD), Dynamic Compound Deposition (DCD), and Thermal Diffusion (TD).

In the coating process a layer of material is coated onto the substrate. This layer is so thin but has an important effect on final product. (Astakhov, 2006)

Carbides are great to be used as the substrate for most of the coatings like TiN, TiAlN, TiCN and solid lubricant or multilayer coatings.

Trent et al. (2000) have had some investigations about carbides coatings. Regarding to their research, in CVD method the substrate is heated to 1000 degrees Celsius. The high temperature in this method decreases the hardness of carbide and its rupture strength. In contrast, PVD is applied at lower temperature near 500 degrees Celsius. In this method, the coating material is deposited onto the substrate in a vacuum chamber (Trent, 2000).

Concerning the materials, coating splits into four principal groups:

- **Titanium based coating materials** like TiN, TiC and Ti (C, N). These coatings could be made adding other metals such as Cr or Al to reach a specific property.

- **Ceramic-type coating materials** like Al_2O_3 (alumina oxide) exhibit, high wear and corrosion resistance, high melting temperature, low thermal conductivity, electrical insulation fairly high toughness and plastic deformation of metals.

- **Super hard coating materials** like chemical vapor deposition (CVD) diamond.

- **Solid lubricant coating materials** like amorphous metal-carbon (Martin, 2009).

Furthermore, concerning the layers, coatings are classified into two principal groups: mono layers or multilayers.

Mono layer coating as it is clear, a layer is coated onto the substrate, but multilayer structures have more than a layer onto the substrate to reach the desired functions like high toughness. In the other words, the sub-layers in a sandwich structure improves crack absorption.

Nanolayer is a fine form of multilayer coating with a layer thickness of less than 20 nm.

Figure 2-2 shows a schematic image of every five different coatings. In mono layer image a TiN layer is coated on the substrate.
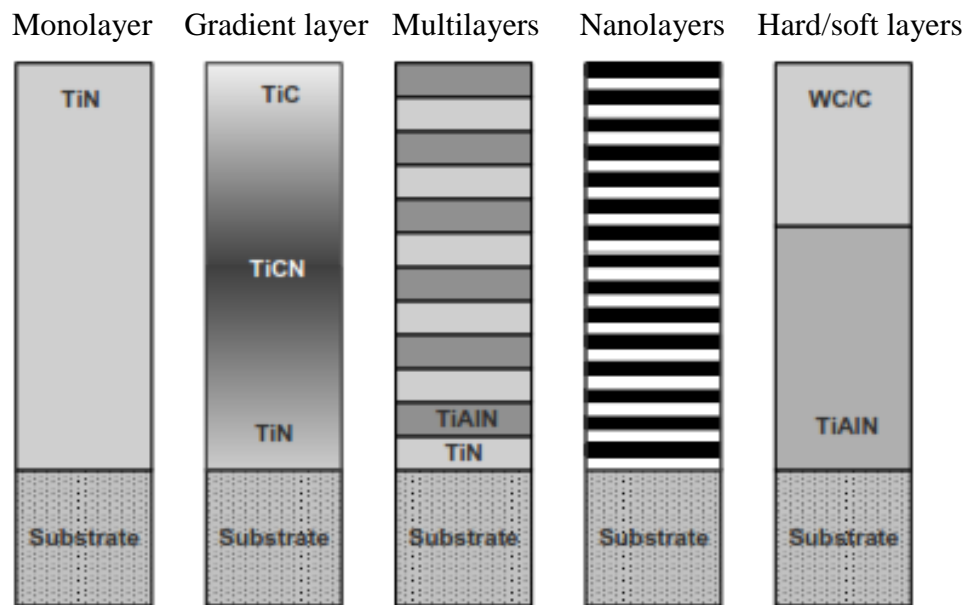
Figure 2-2 : Schematic images of different types of coating (Astakhov & Davim, 2006)

Gradient coating is fairly new. The composition, microstructure and properties of gradient material, all are changed from the substrate to the surface of the material. Usually, the gradient coating is used to improve the resistance against adhesion and to provide other expected functional properties of tools. For example, the problem of adhesion between the layers in multilayer coating is solved by continuous gradient coating. Eventually, to decrease extensive tool wear during the machining a soft coating is deposited onto a hard coating (Dobrzański et al. 2006).

In gradient layer image the darker color represents higher concentration of TiCN in the middle of coating. In multilayer image a TiN and a TiAlN layer is coated one by one. As shown in nanolayer image, the coating is similar to the multilayer but very thinner layers. In hard/soft layers image a WC/C soft layer is deposited on a TiAlN hard layer.

Physical vapor deposition (PVD) coatings

The common PVD coatings are: TiN, TiN (C, N), (Ti, Al) N, and CrN.

Titanium nitride, TiN: With gold color, show high wear resistance in the machining of many materials. Machining speed and feed rate can be increased by using this tool. Also, this coating improves finished surface quality while decreasing welding and galling of work-piece material and increasing tool life two or three times and sometimes eight times.

Moreno et al (2010) had an investigation about wear evaluation of WC Inserts coated with TiN/TiAlN multi and nanolayers. They presented a schematic design of insert with TiN/TiAlN multilayers coated on a WC insert substrate (shown in Figure 2-3).
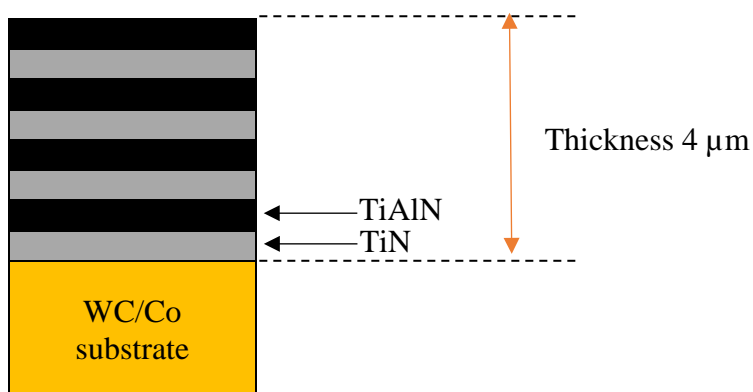
Figure 2-3 : Schematic design of TiN/TiAlN multilayers with the substrate of tungsten carbide (WC) and cobalt (Co) as binder (Inspired of a research done by Moreno et al., 2010)

In this figure, black layers are TiAlN and grays are TiN. The thickness of the coating is about 4 µm. It contains 200 to 300 layers, equivalent to 100 and 150 nanometre layers each one equal to 13 to 20 nm.

On the other hand, PVD TiN coatings have two major weaknesses: low fracture toughness and oxidation resistance which are solved by adding aluminum (Al) into TiN coating while depositing as solid solutions (Moreno et al., 2010).

Titanium carbonitride, TiN (C, N): With bronze color, show high wear resistance in the machining of hard-to-cut materials like cast irons, steels, copper and their alloys, Inconel and titanium alloys. Those improvements are the same as TiNs but also for hard-to-cut materials.

Titanium aluminum nitride, (Ti, Al) N: With purple/black color, show an excellent productivity in the machining of hard-to-cut materials like cast iron, aluminum alloys, steels and nickel alloys. These coatings could be an excellent option for interrupted operations due to their higher oxidation resistance in high temperatures.

Chromium nitride, CrN: With silver color, show high thermal stability and reduce built up edge production in machining of titanium alloys (Astakhov & Davim, 2006).

2.5 Tungsten carbide with the cobalt binder (WC/Co) tools

Cermets are composite materials composed of ceramic and metallic compositions. Tungsten carbides (WC) are cermet and bounded with cobalt (Co) as a binder are the most commonly used for turning and milling process. Concerning WC/Co carbide, the binder phase Co can help better sintering and increases the strength and toughness. Moreover, Co as a binder increases hardness and the material resistance against corrosion and oxidation. On the other hand, the major weakness of adding Co is to weaken the material strength at elevated temperatures (Zackrisson et al., 1999).

Pramanik et al. (2013) found that in the machining titanium alloys with WC/Co carbide inserts, Co binder might be diffused from the tool to the chips through the contact surface. This diffusion may decrease the tool strength which leads to the tool damage, especially at high cutting speeds.

2.5.1 Types of WC tools

Tungsten carbide-cobalt (WC/Co) tools are classified into two general categories:

- The ISO K-type which contains only WC and Co, or straight carbides and normally are used for non-ferrous metals.

- The ISO P-type in which some parts of WC are replaced with compounds such as TiC, TaC, and NbC and normally are used for machining of ferrous metals. These are named as C-type grades too.

For machining both of ferrous and non-ferrous metals, there is an ISO M-type grade as well.

The K-type tool substrates, called straight carbides, contain hard WC-grains and about 4-12% of the Co-binder. Carbide tools with less than 10% Co can resist of plastic deformation at elevated temperatures up to 7000C (Upadhyaya, 1998).

2.5.2 Microstructure

Normally, a carbide grain sizes in cemented carbides are less than l μm. WC/Co alloys contain two main phases: the carbide phase (WC), and the binder phase (Co). Because of the residual stresses during the sintering crystal defect densities in WC are pretty low which are laid to plastic deformation. Cobalt is widely used as a binder due to its presence in the microstructure to separate the carbide particles. Generally, the Cobalt phase is lead to high dislocation density and disordering of crystallographic planes (Upadhyaya, 1998).

Due to the ductility related to cobalt phase and hardness linked to WC phase, WC/Co tools provide high toughness and strength. Owing to the fact that the solubility of WC in cobalt is higher than other binders, such as: Fe or Ni, cobalt is one of the best options for manufacturers to employ as a binder.

2.5.3 Third Phase in WC/Co Tools

Another phase or intermediate layer outside the WC grains was observed by some researcher whereas ignored by others. The presence of this intermediate layer can explain the high transverse rupture strength (TRS) (The amount of energy that tool can absorb before fracture) of WC/Co tools and it is possible also at low percentages of Co concentrations. It was found that the density of this intermediate layer might be about 9g/cm^3 (Upadhyaya, 2001).

2.5.4 Thermo-Mechanical Properties of WC/Co tools

WC particles as the basic part of cemented carbides are fairly hard and brittle while, the cobalt binder phase is pretty soft and ductile. Therefore, the percentage of cobalt (Co) determines the typical mechanical properties.

It can be seen in Figure 2-4 that by increasing cobalt (Co) content, tool wear, while compressive and transverse rupture strength are increased, the hardness is decreased.

Some major parameters of WC/Co tools are:

- Cobalt concentration (percentage of cobalt)

- Carbide grain size (dg)

- Distribution of mean grain size of carbide (Δdg)

- Bonding layer thickness

- Transverse rupture strength (TRS)

Like other tools, the hardness of carbides decreases at elevated temperatures but normally

WC tools keep their functional ability until about 800 ℃ (Upadhyaya, 2001).
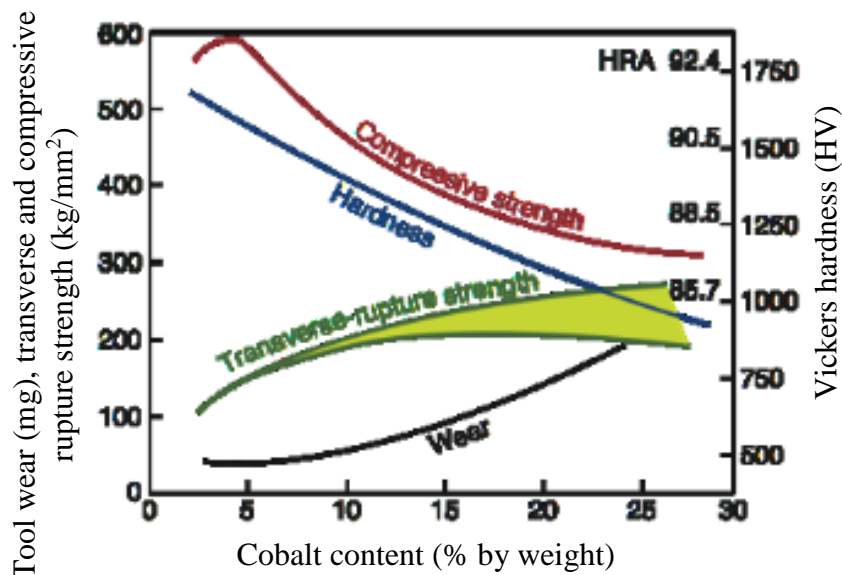
Figure 2-4 : The effect of Cobalt (Co) content on some mechanical properties of WC/Co cutting tools

It can be seen by increasing cobalt (Co) content, tool wear, compressive and transverse rupture strength are increased while the hardness is decreased that hardness is directly related to compressive strength and hence, inversely to wear (Kuttolamadom, 2012)

2.6 Tool Wear

Many factors, such as cutting conditions, cutting tool, work-piece material, machine tool and coolants, play their own roles in tool wear.

Accordingly, quantitative identification of wear mechanisms and chip formation are difficult (Olortegui-Yume & Kwon, 2007).

During the machining, because of the direct contact between tool surface and work-piece and the resulting friction, the tool shears the work-piece material due to the plastic deformation of heated material and generates the chip.

At the beginning of the machining, temperatures in both work-piece material and cutting tool increases rapidly and the cutting tool must resist this thermal shock but after a certain time it is weakened.

The presence of two or more wear mechanisms has been seen in metal cutting in many studies (Shaw, 2005), which makes the tool wear criteria more complicated.

Types of tool wear

The different types of tool wear are shown in Figure 2-5.

This study is focused on flank wear (Figure 2-5 (a)). The other types of wear are specific to work-piece material or cutting conditions or chip hammering (Figure 2-5 (g)) that may happen during the machining of a work-piece of tough and abrasive material, such as stainless steel.

Mechanical (Figure 2-5 (f)) and thermal (Figure 2-5 (e)) cracking are mostly observed in periodic cutting; however, when occurring these tool wear types can result in breakage or tool chipping.

Despite the BUE formation not categorizing as a tool wear process, it can speed up adhesive and abrasive wear. The major plastic deformation may change the shape of a tool thereupon modifying the wear process, cutting forces and temperature. Eventually, large fractures may occur at the beginning of the machining process or after machining for a while (Astakhov, 2006).
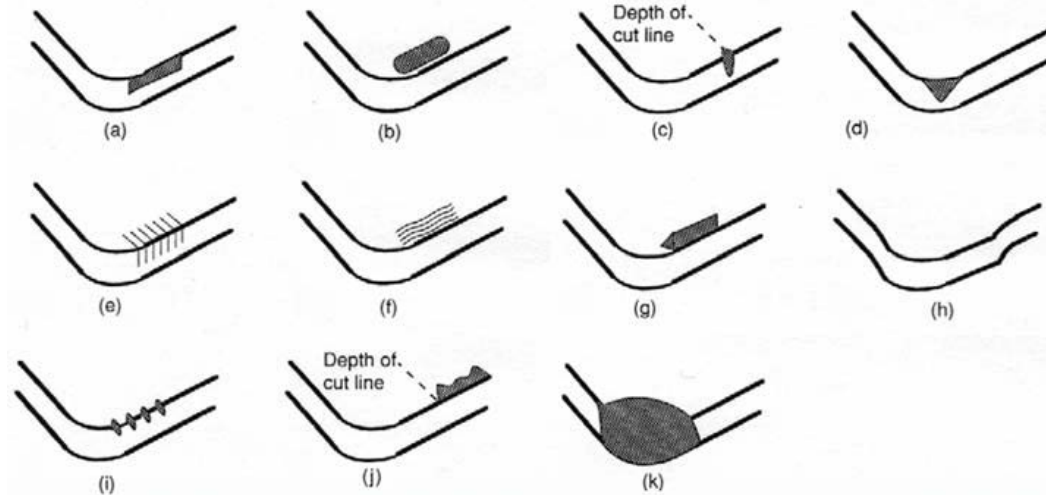
Figure 2-5 : Tool wear types (a) is flank wear, (b) is crater wear, (c) is notch wear, (d) is nose radius wear, (e) is thermal cracking, (f) is parallel cracking, (g) is built-up edge (BUE), (h) is gross plastic deformation, (i) is edge chipping, (j) is chip hammering and (k) is gross fracture (Stephenson & Agapiou, 2006)

For measuring tool wear according to the standard (ISO. 3685, 1993), there are three regions on the main cutting edge, as shown in Figure 2-6:

- Region N is formed outside of the area of contact between the tool and work-piece for approximately ¼ of the worn length b and the type of wear is notch wear.

- Region C starts at the corner of the tool from the curved part.

- The area between region N and C is Region B.

Plane P_s is the surface in contact with work-piece and linked to the flank wear. Normally, VB_B is frequently used as the tool wear criteria and measured inside zone B from the previous position of cutting edge to the end of actual worn out region.

The maximum distance between the crater bottom and the original face in region B is named the crater depth (KT) (Astakhov & Davim, 2006).
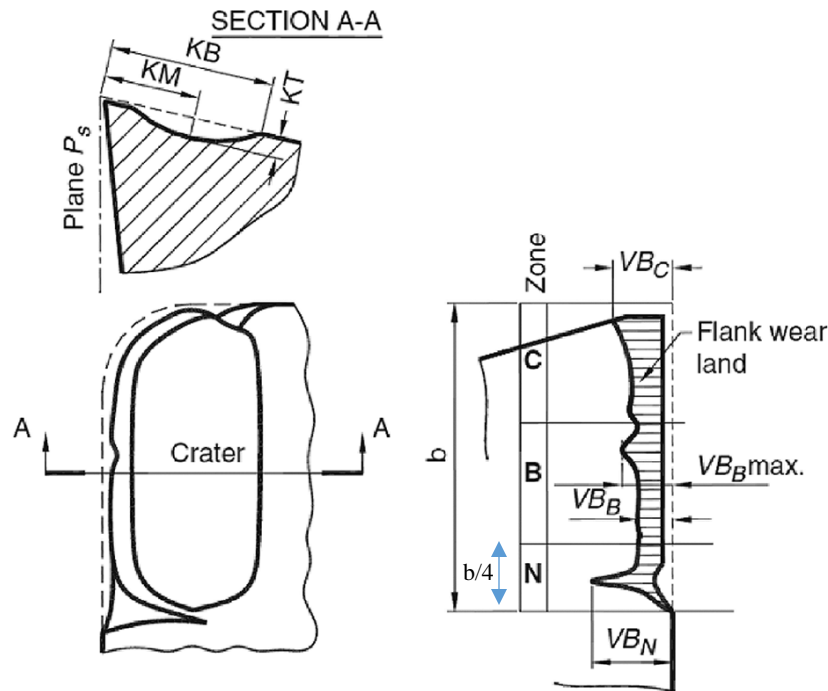
Figure 2-6 : Tool wear criteria according to Standard (ISO.3685, 1993). Section A-A shows the crater wear parameters in rake face

Mostly, the tool wear is measured using a Toolmakers-Mitutoyo microscope (shown in Figure 2-7). As it can be seen in the image, the least count (L.C.) of microscope of 100 equal divisions and of pitch 0.5 mm is 0.5/100 = 0.005 mm.
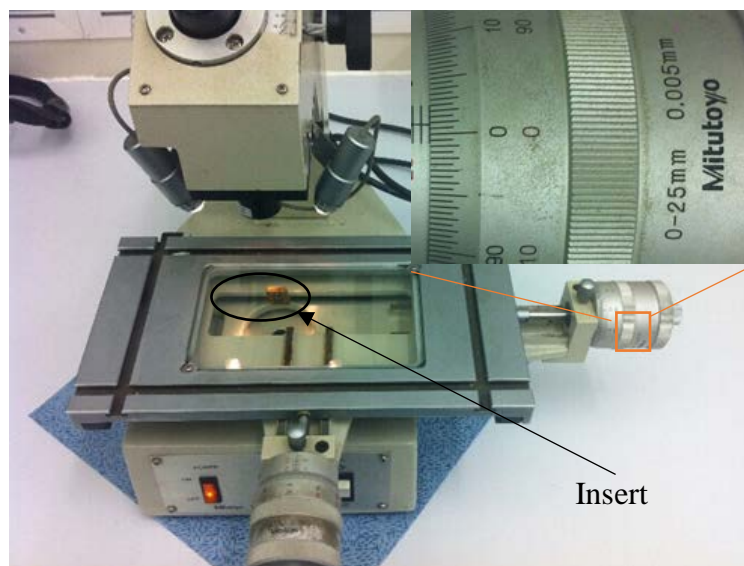
Figure 2-7 : Toolmaker microscope, used in this study to measure the tool flank wear

2.7 Tool Wear Progress

In comparison with aluminum alloys, the tool wear rate is much higher in the machining of the titanium alloys. Soboyejo et al. (2006) found that this could be due to the low thermal conductivity of titanium alloys and high normal stress at very small region of the contact between work-piece and tool surface result in high temperatures.

Tool wear curves show the relation between flank wear and the cutting time or length of cut. As shown in Figure 2-8 (a), there are three individual regions:

The first region (region I) is the region of initial or primary or break-in wear. Tool wear rate in this region is high since the sharp tool tip is subjected to high pressure and breaks away. Tools normally become worn out quickly at this stage. The second region (region II) is the steady-state wear region and usually the normal operating region of the tool. The tool wear rate decreases within the steady-state wear stage. The third region (region III) is the tertiary or accelerated wear region. Tool wears fast in this region due to the high amounts of machining forces rooted in high temperature.
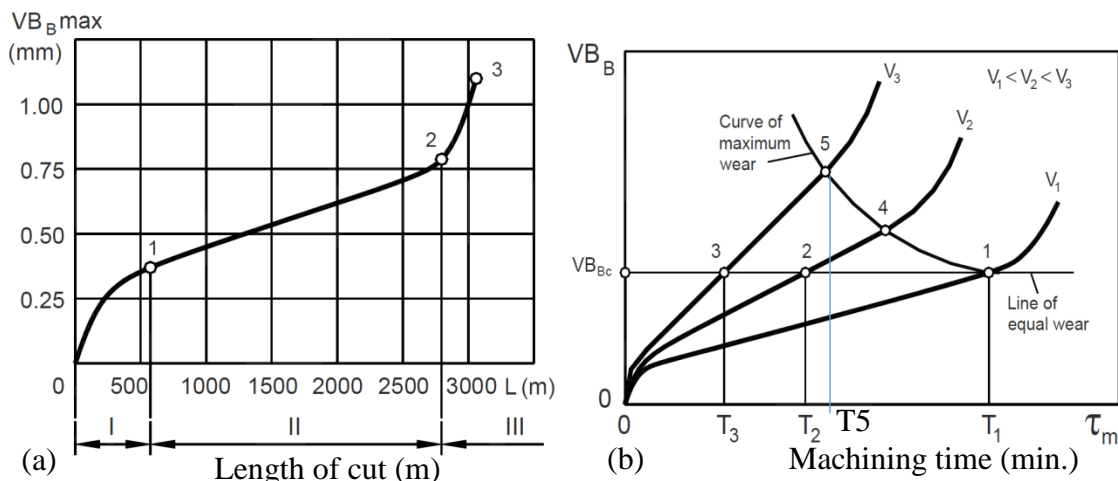
Figure 2-8 : (a) Typical stages of tool wear in the machining (b) three tool wear curves related to three different machining speeds (Astakhov & Davim, 2006)

It was found by Sharif et al. (2012) that the cutting speed is one of the most important parameters and has the most influences on wear mechanisms dominant in the machining.

In Figure 2-8 (b) three typical tool wear curves at three different machining speeds are shown. T_1, T_2, and T_3 are the machining times at different speeds of V_1, V_2, and V_3. It can be seen that if the machining is done with the higher speed, tool wears out sooner than machining at lower speeds.

Furthermore, as long as the desired purpose of the machining are met, the speed related to the wear in the curve of maximum wear, could be used as an alternative of the speed linked to the wear in the line of equal wear. For example, if the surface integrity is not so important in the machining instead of machining at the speed of V_1 in time T_1, it is possible to cut at the speed of V_3 in time T_5.

It is clear that the tool wear rate at higher speed is faster. VB_{Bc} is the acceptable tool wear in the range of 0.15–1.00 mm and depends on the type of machining operation and desired quality of the operation. The curve of maximum wear shows the possible speed could be chosen in a machining process based on possible surface integrity (surface condition of the work-piece after being machined). Also, based on ASME Standard (ASME, 1985) the tool should be considered worn when the flank wear criterion VB_B is 500 µm. This is the time for replacing the tool.

In Table 2-2 three images of the CNMG carbide TiAlN/TiN coated in which tool wears (VB_B) are at three different regions of tool wear curve (Figure 2-8 (a)) are shown. In region I after only 0.2 second of machining the edge in contact with work-piece was worn out. After 23 seconds of machining tool wear is located in region II and the tool wear is typical. After 93 seconds of machining tool is completely worn out and trace of oxidation is clearly shown.

2.8 Tool wear mechanisms
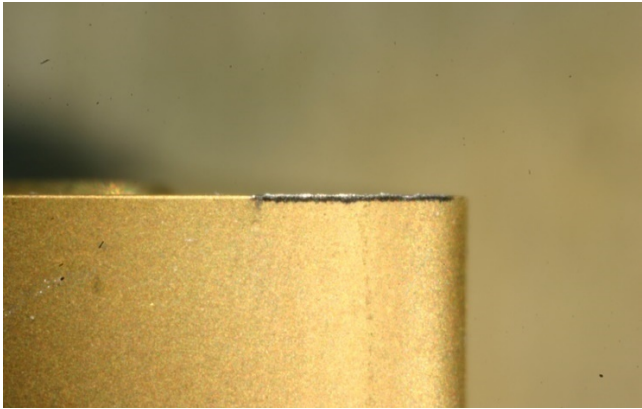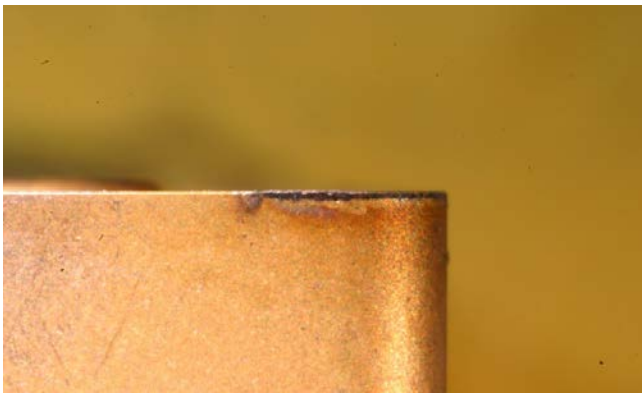
In order to improve the tool life and have more effective machining tool wear mechanisms present in machining and their causes are investigated. After this it could be reduce the effects of tool wear in the machining process.

Some tool wear mechanisms which are commonly accepted among the scientists are: adhesion, abrasion, diffusion, dissolution, chemical reaction, and oxidation (Olortegui-Yume & Kwon, 2007).

It should be noted that, sometimes two or more mechanisms have their own influences on tool wear simultaneously that make it harder to understand.

In the upcoming sections, some explanations for tool wear mechanisms are presented.

Table 2-2 : Flank tool wear of a carbide insert in three different machining times. Tool wear criterion of this insert (VB_B) is at different regions of tool wear curve (Figure 2-8 (a))

Carbide TiAlN/TiN coated flank face	Machining parameters
	Machining time = 0.2 second Cutting speed Vc = 50 m/min Feed rate f = 0.15 mm/rev Depth of cut a_p = 1.5 mm Material: Ti-MMC Region I
	Machining time = 23 seconds Cutting speed Vc = 50 m/min Feed rate f = 0.15 mm/rev Depth of cut a_p = 1.5 mm Material: Ti-MMC Region II
	Machining time = 93 seconds Cutting speed Vc = 50 m/min Feed rate f = 0.15 mm/rev Depth of cut a_p = 1.5 mm Material: Ti-MMC Region III

2.8.1 Adhesion

During the sliding of two surfaces on each other, some parts of one surface (normally from the weaker material) adhere to the other surface and become a part of the new surface. This is called Adhesion and occurs under high temperature and pressure from strong bonds. At the atomic scale, when two atoms get close to each other under high pressure and temperature adhesive forces increase, and then strong bonding shapes and cause adhesion (Ernest, 1995).

In summary, adhesive wear is the formation of a junction as a result of bonding between work-piece or chip and the tool.

Rabinowicz et al. (1977) focused on some experimental studies about adhesion and determined the following laws of adhesive wear:

- The load between two contact surfaces affects directly tool wear.

- The sliding distance affects tool wear.

- The hardness of the material being worn away affects tool wear inversely.

At medium temperatures, because of the softening at high temperatures and minimum tendency at low temperatures, adhesion is the dominant mechanism (Childs, 2000).

When machining soft materials like aluminium alloy, adhesion is an important problem due to separated materials from work-piece being gathered on the tool possibly breaking it. It is also a problem in low speed machining with High speed steel (HSS) tools (Stephenson & Agapiou, 2006).

2.8.2 Abrasion

Based on Ernest et al. (1995) 's studies, when a hard surface or hard particles slide on a softer surface, abrasive wear occurs and causes a material loss by the act of scratching on the surface.

In machining, abrasive wear occurs as a result of work-piece abrasive particles. If the abrasive phase has complex morphologies, then the result is a 2-body abrasion whereas the abrasive that has simple morphologies causes a 3-body abrasion (Figure 2-9) (Neale & Gee, 2001).

Movement direction

(a)   (b)
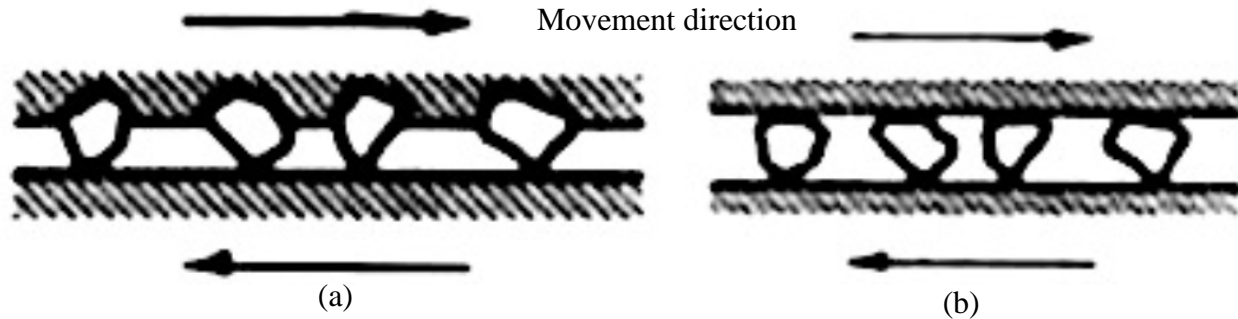
Figure 2-9 : Schematic images of two kinds of abrasive wear (a) two body wear; (b) three body wear (Neale & Gee, 2001)

A methodology of predicting the tool wear progression over time in turning of MMCs was presented by Kannan et al. (2013). They formulated the wear volume due to two or three body abrasion mechanism.

There is another classification presented by Davis (2001) and is founded on the applied load. In his book, he separated abrasion into low stress and high stress abrasion.

Low stress abrasion: it happens when particles have a light contact with the surface and it is not enough to deeply scratch the surface. The contact surface exhibits scratching with very low subsurface plastic flow. Thus, work hardening does not happen. This kind of abrasion normally seen in oil and mining sands extraction.

High stress abrasion: it occurs when particles crush the surface are interacting with and lead to coarse grooving and gouges.

Kwon et al. (2002) did some studies about the phase transformation. They found that at a higher cutting speed when the temperature passes a certain amount, pearlites transfer into austenite.

They analysed the surface of the machined work-piece using XRD technic and found some austenite on it. It was concluded that the alloy elements have direct influence on phase transformation and changing the phase changes structure and transformation temperature.

2.8.3 Diffusion

Diffusion happens from the higher atomic amount to low atomic amount regions and the rate grows exponentially by increasing the temperature. In particular, during the machining the high concentrated temperature on a very small surface is enough to have diffusion. Normally, high

cutting speeds and feeds or intense friction result in high temperatures and lead to diffusion. Moreover, it is generally linked to the crater wear which decreases the tool mechanical resistance and its productivity. Wright et al. (2000) found the evidences of existence of tungsten, cobalt, and carbon (tool elements) within the chip at the tool–chip interface.

Studying diffusion and the factors causing it could be difficult due to the acting of two or more mechanisms at the same time in tool wear and being rooted in high temperature (Shaw, 2005).

Hua et al. (2005) established an analytical wear model of cobalt diffusion from carbide tool to titanium chips for predicting crater wear in machining of the titanium alloys. They found that the high chemical reactivity of titanium results in the diffusion wear mechanism. The carbon atoms of carbide can be transferred into the mating Ti alloy surface by diffusion and therefore causes the loss of carbide.

However, in their experiments there was not any evidence of TiC existing on the worn surface of the insert, which implies that TiC is not the final bond and titanium mostly oxidized to the form TiO_2.

2.8.4 Dissolution

Dissolution is the formation of a solid layer transferred from the tool material into the chips. While the chips pass over the rake face, depends on the chemical inertness of the tool elements and their affinity with the work-piece material, high temperature causes dissolution in the rake face. It might happen at a relatively high cutting speed. In machining with carbide tools, coated carbide tools and ceramic tools dissolution wear is common due to the solubility of the elements of these tools in materials like steel. Among the tool ingredients, WC has a weak wear resistance versus dissolution contrary to Alumina Al_2O_3 which has the most dissolution wear resistance (Wong et al., 2004).

2.8.5 Chemical reaction

After diffusion in machining of some extremely reactive materials like titanium, a chemical reaction happens. This is not a wear mechanism but can reduce tool productivity. When the tool elements react with the oxygen in the air, oxidation as a chemical reaction occurs.

Normally in most conventional machining oxidation occurs and the result is changing the colour of the oxidised region and sometimes notch wear (Stephenson & Agapiou, 2006).

As a general conclusion, for the steady-state tool wear period during the machining three wear mechanisms have been recognized: abrasion, generalised dissolution and adhesion. The dominant mechanisms at low cutting speeds might be adhesive and abrasive wear. However, at high cutting speeds, dissolution, diffusion, chemical reaction and oxidation are more relevant (Stephenson & Agapiou, 2005).

During the machining of steels, carbide tools wear simply by dissolution (Kramer & Suh, 1980) whereas in machining of titanium alloys they show better wear resistance due to the reaction between carbon from carbides and titanium and the formation of a protection layer (Hartung, Kramer & Von Turkovich, 1982).

Flank wear can be created by the abrasive particles in the work-piece whereas crater wear can be a complex combination of two or more wear mechanisms such as abrasion, adhesion, dissolution and diffusion. Contact conditions, the interface between tool work-piece, and cutting temperatures are the most important factors in wear mechanisms (Kwon, 2000).

Higher cutting speed causes higher cutting temperature, making tool material softer, which causes abrasion to be the dominant mechanism.

2.8.6 Oxidation

Oxidation wear (corrosive wear)

The chemical reaction between the tool surface and oxygen at high temperature, which results in the discoloration of material is called oxidation. In this process a layer of oxides on the surface is formed and when abrasion destroyed this layer during the machining process another layer form. This is a repetitive process which forms, then destroys but sometimes this slight layer helps to reduce the tool wear by isolating the tool and the work-piece.

2.8.7 Edge chipping (premature wear)

Normally, it occurs in the machining with the variable depth of cut and some small parts of cutting edge are broken away due to the sudden shocks.

2.9 Chip morphology

It is shown in Figure 2-10 that different cutting speeds result in different chips such as wavy, developed and saw toothed form. Also, different types of grains are seen in the chips at different cutting speeds.
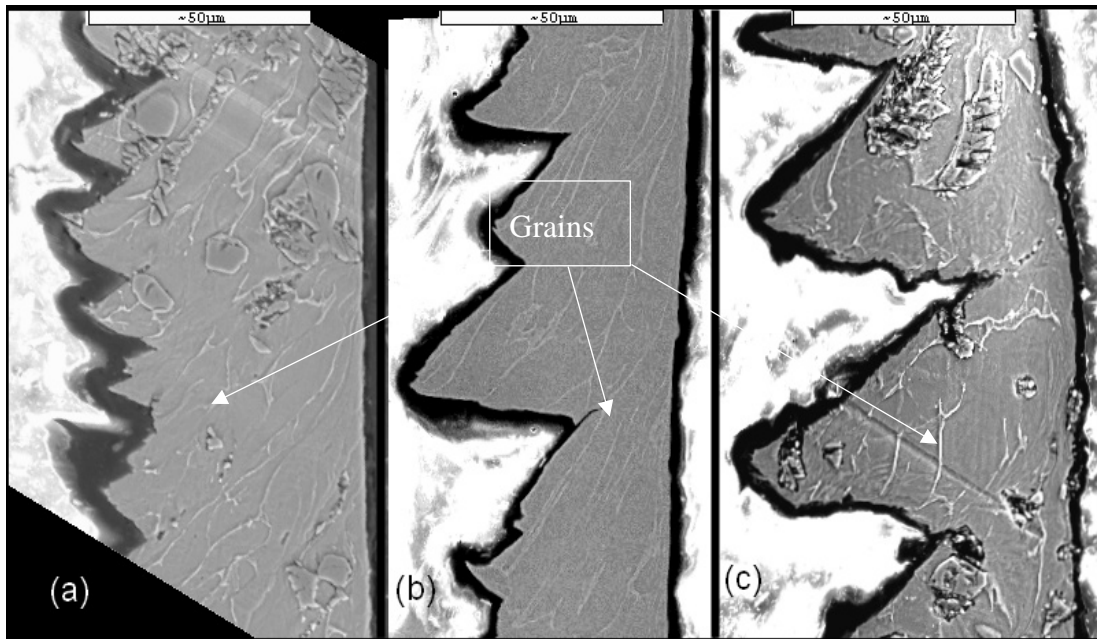
Figure 2-10 : Segmented chips at the speed of (a) at 60 m/min the wavy chips are formed, (b) at 100 m/min the chip segmentation is developed and (c) at 230 m/min the saw toothed chips are formed. Also, different forms of grains are seen at different speeds (Bejjani et al., 2012)

Since the early twentieth century, researchers started to study chip morphology because of its important influences on machining quality and other parameters like power consumption or tool wear. Depending on the properties of the work-piece material such as hardness, yield strength or ductility, chip formation varies in machining. Materials with high ductility have continuous chips while brittle materials have discontinuous chips. Cutting conditions such as cutting speed or feed rate also play an enormous role in chip formation (Miracle et al., 2001).

Bejjani et al. (2012) found that at lower cutting speed there is a wavy free surface of the chip whereas at higher cutting speeds, the chip segmentation is developed and the saw toothed chip form is shaped. In his study, by analyzing the chip morphology he revealed how the formation of a complete saw toothed chip is influenced by the cutting parameters.

2.10 Metal matrix composites (MMCs)

Metal matrix composites have solved a lot of industrial or biomedical problems and improved many processes which had faced various problems using monolithic materials before.

The reinforcements in MMCs can be particles, continuous fibers, or discontinuous fibers in the form of whiskers.

Even though producing particulate composites is easier and cheaper, ceramic fibers are used the most as the reinforcements in MMCs and greatly improve strength, stiffness and temperature resistance.

As reinforcement, particles can be distributed in the matrix better with any size, shape or arrangement. Moreover, breakage is seen less in particles compared to whiskers. Also, they can be oriented in matrices randomly or aligned; however, mostly they are distributed without any orientation (Soboyejo & Srivatsan, 2006).

Normally, particles as the reinforcement improve many material specifications, such as stiffness and abrasion resistance at high temperatures. This minimizes the manufacturing costs and blocks the displacement of the material's elements which leads to a decrease in plastic deformation and increase in strength. Some industries, like aerospace, started to use MMCs in 1970 and automotive in 1980. At the present time, MMCs are used in many domains, not only in industries, but also in other domains like biomechanics or painting (Davim, 2014).

Some of their usages are shown in Figure 2-11 and Figure 2-12.

The engine systems with lightweight connecting rods have a lower polar moment of inertia result in faster acceleration (Elite engine system, 2006).

Pushrods

(a)   (b)
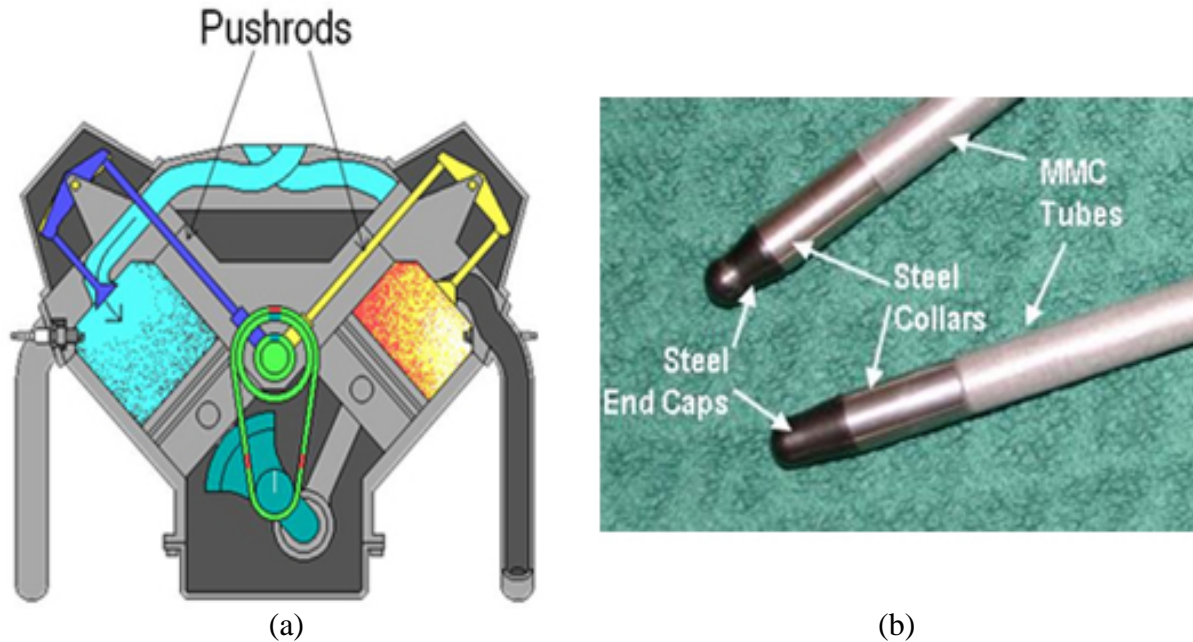
Figure 2-11 : (a) Metal matrix composite pushrod, a highly stressed component in high speed spark ignited engines (b) magnified image of the pushrods. Due to the different conditions of three sections of the rod, these sections are made with three different materials, as shown in the picture (Coupal, 2012)

The connecting rod needs to be strong, light and stiff and by using of a lower mass metal matrix composite, the mechanical requirements of the engine system are met.

Figure 2-12 : Connecting rod (Elite engine system, 2006)

Titanium Metal Matrix Composites

Titanium MMCs, having the advantages of both TiC particles and titanium, display a mixture of desirable properties such as: high stiffness and elastic modulus, increased strength, and low density. With all these beneficial properties, there are some disadvantages, in particular poor machinability due to the existence of enormously abrasive reinforcements. Because of their manufacturing process, finish machining is required (Pramanik, Zhang & Arsecularatne, 2008).

The difficulty of machining is caused by the interface between the TiC particles of the work-piece and the tool. The factors which have the most consequences in the surface roughness are cutting conditions, tool characteristics and the work-piece material.

Manna et al. (2003) found that higher cutting speeds can cause better surface finish when machining metal matrix composites in the turning process. Also, for evaluating machinability of MMC, tool life and tool wear tests are used more than the other parameters (Davim, 2014).

Ti-MMCs, due to their difficulty in machining, are mostly produced close to final shape to minimize machining. The production process is named CHIP (Cold and Hot Isostatic Pressing).

Firstly, raw material powders are blended in a blender, and then by a pressing machine the powders, ejected from the blender, are pressed under high hydrostatic pressure at room temperature to be compacted, named CIP (Cold Isostatic Pressing).

After that, the outlet goes to the sintering machine. The process is done at high temperature and very low pressure to change the compacted powders into the form of an alloy.

Finally, depending on the type of desired product and increase in mechanical properties, HIP (Hot Isostatic Pressing), CHIP or forging is applied. In HIP process, to close the residual porosities and improve some mechanical properties of material, argon gas is ejected into the machine under high pressure and proper temperature.

In CHIP process, as in conventional extrusion, pasty sintered materials are forced to pass through a nozzle and normally the result is the final product. Figure 2-13 shows a schematic process of producing Ti-MMCs (Aramesh, 2015).
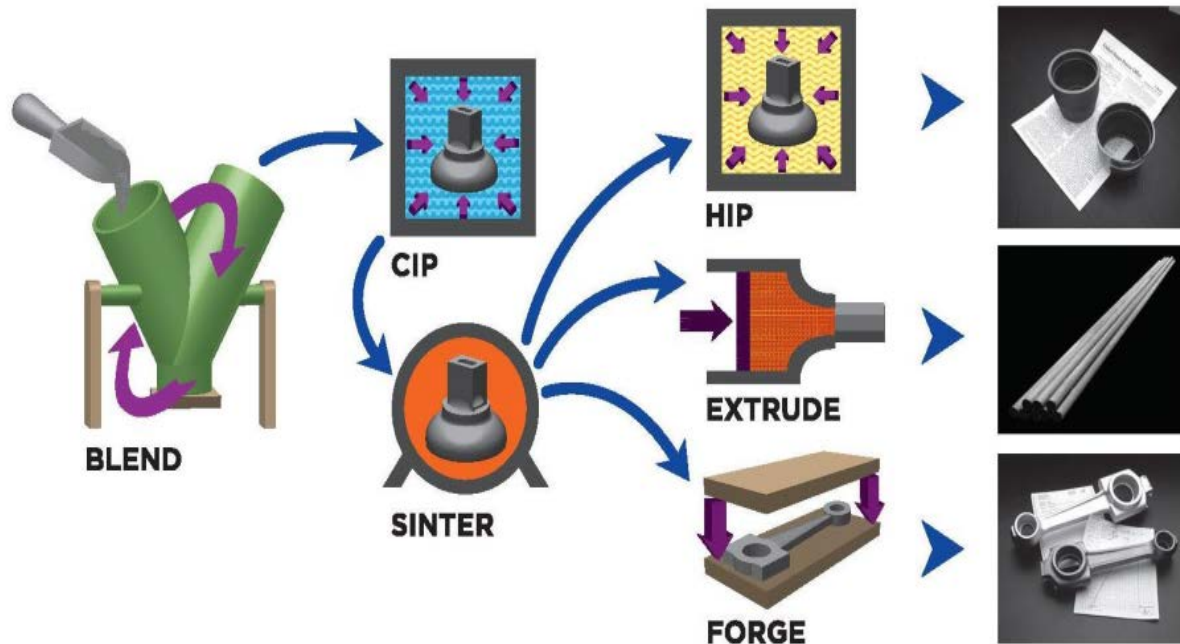
Figure 2-13 : Three different ways to produce Ti-MMCs products (Aramesh, 2015)

After being produced close to final shape, Ti-MMCs need to be machined to achieve the final desired product. (Niknam, Khettabi & Songmene, 2014).

Some mechanical properties of Ti-MMC and Ti6Al-4V are shown in Table 2-3. It can be seen that most Ti-MMCs mechanical properties are higher than those in Ti-6Al-4Vs.

Table 2-3 : Mechanical properties of Ti-MMC and Ti-6Al-4V (Dynamet Technology Inc.)

Material	Yield strength (MPa)	Tensile strength (MPa)	Elastic Modulus (GPa)	Shear Modulus (MPa)	Fracture Toughness (MPa/m$^{1/2}$)
Ti-MMC	1014	1082	135	51.7	40
Ti-6Al-4V	862	965	116	44	80

2.11 Tool wear in machining of Ti-MMCs

Due to the presence of hard and abrasive TiC particles as the reinforcement in Ti-6Al-4V the abrasive wear which is common in the machining is different in Ti-MMCs. Not only does a two-body abrasion mode exists in the wear mechanism, but a three-body abrasion mode also plays a role at the same time (Kishawy et al. 2005).

As mentioned in section 1-8-2, the two-body abrasion mode occurs while a smooth and hard surface rubs toward a softer surface. The three-body abrasion mode happens while a hard particle is rubbed between two surfaces and scratches both surface materials (Olortegui-Yume & Kwon, 2007).

Due to the existence of hard and abrasive particles in Ti-MMCs, flank wear is the first criterion in their machining. Because of the high importance of some uses of Ti-MMCs, such as engine parts of airplanes or cars, sometimes having a good surface finished is more important than machining costs. Theoretically, two factors can play a more important role in surface roughness: feed rate and tool geometry (Veiga, 2013).

2.12 Machining of titanium alloys using carbide tools

Gerez et al. (2009) performed some analysis of surface changes of WC/Co inserts in 10 first seconds dry turning of Ti-6Al-4V. The formation of built up edge (BUE) was observed in their experiments. Also, abrasion wear and a thin titanium oxide layer in the cutting area on the tool surface was detected.

Hartung et al. (1982) had some experimental studies about WC/Co tools in the turning of Ti-6Al-4V. They found that crater is a dominant wear at the cutting speed 61 to 122 m/min and higher than 122 m/min plastic deformation is the main wear mechanism. At the speed of 61 m/min and 30 seconds of machining they observed an adhered layer of titanium on rake face of tool. They suggested that this adhered layer decreases the tool wear rate by reducing the diffusion rate of work-piece elements through the insert. Then, they removed this layer by etching in hydrofluoric acid for 20 minutes and analyzed the actual worn out surface. Based on their research, a chemical reaction happens between the work-piece and the insert elements and forms an adherent layer of TiC on the crater.

Ezugwu and Wang (Ezugwu & Wang, 1997) had a review of the main problems related to titanium machining such as tool wear and the mechanisms which cause tool failure. They suggest that the uncoated WC/Co cutting tools are better than most coated cutting tools for machining titanium alloys due to the chemical activity of titanium with the work-piece material.

Moreover, they proposed that the high localized temperatures at the contact region, increase the reactivity of titanium, quicken the tool wear rate, and lead to chipping and premature tool failure.

Chou and Evans (Chou & Evans, 1997) focused on some experimental tests about the effects of microstructure of the tool and work-piece material on tool wear mechanisms. They observed a coating on the flank and the rake face which consisted of compounds of elements of the insert and work-piece material. Based on their results, a protective built-up layer is formed at low cutting speeds (between 15 to 60 m/min), but at high cutting speeds (more than 120 m/min) the built up layer is removed and high wear rates are observed.

Yousheng and Jianxin (Yousheng & Jianxin, 2008) observed that high cutting temperatures in the machining of titanium alloys using WC/Co cutting tools increase diffusion wear mechanism. They had some experimental studies in dry machining of Ti-6Al-4V with a WC/Co cutting tool. The machining parameters were: feed rate 0.1 mm/rev, depth of cut 0.5 mm, and cutting speed in the range 20 to 120 m/min.

Based on their results the flank wear increases when the cutting speed was increased from 20 to 120 m/min. They measured the cutting forces during the machining at 60 m/min and found that these forces are pretty stable when the tool wear rate is steady. They performed some high speed machining experiments and then analysed the inserts through SEM analysis with an Energy Dispersive Spectroscopy (EDS) detector. According to the observations made in their study, the main wear mechanisms were diffusion and adhesion.

Zlatin et al. (1973), found that titanium and its alloys have a Strong tendency to weld to the cutting edge, particularly after the initial tool wear period.

Rabinowicz (Rabinowicz, 1977), had some studies about adhesion wear and demonstrated the correlation between friction and wear because of the same adhesion factors which influence both of them.

R. Bejjani (2012), M. Aramesh (2015) and X. D. Troung (2015) have investigated three different aspects of the machining of Ti-MMCs.

R. Bejjani et al. performed some experimental studies about the machining of Ti-MMCs and an optimization process with two different speeds using PCD and carbide inserts, but his results could be extended with the other cutting parameters or with different speeds.

They found that at a speed of 90 m/min, feed rate 0.2 mm/rev and depth of cut 0.15 mm, machining has the optimal conditions, meaning less tool wear and better surface roughness (Bejjani, 2012). In contrast, X. D. Troung et al. (2015) found that at lower speeds like 20 m/min tool wear is less than higher speeds like 30, 50 and 60 m/min (shown in Figure 2-14).

Basavarajappa et al.'s studies (2006) separated the most important parameters in the machining of particulate metal matrix composites into two groups: intrinsic and extrinsic. Intrinsic parameters are: feed rate, cutting speed, and depth of cut. Extrinsic parameters contain: reinforcement size and volume fraction.
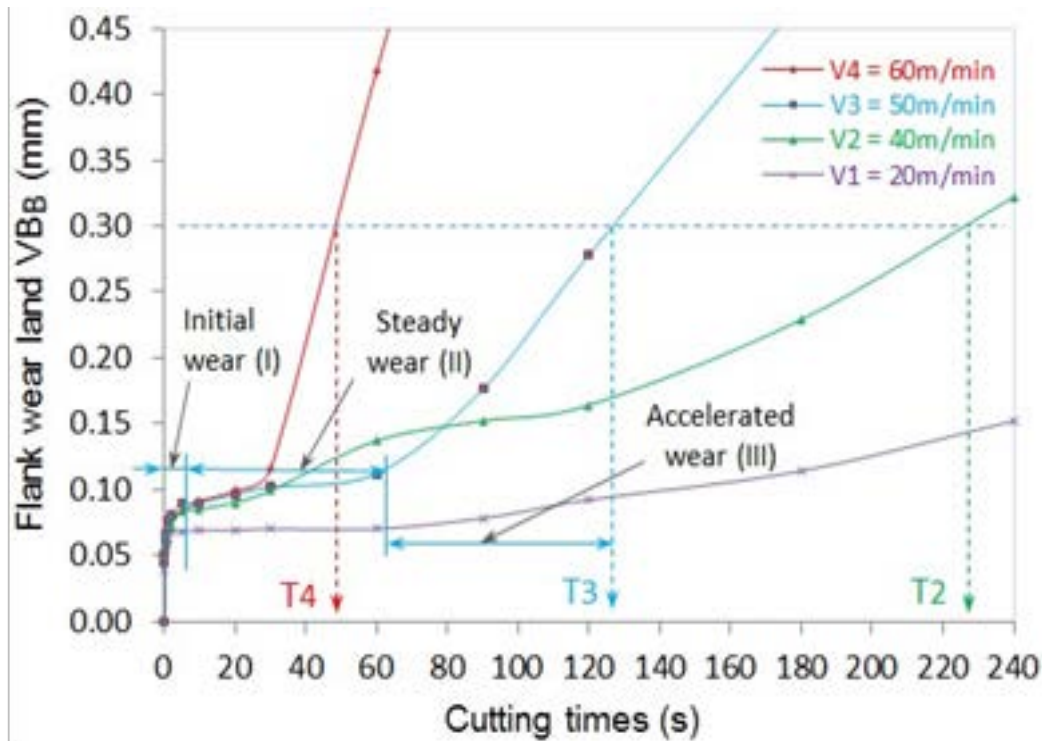
Figure 2-14 : Tool wear with different speeds in machining of Ti-MMC (Troung et al., 2015)

X. D. Troung et al. had some experimental studies about the initial tool wear in the machining of Ti-MMCs and found a protective layer forming in the first stage of tool wear which could have some influences on the tool life. Also, he presented a new theory to relate the initial moments of machining to the rest of the process, but some of his test results such as the initial wear mechanism were different with R. Bejjani and M. Arameh.

2.13 Summary of the literature review

Due to the existence of hard and abrasive particles in Ti-MMCs, flank wear is the first criterion in their machining. The initial period of tool wear is an area that needs more research. Furthermore, not many studies have approached to the initial tool wear in machining of TiMMCs. Also, identifying the initial mechanism of the primary stages of tool wear becomes more significant due to its direct influences on the tool life.

As a result, this study's aim is to continue the research in the field of initial tool wear mechanisms in the first moments of machining of Ti-MMCs.

CHAPTER 3   EXPERIMENTAL PROCEDURE

In this study, all the tests were performed under dry machining. Cutting tools, tool holder, machining parameters, and conditions were selected based on the previous research in this domain (Bejjani et al., 2012 & Troung et al., 2015).

3.1 Cutting tools and tool holders

Some specifications of the insert and tool holder, used in this research, are shown in Figures 3-1, 3-2, and Table 3-1.

Table 3-1 : CNMG 432-MF4 TS2000 insert with the specifications

Application	turning
Insert style	CNMG
Insert size	432
Chip breaker type	MF4
Inscribed Circle	0.5 Inch
Included angle	80 degrees
Grade	TS2000
Material	carbide
Coating	TiAlN/TiN
Coating process	PVD
Thickness	4.76 mm

Turning – Inserts

SECO

CNMA, CNMG

				Dimensions in mm			
Size				**d**	**l**	**s**	**h**
1204				12,70	12,9	4,76	5,2
1606				15,88	16,1	6,35	6,4
1906				19,05	19,3	6,35	7,9

Tolerances:
d = ±0,08
d = ±0,10
s = ±0,13
r$_\varepsilon$ = ±0,1

Size:
12
16, 19
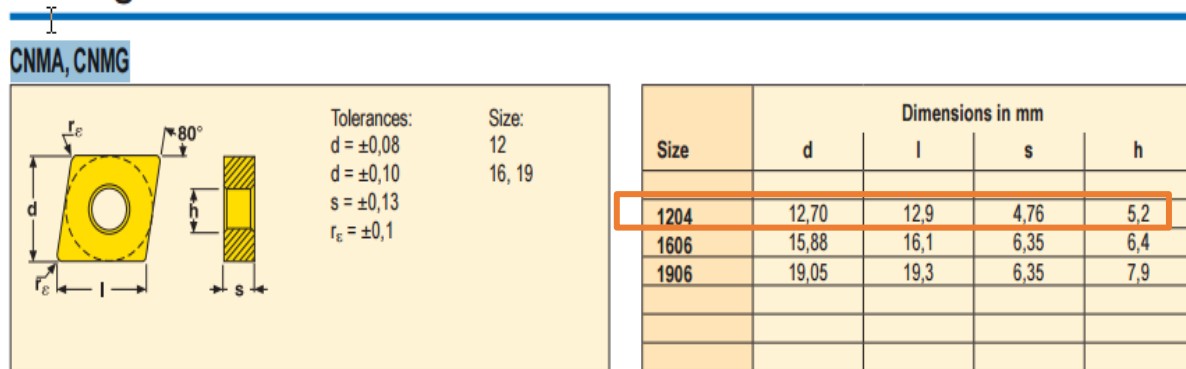
Figure 3-1 : Carbide TiAlN/TiN coated insert specifications (Seco, 2011)

DCLNR/L

Right-hand version shown
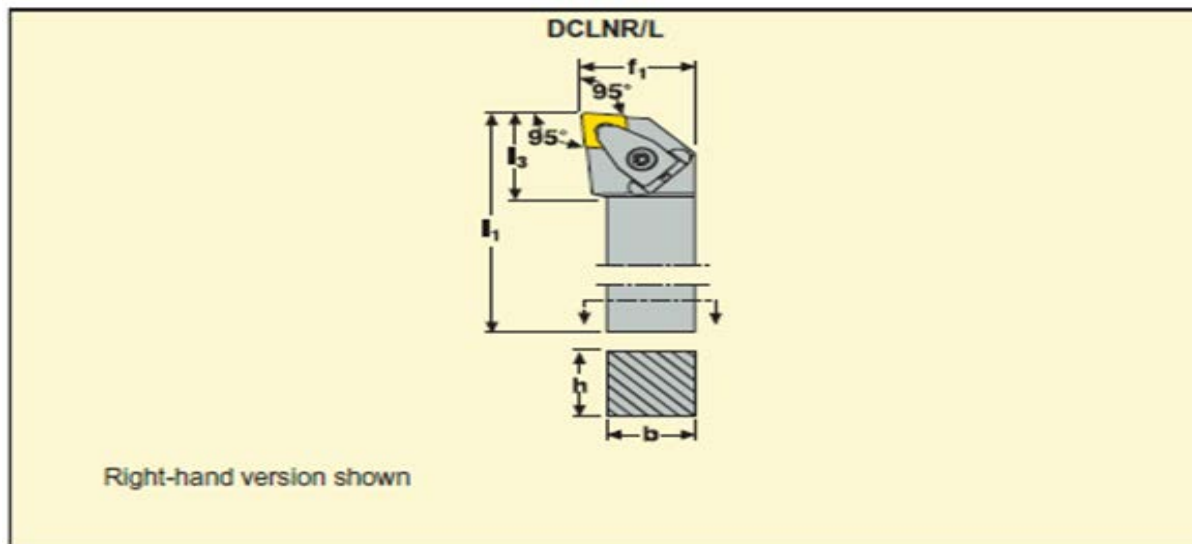
Application	Insert I.C.	EDP No.	Part No.	Dimensions in Inch					$\gamma_o°$	$\gamma_p°$	lbs	
				h	b	l_1	f_1	l_3				
95°												
	1/2	31061	DCLNL 12 4B	0.75	0.75	4.5	1.00	1.30	-6	-6	0.7	CN..43.
		31003	DCLNR 12 4B	0.75	0.75	4.5	1.00	1.30	-6	-6	0.7	CN..43.
		31062	DCLNL 16 4C	1.00	1.00	5.0	1.25	1.30	-6	-6	1.4	CN..43.
		31057	DCLNR 16 4C	1.00	1.00	5.0	1.25	1.30	-6	-6	1.4	CN..43
		32304	DCLNL 16 4D	1.00	1.00	6.0	1.25	1.30	-6	-6	1.7	CN..43.
		32303	DCLNR 16 4D	1.00	1.00	6.0	1.25	1.30	-6	-6	1.7	CN..43.
		31064	DCLNL 20 4D	1.25	1.25	6.0	1.50	1.30	-6	-6	2.7	CN..43.
		34513	DCLNR 20 4D	1.25	1.25	6.0	1.50	1.30	-6	-6	2.7	CN..43.

Figure 3-2 : Tool holder used in the tests (Seco, 2011)

Based on recent research, Polycrystalline Diamond (PCD) tools are the first choice for machining of Ti-MMCs (da Silva et al., 2013). Cubic Boron Nitride (CBN) and carbide TiAlN/TiN coated

tools are the other options for machining Ti-MMCs according to manufacturer's recommendations. In keeping with the purpose of this study, the tool wear should not be too fast to have the needed average accuracy or too slow to decrease the experimental costs. Moreover, to address the other question of this study that was the difference between two previous studies done with carbide tools, WC/Co substrate TiAlN/TiN PVD coated was selected.

Dynamet Technology Inc supplied the work-piece material and the Drillmex Company supplied the inserts and tool holder.

3.2 Equipment and work-piece material

All the experiments were done using a 6-axis Mazak QT-Nexus-200, CNC turning center (shown in Figure 3-3).
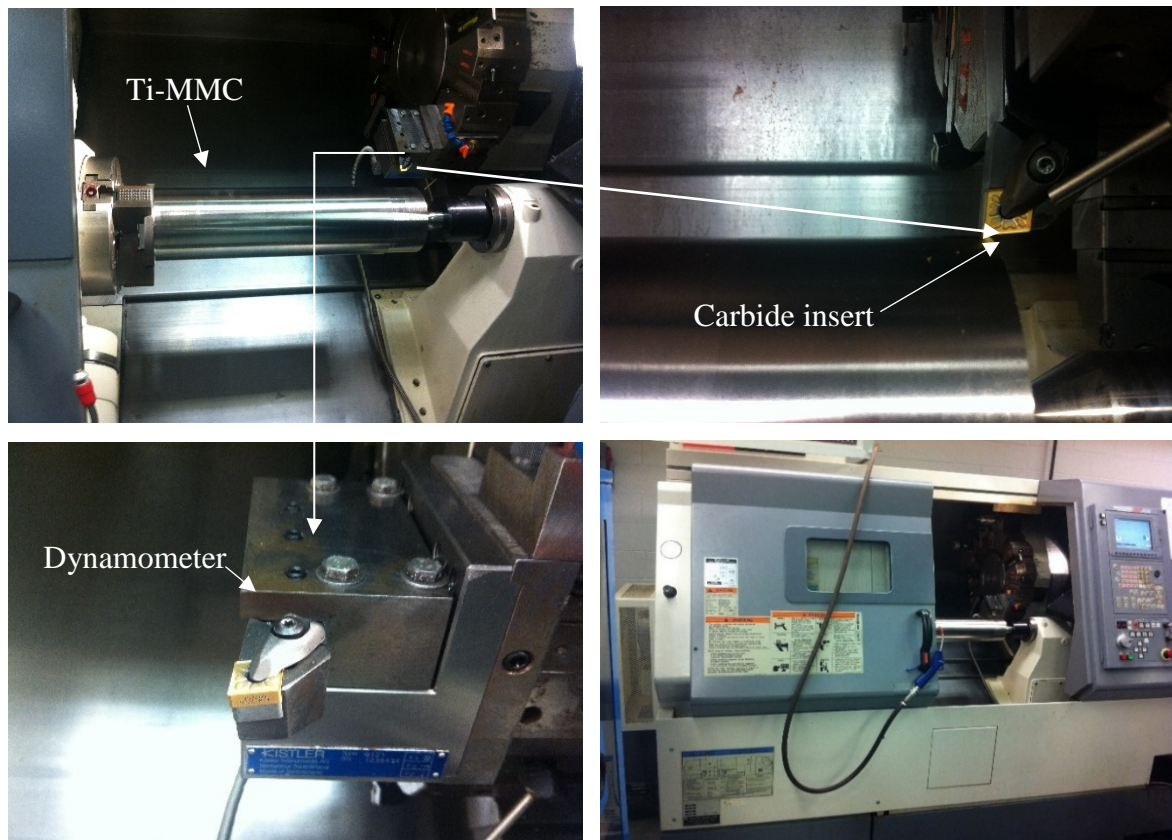
Figure 3-3 : Lathe, insert and dynamometer images at virtual manufacturing research laboratory (LRFV)

Cutting force components were measured and registered using a Kistler dynamometer (type 9121) connected to the LabVIEW software. The tool wear was quantified by measuring the flank wear of the inserts and plotting it versus cutting time (ASME Standard, 1985).

Dynamet Technology, Inc. is one of the pioneers in Ti-MMCs production. All the tests, done in this study, were performed using one of their products, Ti-6Al-4V with 10-12% volume fraction of TiC particles with irregular shapes and 10-20 μm size. The turning tests were performed with 140 mm diameter cylindrical CermeTi-MMCs.

Procedure of data collection

Each insert was given a number and cleaned before machining started. A divider was put between the cutting parts and the bed of the lathe machine to separate the chips of each pass. After each test, all the produced chips were collected and labelled with machining parameters like cutting time feed rate and speed for further metallographic analysis. Then, the divider was cleaned and replaced.

3.3 Methodology

To start the preliminary tests, the cutting conditions were chosen to match manufacturer's recommendations and the same as in the research done by Troung et al. (2015) Each edge of the tool was used in the machining until a certain period of time and for all experiments the cutting speed was 50 m/min, feed rate 0.15 mm/rev and depth of cut 1.5 mm.

In order to have an accurate result, each test was performed with an edge of the insert, which means 4 tests for each insert.

To prevent the influences of the previous cutting on the work-piece and tool elements, every new test was done using an unused edge of the insert. All the tests were repeated a further two times to ensure that the tests are carried out correctly.

Tool wear (VB_B) was measured using a Toolmaker-Mitutoyo optical microscope (Figure

3-4 (a)) and by counting the pixels in the photos captured with Canon EOS 300D digital camera

(Figure 3-4 (b)).
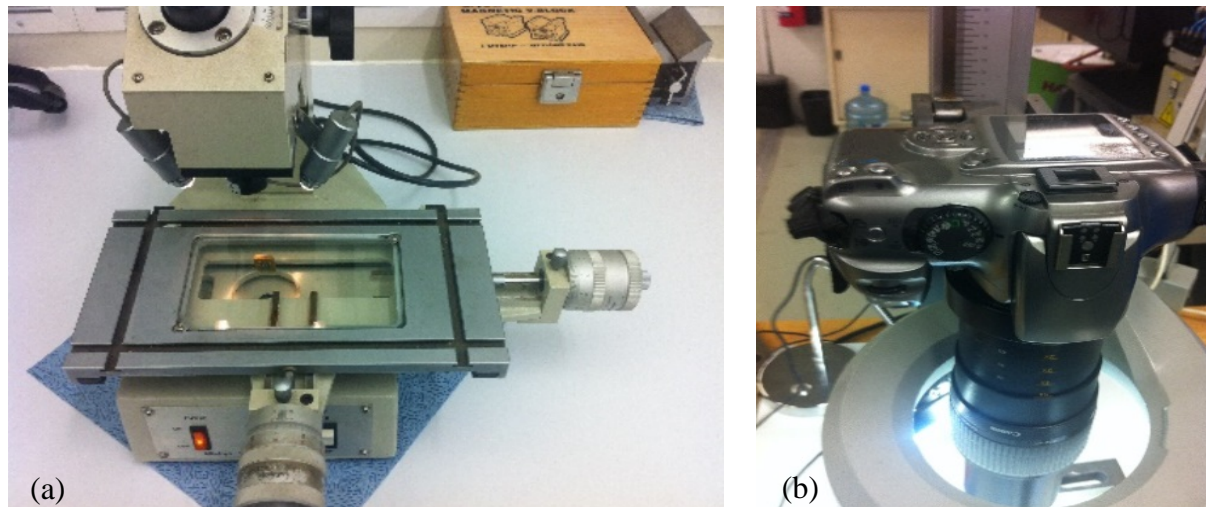
Figure 3-4 : Measuring of VB_B by; (a) Mitutoyo microscope and (b) Canon digital camera

A typical worn out flank face is shown in Figure: 3-5. To measure VB_B, first, worn out length (b) was measured with the Toolmaker optical microscope having the unit of precise measurement 0.005mm. Then, near zone N whose length is equal to b/4, VB_B was measured. VB_B is the distance between the rake face plane and the end of the worn out region. In order to have a precise measurement, at first, a photo of all worn out flank faces was taken with the camera and then, VB_B in the photos was measured by counting the pixels. To have the same conversion factor in all photos, the camera was fixed at the exact same distance from the inserts and with exactly the same zoom setting. Also, for each insert in the same place in the picture, as well (in the center to avoid distortion).
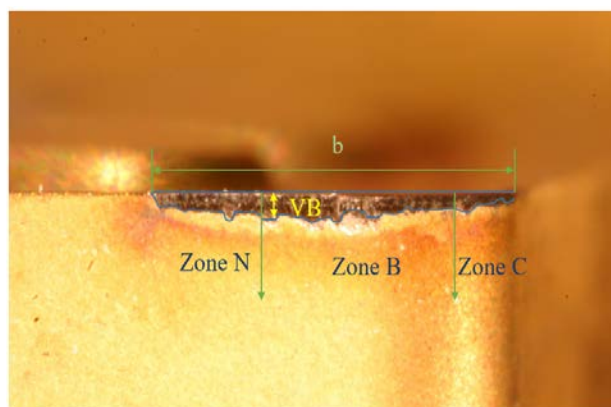
Figure 3-5 : Typical flank tool wear with three zones

VB can be measured using an optical microscope directly or taking the photo and converting the pixels into millimetres

It should be noted that with this method, it is not possible to adjust the focus by changing the distance between the lens and the insert otherwise it is needed to include a ruler to get the new conversion factor. The best way to avoid any mistake is to always add a ruler in the photo.

Tool wear in a brand new tool was measured (shown in Figure 3-6) to prevent any default in further measurements.

Figure 3-6 : Zero tool wear in a brand new insert

To answer the question of what is happening in the first transition period resulting in lower tool wear rate comparing to that before the first transition time, some EDS analyses of flank worn out surface were performed. In addition, to find the composition of the elements on the surface of a brand new insert and raw work-piece material, Energy Dispersive Spectroscopy (EDS) and X-ray Photoelectron Spectroscopy (XPS) techniques were applied.

3.4 X-ray photoelectron spectroscopy (XPS) analysis

The XPS technique can be applied to investigate and reveal the chemical compositions of the surface containing elements and bonds. It is a quantitative surface sensitive spectroscopic technique which measures the elemental composition in the parts per thousand range. The method requires high vacuum (10^{-6} Torr) and detects surface elements with the atomic mass number between lithium (3) and lawrencium (103). In this method, X-rays force the surface elements electrons to pass through a detector to determine their binding energy. The electrons having lower binding energy (BE) form weaker bonds, and the electrons with higher BE form stronger covalent bonds.

In this study, to further confirm the EDS results, XPS analysis of a round Ti-MMC material (work-piece) and a brand new carbide TiAlN/TiN coated insert (tool) were carried out.

Preparation:

Before XPS operation, all the specimens were cleaned by hexane, acetone, and isopropyl alcohol.

At first all the specimens were cleaned with hexane using an ultrasonic bath for 20 minutes. Hexane is a solvent which is used to solve oil on the parts. It dissolves oil better than other organic solvents. Then, the process repeated using acetone for another 20 minutes. Acetone leaves a residue after evaporating, hence a rinse with IPA is needed to remove the residue. Therefore, the cleaning process was repeated using IPA for 20 minutes. Eventually, nitrogen gas was blown to the specimens to dry them.

The next step was to identify the chemical state of the main elements of the specimens with XPS experiments.

Experimental conditions

The experimental conditions are presented in Table 3-2. As it can be seen, all survey scans were obtained at 100 eV pass energy with the energy steps 1 eV and in core level spectra, at 20 eV pass energy with the energy steps 0.05 eV.

Table 3-2 : Experimental conditions of XPS analysis

Apparatus		VG ESCALAB 3 MKII
Source		Mg Kα
Power		300 W (15 kV, 20 mA)
Pressure in analysis chamber		3.0×10^{-9} Torr
Analysed surface		2 mm x 3 mm
Electron takeoff angle		90 degrees
Analysed depth		< 10 nm
Detection limit		~ 0.1 % atomic
Survey scans	Energy step size	1.0 eV
	Pass energy	100 eV
High resolution scans	Energy step size	0.05 eV
	Pass energy	20 eV
Background subtraction		Shirley method
Sensitivity factor table		Wagner
Charge correction with respect to C1s at		285.0 eV

It is important to note that the analyzed depth was less than 10 nanometers, which means just the surface composition is analysed. The spectra were fitted with Gauss-Lorentzian peaks and the compositions were gained using the area under the related core level spectra and their respective atomic sensitivity factors by comparing to the handbooks of the spectroscopy.

3.5 Scanning Electron Microscopy (SEM)

A scanning electron microscope (SEM) followed by Energy Dispersive Spectroscopy (EDS) is commonly used to reveal the chemical composition or crystalline structure of a material.

SEM/EDS commonly operates in a vacuum, and the magnification of images may vary between 20 to 300000X.

A high-energy source produces an electron beam and bombards the sample to interact with the atoms within it to produce certain signals and reveal the chemical compositions of the specimen. The amounts of X-rays released from the sample material are measured with an EDS detector and normally a spectrum is plotted as x-ray counts versus energy. The peaks in the spectra relate to the distinct elements in the material and the higher peak in the spectrum of EDS presents the more concentrated element in sample.

To study the initial tool wear mechanisms, two SEM (Jeol, JSM -840A and Jeol JSM 7800F FEG-SEM) equipped with an Oxford X-ray detection system (AZtec EDS) for elemental analysis and quantitative mapping were used. Moreover, Joel JSM is a field emission SEM equipped with field emission guns (FEG) which provides the extreme resolution of 0.8 nm at 15 kV and 1.2 nm at 1 kV. The micrographs of the microstructures were captured at a low magnification and at a high magnification.

3.6 Focused Ion Beam (FIB) application

In order to measure the length and depth of the adhered layer and to find out what elements or sub-layers are under the layer that perform during the machining, a focused ion beam (FIB) technique was applied.

To prepare the sample for cross sectional removal with FIB technique, the sample must be prepared by cutting the insert with cut-off saw (Figure 3-7).

In the cutting operation, attention is paid to avoid to damage the sample. After preparing the specimen and cleaning it using an ultrasonic bath with acetone and IPA for 20 minutes, the layer to be cross-sectioned was first selected and located within the FIB workstation. Then, by using a high current beam, a wedge with certain dimensions was cut and a vertical wall was attained.
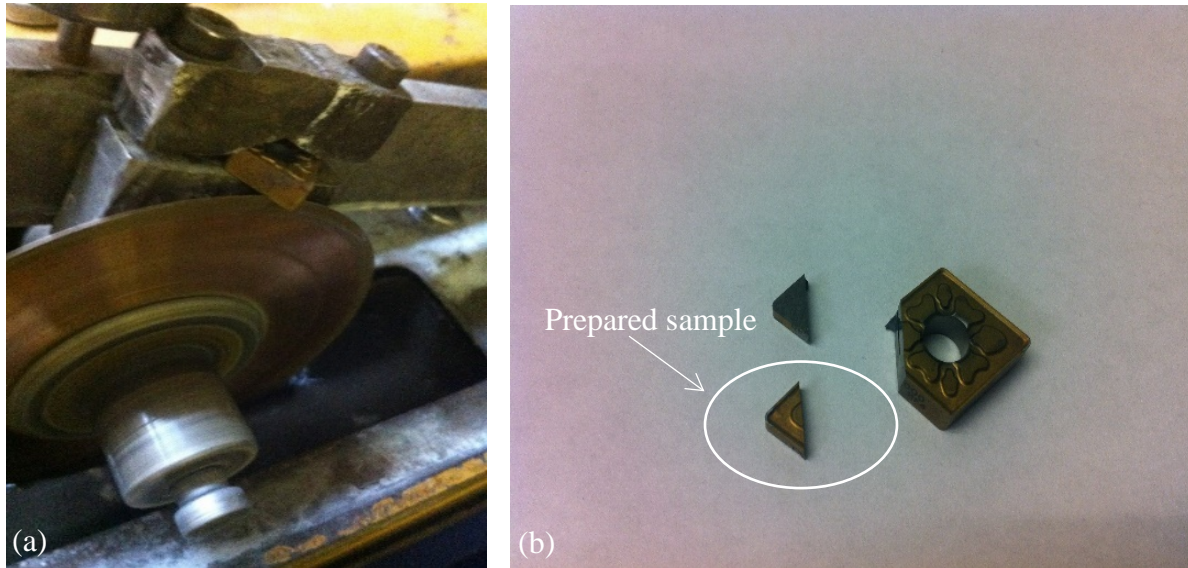
Figure 3-7 : Preparation of the sample for FIB technique (a) cutting the insert using a cut-off saw (b) prepared sample for FIB technique

Usually, a cross section with FIB technique is similar to SEM except FIB uses the focused ion beam instead of electrons. FIB is performed by orienting the sample surface perpendicular to the released ions direction and the surface is hit and sputtered by ions. A final polish is done with the ion beam parallel to the cross-sectional surface. This polishing, helps to clean up the cross-sectional wall. The result is an FIB cut that has no depth at the top and is fairly shallow at the end. The sectioning was made wide enough to show the sub-surface features in both rake face and flank face.

CHAPTER 4   RESULTS AND ANALYSES

In this chapter the results of the machining tests and the analyses which help to have a better understanding of the initial tool wear mechanisms are presented. The results of the tool wear measurements are provided in Figure 4-1.
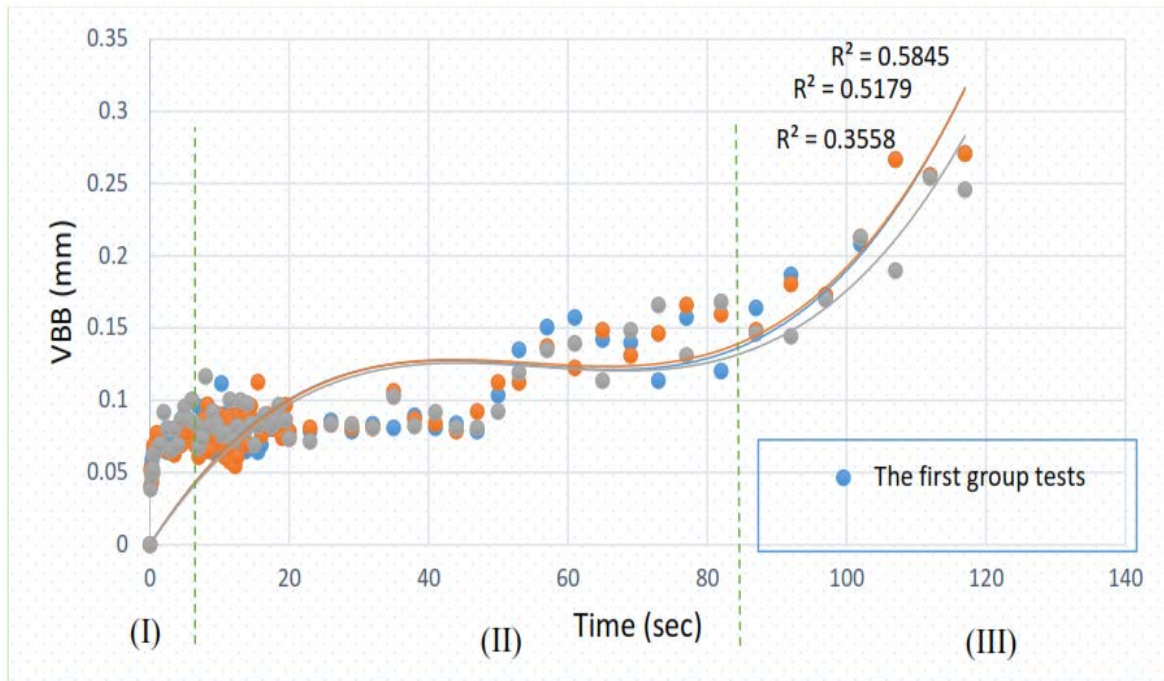
Figure 4-1 : Tool wear progression of different inserts at different times and fitting a polynomial regression of order 3 (polynomial of order 3 was chosen based on the previous study (Troung et al., 2015))

As a first attempt to find the transition point, polynomial regression was applied to fit the trend line, but comparing the progression of the points with the progression curves, shows that the values do not match data and the fitting polynomial trend line seems to be wrong especially for initial points.

Also, it is well-known that the R-squared value in a reliable trend line is 1 or near it. In this case as it is shown in Figure 4-1 R-squared values are: 0.5845, 0.5179 and, 0.3558 which obviously are not close to 1. Hence, another type of trend line with linear regression which seems to be more fitted and R-squared closer to 1, was chosen (Shown in Figure 4-2).

To add the linear trend line, each group of the test was divided into three sub-groups. Then, for each sub-group a linear regression was fitted.

In order to find the best data dividing as a sub-group (highlighted in Figure 4-3 (a)), it was noted that the trend line should not be extended too far outside the data set and be close to 1. This was done by guesswork that means: at first, a group of data was selected and its R-squared was calculated then another group and determining another R-squared. This process repeated to find the closest R-squared to 1. This method was applied to all 9 sub-groups.
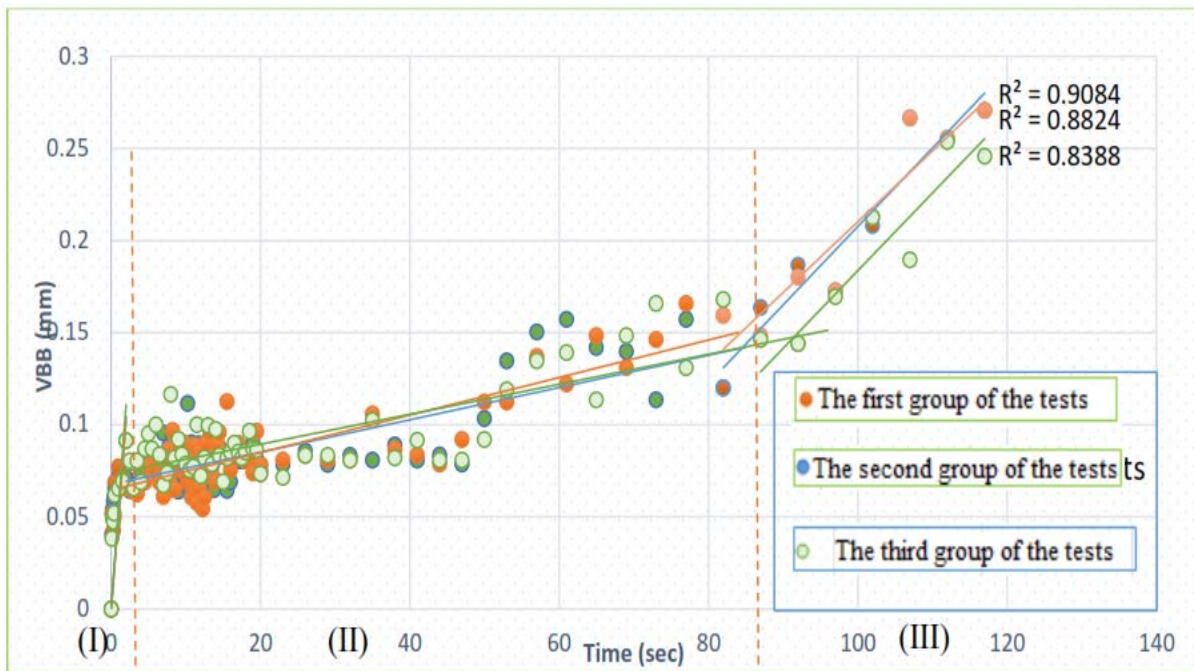
Figure 4-2 : Tool wear progression chart for different inserts with linear regression

Regarding Figure 4-2, tool wear rate is too high in less than a second of starting machining (region I) with the speed of 50 m/min and the transition period starts around that time. After that, tool wear rate decreases rapidly and the steady-state tool wear region is achieved (region (II)). Eventually, after about 83 seconds of machining, the time tool wear rate changes to a higher amount and enters the third region (region (III)). It is determined using Figure 4-3 that the first transition time happens before the first second of machining and the second transition period is after about 85 seconds of machining.
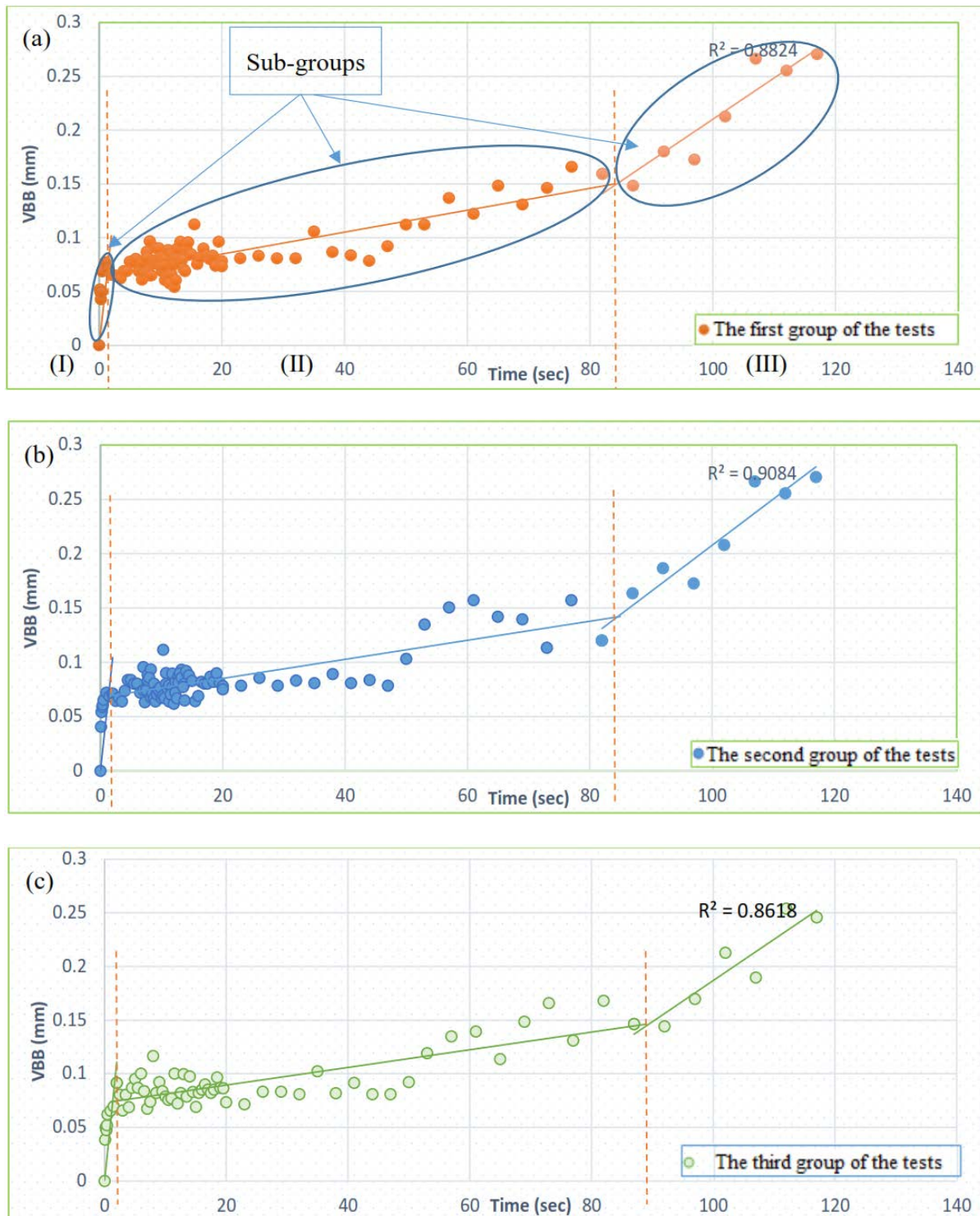
Figure 4-3 (a), (b), and (c) : Tool wear progression chart for different inserts with three groups of machining results (c) The sub-groups are highlighted in the first group of the results

The transition points are considered important machining data due to their influence on the entire machining process. The second transition time is particularly important because of the high tool wear rate in its third state (Astakhov, 2006).

Mostly, the tool wear is linked to the point called the permissible tool wear VB$_{BC}$ (as mentioned in the section 1-6) which is often the acceptable tool wear. Moreover, a precise estimation of this point is necessary with the purpose of preventing harmful effects on the work-piece and the machine tool from entering the rapid wear region. Thus, using the data on the first and second transition points could help manufacturers to reduce machining costs.

First transition point

As shown in Figure 4-4, in all three times of the experiments, by drawing the trend line, the transition time occurs at less than one second of machining. The tool wears out extremely fast before reaching this point.
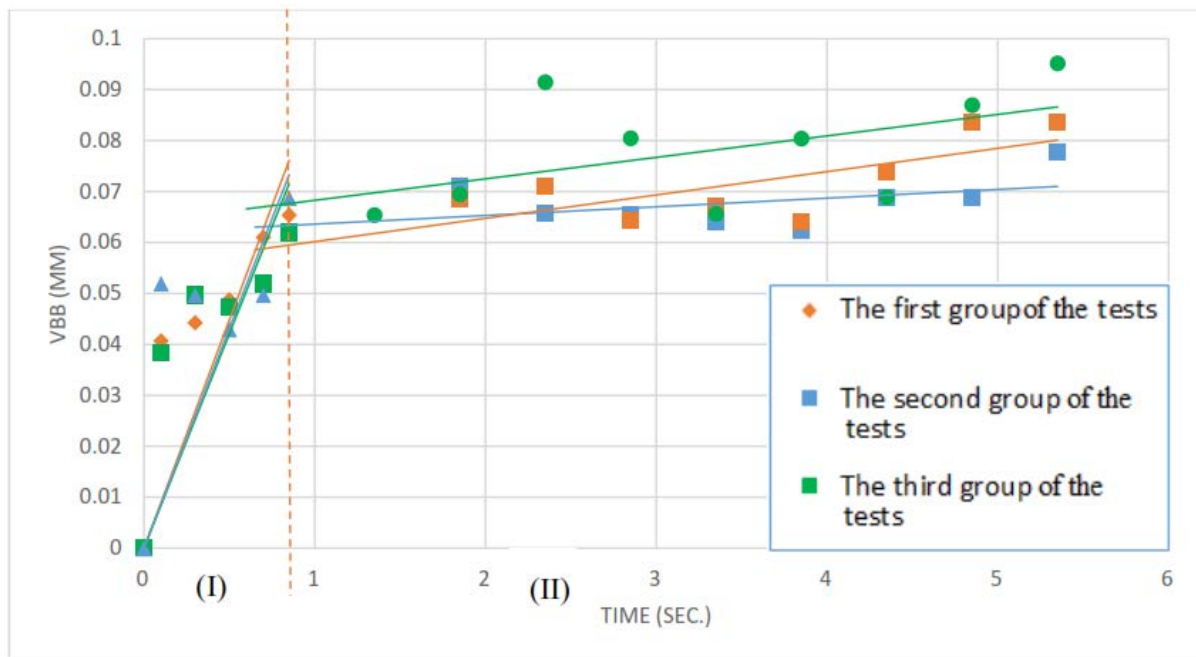
Figure 4-4 : Tool wear progression within 6 seconds of machining showing the first transition point at less than a second of machining

4.1 Cutting force during the initial tool wear period

Ravindra et al. (1993) found out that there is a direct correlation between the cutting forces and the progressive tool wear. Due to the important influences of tool wear on the finished surface of work-piece, using force monitoring could be one of the best choices for indirect tool life estimations. Moreover, other signals such as cutting temperature, vibration, acoustic emission, surface finish and process power consumption are used (Dimla Snr, 2000).

A piezoelectric quartz crystal dynamometer was used to measure cutting force components during the machining.

The cutting forces in machining of Ti-MMCs are mainly depend on the friction between the work-piece material and the insert, the mechanism of chip formation, the deflection of the chips, and the material separation. Afterwards, in turning, at higher cutting speeds lower cutting force has been observed (Veiga, 2013).

Cutting force components direction are presented in Figure 4-5.
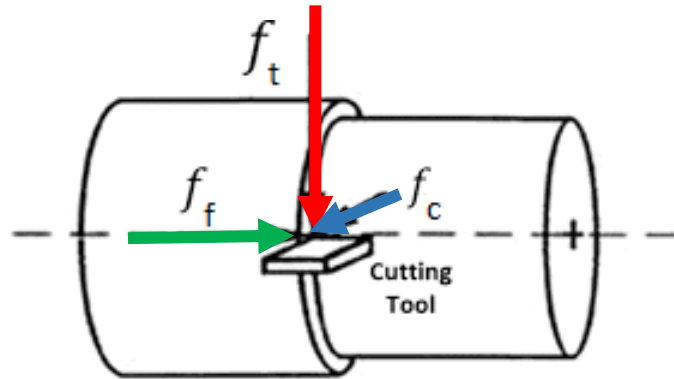
Figure 4-5 : cutting force components direction

After recording cutting force components during the initial moments of machining, the forces were plotted using Matlab software to see the variation of cutting force components within a certain time. The results were shown in Figure 4-6 (a) to (j). It can be seen that the amounts of cutting force components stabilize at around 1 second but until this time all forces increase rapidly. As shown in Figure 4-6 (a) the highest amount of tangential force (Ft) is 350 N, Fc = 190 N, and Ff = 60 N at 0.5 second of the machining. Then, at the first second of machining

Ft = 450 N, Fc = 250 N, and Ff = 120 N (Figure 4-6 (b)).
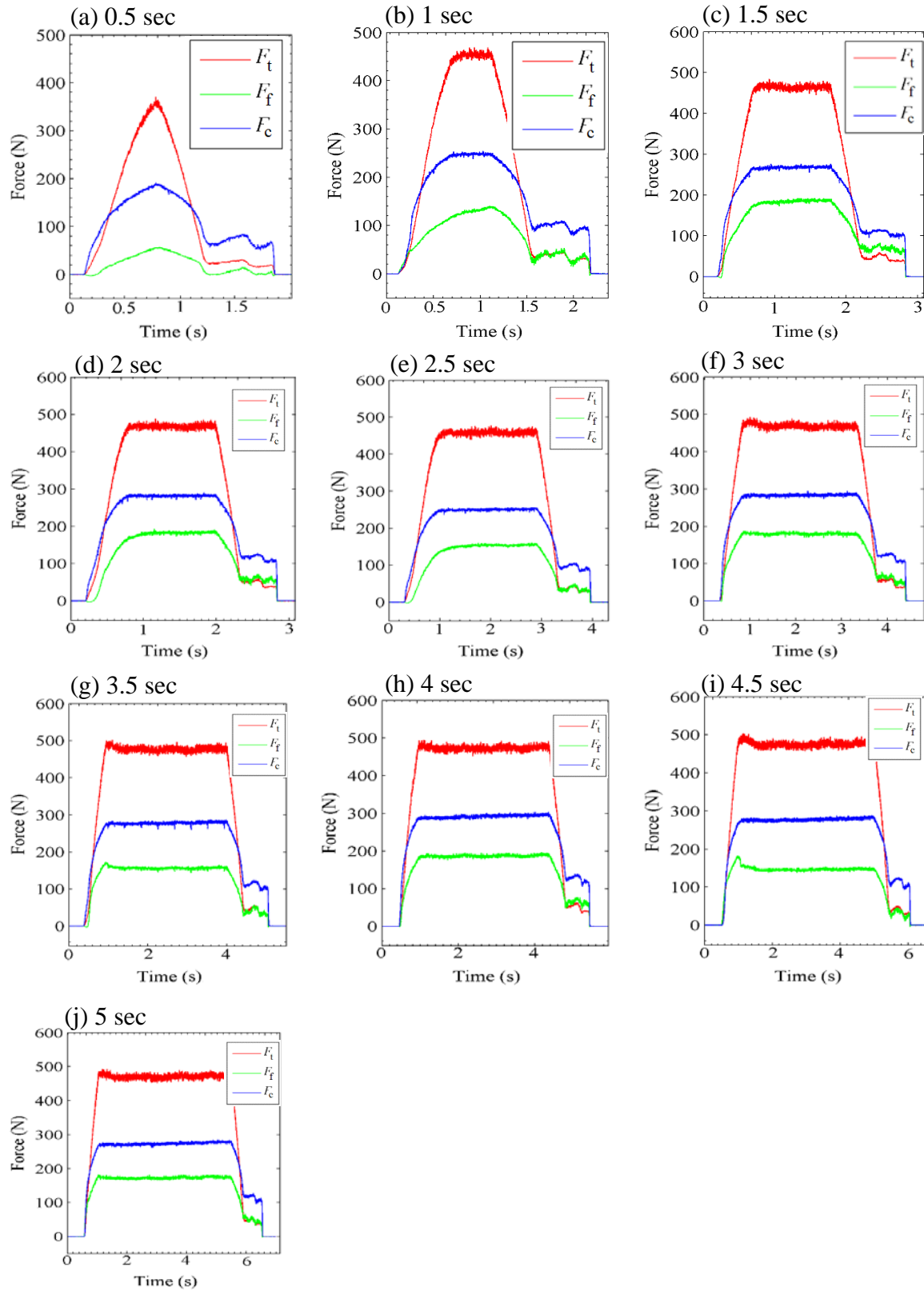
Figure 4-6 : (a) to (j) cutting force diagrams, registered in the first five seconds of machining and (k) cutting force components direction

Since the results should be validated, all the tests were repeated two times. The results show that when machining starts, the amount of each cutting force component (F_t, F_c, and F_f) increases fast and becomes almost constant around 1 second.

The correlation between the cutting force and the initial tool wear progression will be discussed in section 5.5.

The chemical composition of a round Ti-MMC material (work-piece) and a brand new carbide TiAlN/TiN coated insert (tool) were analysed by applying XPS method.

Ti-MMC surface chemical characterization with XPS

A typical survey XPS spectra of Ti-MMC is shown in Figure: 4-7 and the results are presented in Table 4-1 and Table 4-2.

It can be seen that the dominant signals are O, Ti and C, with weaker contributions from N and Al. Moreover, small signals from Ca, Zn, and Pb were observed. Since Zn and Pb peaks do not belong to the Ti-MMX, these elements might be some debris present as contaminants in the outermost surface atomic layers due to the process used to prepare the unpolished sample. Chloride (Cl) was also detected on the Ti-MMC sample with the binding energy of 199.4 eV, which could correspond to chloride salts (Moulder, 1992). Furthermore, in Figure 4-7 an Auger peaks relate to O due to the self-orbital coupling of O 1s and Ti 2p and do not correspond to the other elements (Moulder, 1992).
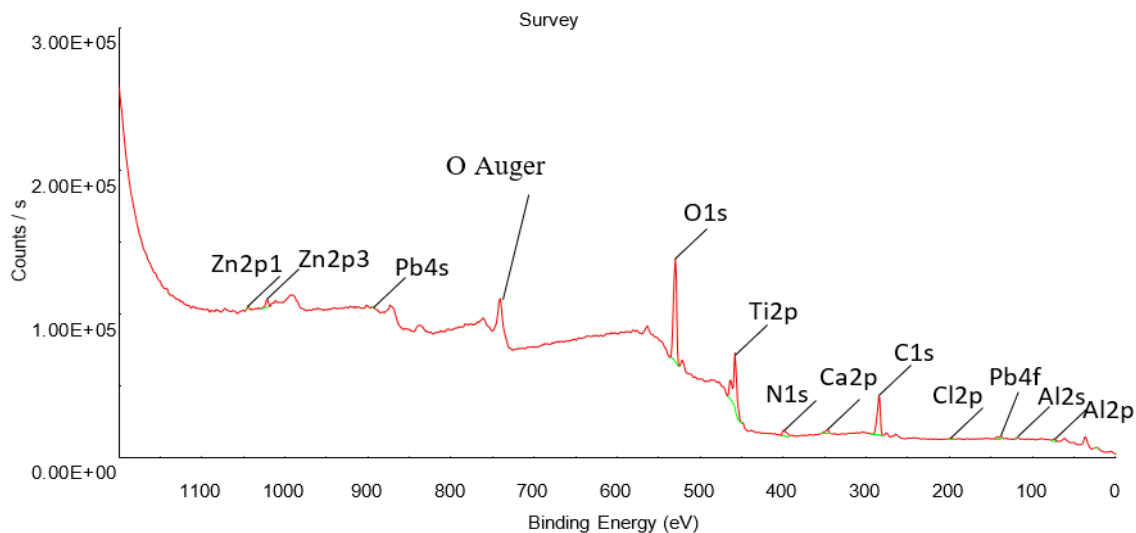
Figure 4-7 : Survey spectra of Ti-MMC sample

Table 4-1 : Chemical composition of the survey spectra of Ti-MMC sample

Name	BE	At. %
		Ti-MMC
Al	74.4	1.8
Pb	138.2	0.1
Cl	199.4	0.4
C	285.8	38.6
Ca	348.1	0.9
N	397.8	3.6
Ti	459.0	10.6
O	530.9	43.3
Zn	1021.2	0.7

Table 4-1 shows that O (43.3%), C (38.6%), and Ti (10.6%) have the highest percentage in surface chemical composition of the sample. In this table, "NAME" means the name of elements, BE is the abbreviation of the binding energy of corresponding atomic orbital, and at. % is the relative atomic percentage.

In Figure 4-8, the survey XPS core-level of Al2p, Ti 2p, N1s, C1s, and O1s are presented. The integrated intensity of separate components after peak fitting is provided based on the standard data on the binding energy of the titanium and aluminum oxides and nitrides (Moulder et al., 1992).

Here are some discussions about the elements and bonds, detected by XPS:

C1s

Figure 4-8 (a) shows the C1s spectra of the Ti-MMC sample by XPS measurement. According to the handbook (Moulder et al. 1992) the C1s peak of TiC should appear around 281.9 eV but here as it is clear there is not a major peak around 281.9 eV. It is possible that the TiC particles were partly oxidized or there was not any TiC particle on the fairly small analysed surface.

O 1s

The high resolution O 1s spectra (shown in Figure 4-8 (b)) revealed three Gaussian-shaped peaks at 530.0, 531.8, and 533.3 eV. The first and main peak is due to the O-metal band and might originate from Ti O bond relating to the thin TiO film formed on the surface.
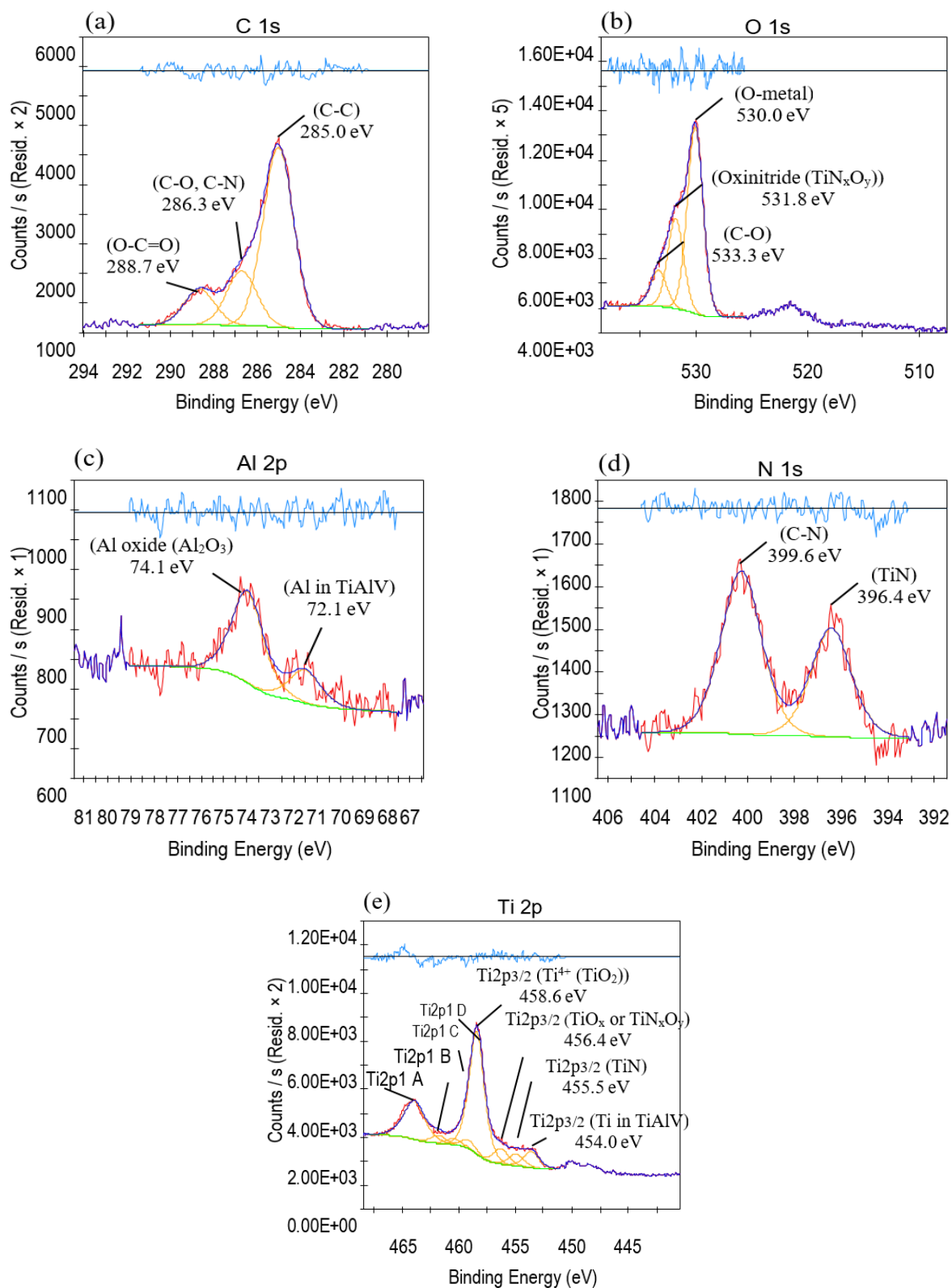
Figure 4-8 : Survey XPS core-levels of Ti-MMC sample

Table 4-2 : High resolution surface chemical composition of Ti-MMC sample

Name	BE	Identification	At. % Ti-MMC
Al	72.1	Al in TiAlV and/or metallic Al	0.6
	74.1	Al oxide (Al_2O_3)	1.5
C	285.0	C-C	24.2
	286.3	C-O, C-N	7.4
	287.3	C=O	
	288.7	O-C=O	4.9
	290.0	-CO_3	
N	396.4	TiN	1.6
	397.1	TiN_xO_y	
	399.6	C-N	
	400.3		2.4
	401.0	Other C-N	
Ti	454.0	Ti in TiAlV	1.2
	455.5	TiN	0.9
	456.4	TiO_x ($2 \leq x \leq 3$) and or TiN_xO_y	1.2
	458.6	Ti^{4+} (TiO_2)	9.4
O	530.0	O-metal	26.6
	531.8	Oxinitride (TiN_xO_y)	12.9
	533.3	C-O	5.2

Al 2p

Figure 4-8 (c) shows the Al 2p spectra. The Al 2p peak has two components. The distinct peak at a binding energy of 74.1 eV, corresponds to Al_2O_3.

The peak at a binding energy of 72.1 eV corresponds to metallic Al (TiAlV) and could come from the underlying metal matrix.

N 1s

The high resolution N 1s spectra (shown in Figure 4-8 (d)) has two separated components, TiN bond at 396.4 eV which probably indicates the formation of small amounts of titanium nitride in the surface film and C-N at 399.6 eV (Variola et al., 2008).

Ti2p

Figure 4-8 (e) shows the Ti 2p spectra. A peak at 454.0 eV correspond to the Ti 2p3/2 of the titanium in TiAlV form, 455.5 eV to TiN, and 456.4 to TiO_x or TiN_xO_y (Moulder et al. 1992).

It can be seen that Ti is mostly present on the surface as Ti^{4+} (the major peak at 458.6 eV). Thus, it can be suggested from the peaks at 458.6 eV and 464.7 eV which correspond to the Ti 2p3/2 and Ti 2p1/2 A, that the surface of the sample was dominated by TiO_2. It strongly agrees with the O 1s spectra analysis. The TiO bond observed at 455.5 eV probably indicates that the oxide film is thin and the electron could escape of this layer (Ask et al., 1989).

V 2p

Despite the high resolution surface chemical composition of Ti-MMC sample, which shows that Al with 0.6 % (relative atomic percentage) and Ti with 1.2% correspond to TiAlV bond, XPS did not detect any vanadium concentration at the outermost surface in survey even in high resolution scan. The vanadium peak (V2p3/2) is expected to reveal at a binding energy between 512 eV and 517.5 eV.

According to the results, the second aluminum peak at 74.1 eV corresponds to Al_2O_3.

The first aluminum peak at 72.4 eV and the first titanium peak at 454. eV correspond to TIAlV. The fourth titanium peak at 458.6 eV and the first oxygen peak at 530 eV suggest the presence of TiO_2. Fist nitrogen peak at 396.4 eV and second titanium peak at 455.5 eV correspond to TiN. Eventually, carbon C-C and O-metal are two main bonds on the surface detected by XPS.

4.2 Carbide TiAlN/TiN coated insert chemical characterization by XPS method

A typical survey XPS spectra of an unused carbide TiAlN/TiN coated sample is shown in Figure 4-9. The dominant signals are C, O, and Ti with weaker contributions from N. Besides, small signals from Ca was observed.

The intensity of different components after peak fitting based on the standard data on the binding energy of the titanium and aluminum oxides and nitrides is presented (Moulder et al. 1992).
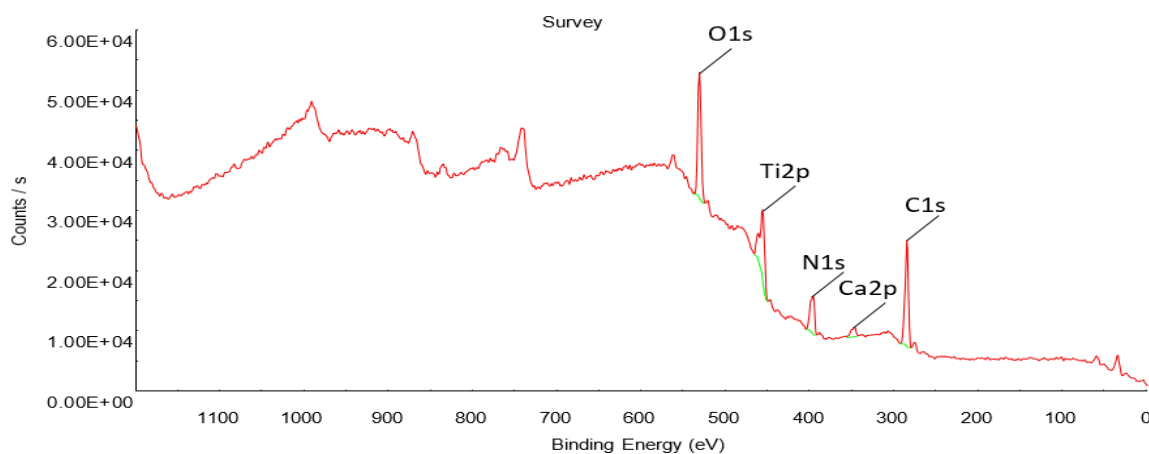
Figure 4-9 : Survey spectra of an unused carbide TiAlN/TiN coated sample

Surface chemical compositions of the survey spectra of insert sample are presented in Table 4-3. The XPS results of carbide sample and the core–level emissions from C1s, O1s, N1s, and Ti2p levels are shown in Figure 4-10.

Photoelectron spectra of insert sample have many interesting features, discussed below:
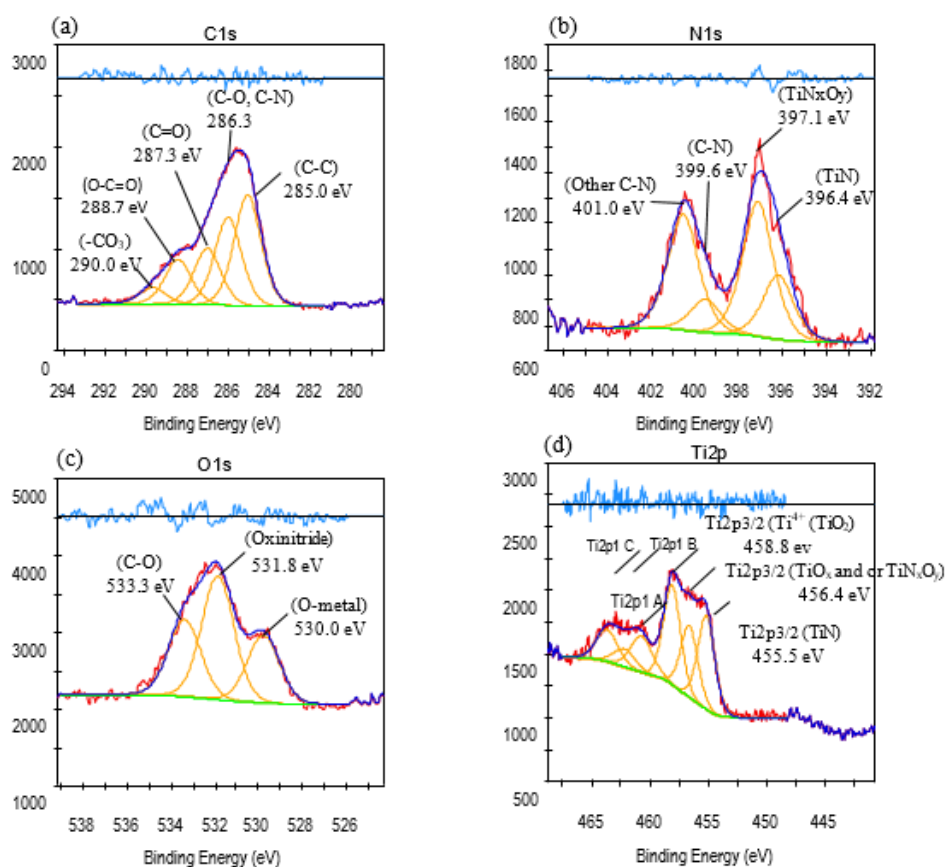
Figure 4-10 : XPS core-levels of insert sample

Table 4-3 : Surface chemical composition of the survey spectra of insert sample

Name	BE	At. %
		Insert
C	285.8	50.2
Ca	348.1	1.0
N	397.8	15.0
Ti	459.0	7.4
O	530.9	26.4

The detailed information about the binding energy of various elements and their bonds are listed in Table 4-4.

Table 4-4 : High resolution measurements to identify the chemical states of the insert main elements with the detailed information about the binding energy of various elements

Name	BE	Identification	At. %
			Insert
Al	72.1	Al in TiAlV and/or metallic Al	-----
	74.1	Al oxide (Al_2O_3)	-----
C	285.0	C-C	17.2
	286.3	C-O, C-N	13.7
	287.3	C=O	8.7
	288.7	O-C=O	6.8
	290.0	$-CO_3$	2.5
N	396.4	TiN	2.8
	397.1	TiN_xO_y	5.8
	399.6	C-N	1.5
	400.3		-----
	401.0	Other C-N	5.0
Ti	454.0	Ti in TiAlV	-----
	455.5	TiN	3.0
	456.4	TiO_x ($2 \leq x \leq 3$) and or TiN_xO_y	2.3
	458.6	Ti^{4+} (TiO_2)	3.2
O	530.0	O-metal	7.0
	531.8	Oxinitride (TiN_xO_y)	12.6
	533.3	C-O	7.9

C1s

In Figure 4-10 (a), the main peak at 285.0 eV assigned to aromatic carbon (C-C) while the peak at 286.3 eV can be assigned to C-O, C–N bond.

O 1s

The spectrum for O 1s is shown in Figure 4-10 (c). It is centered at 531.8 eV (Oxinitride) and peaks at 530.0 eV and 533.3 eV correspond to O-metal and C-O.

Ti 2p

Ti 2p XPS spectra of the sample are shown in Figure 4-10 (d). The Ti2p peak separates into

Ti $2p_{3/2}$ (458.8 eV) and Ti $2p_{1/2}$ (464 eV). It can be seen that Ti^{4+} is dominant on the surface.

As mentioned above, the binding energy of Ti $2p_{3/2}$ is 458.6 eV in the sample and there should be many oxygen defects on the film surface which imply that a layer of TiO_2 formed on the surfaces (Moulder et al. 1992).

N 1s

N 1s XPS spectra of the sample are shown in Figure 4-10 (b), indicating two major peaks at 397.1eV related to TiN_xO_y bond and at 401.0 eV related to C-N bond. TiN bond at 396.4 eV and another C-N bond at 399.6 eV are detected.

Detection of TiN bond on the surface implies that the outermost coated layer might be TiN and TiAlN layer is under it.

Co $2p_{3/2}$

The XPS peaks of cobalt could have appeared at 778.1 eV but due to the presence of cobalt in the substrate of the insert as binder, XPS could not detect it.

Ca 2p

A small amount of calcium was detected by XPS at 348.1 eV which probably corresponds to the ionic compound of calcium and chlorine $CaCl_2$. It is a kind of salt highly soluble in water and here could be a contamination or the samples might be touched by a human body (Atnafu, 2013).

Al 2p

In survey scans, aluminum was not revealed even in high resolution scans which means that the concentration is less than 0.1% and could not be detected by XPS. The most intense of the Al peak (Al 2p) is expected to be at a binding energy 74.4 eV as Al_2O_3 bond. It might be due to the TiO2 layer on the surface that the electron could not escape depth. Other possibility is that the TiAlN coated layer could be under the TiN coating and XPS is not able to detect it. This is powered by the Ti 2p and N 1s spectra which show that TiN was detected in Ti 2p spectrum at 455.5 eV and in N 1s spectrum at 396.4 eV.

4.3 Ti-MMC chemical characterization with EDS

Two SEM micrographs of an unpolished Ti-MMC sample is shown in Figure 4-11 (a) and (b). The diameter of a TiC particle was measured and it was 2.3 µm. Also, the elemental mapping of the distributions and relative proportions (intensity) over the scanned area are demonstrated in Figure 4-11 (c).
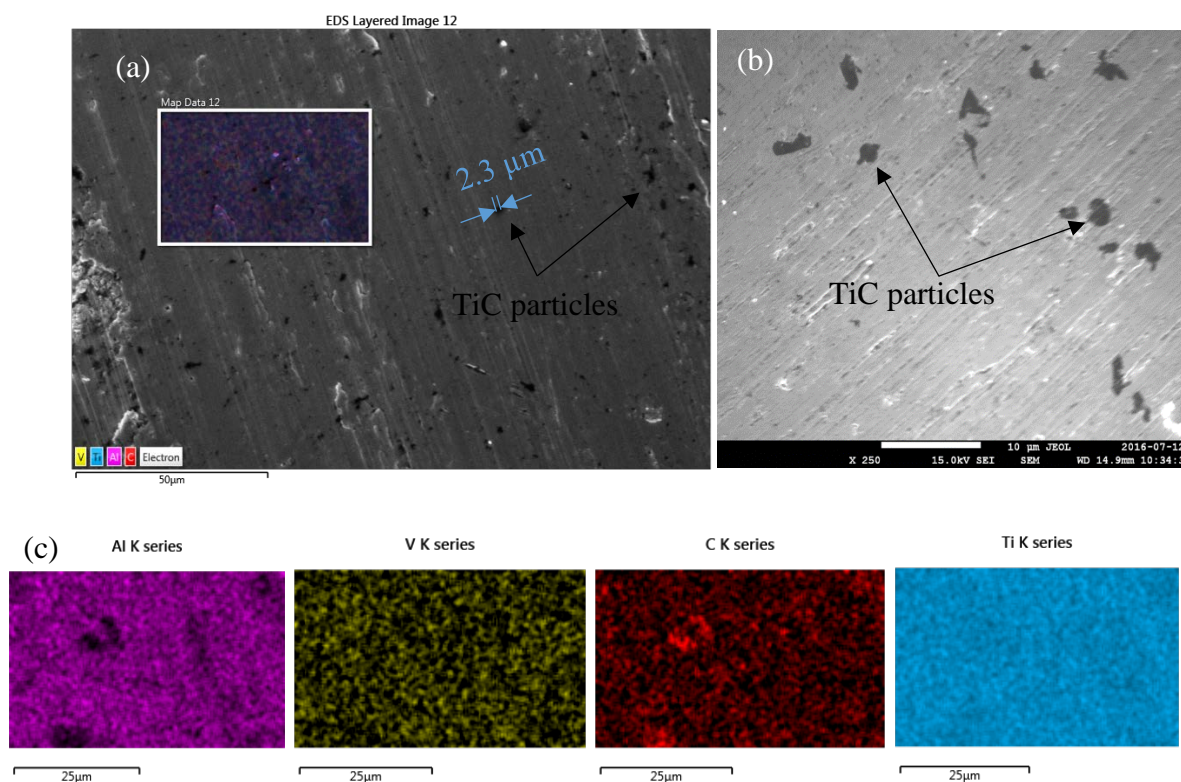
Figure 4-11 : (a) SEM micrograph of an unpolished Ti-MMC sample the TiC particles dispersed into the material are specified, (b) higher magnification of the surface and TiC particles (c) mapping of different chemical composition of Ti-MMC sample

EDS revealed that the elements in chemical composition of the sample are: titanium (Ti), aluminium (Al) and vanadium (V) that belong to the matrix material (Ti-6Al-4V) and carbon (C) that probably belongs to TiC particles.

Below, the corresponding EDS spectrum of the selected scan area of the sample (shown in Figure 4-11 (a)) is presented.

As it is observed and was expected as well, the dominant elements in chemical composition of the selected surface are: 88.5% titanium (Ti), 5.6% aluminum (Al), 3.7% vanadium (V), that are the constituent components of Ti-6Al-4V matrix and 2.2% carbon (C) belongs to TiC particles as reinforcement in Ti-MMC.
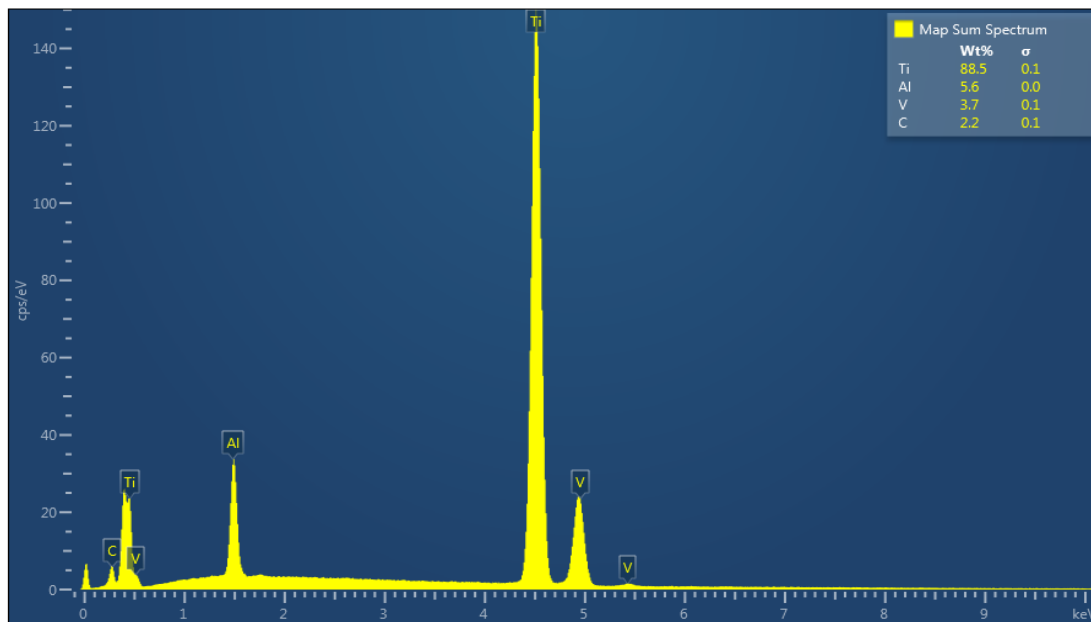
Figure 4-12 : EDS analysis on the surface of the sample which was shown in Figure 4-11 (a). The elemental chemical compositions of Ti-MMC sample were obtained with the element content table

4.4 Carbide TiAlN/TiN coated chemical characterization with EDS

Two micrographs of a brand new carbide tool flank face, and an EDS elemental mapping of a selected surface on flank face are shown in Figures 4-13 and 4-14.

The results show tool elements such as: titanium (Ti), nitrogen (N), and aluminum (Al) which typically exist in tool surface and tungsten (W) and cobalt (Co) refer to the substrate of the insert (as mentioned earlier, the insert is a TiAlN/TiN coated WC/Co).

Some constituents of the tool material such as: titanium (Ti), carbon (C) and aluminum (Al), frequently exist in the both of work-piece and tool material and just vanadium (V) exists in work-piece material.
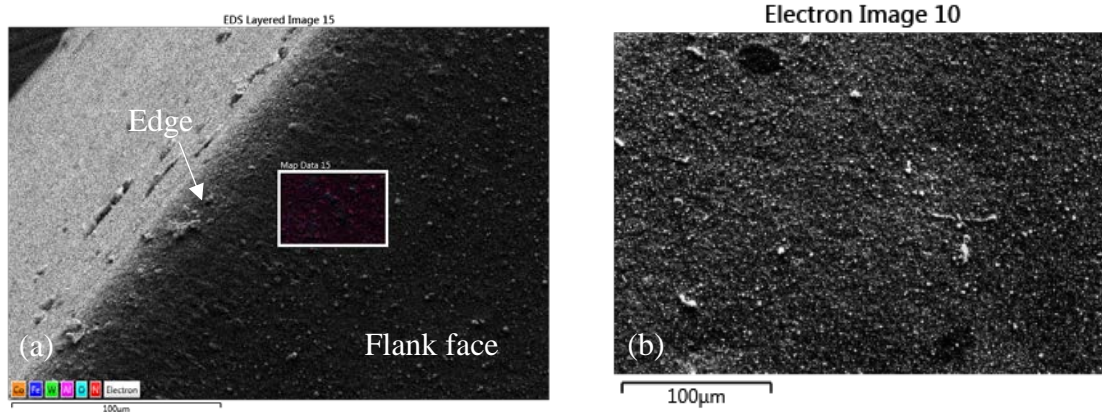
Figure 4-13 : SEM micrographs of the flank face of an unused carbide tool. (a) An area of flank face near the edge was selected for EDS elemental mapping analysis (b) another image of the insert surface showing the external coated layer
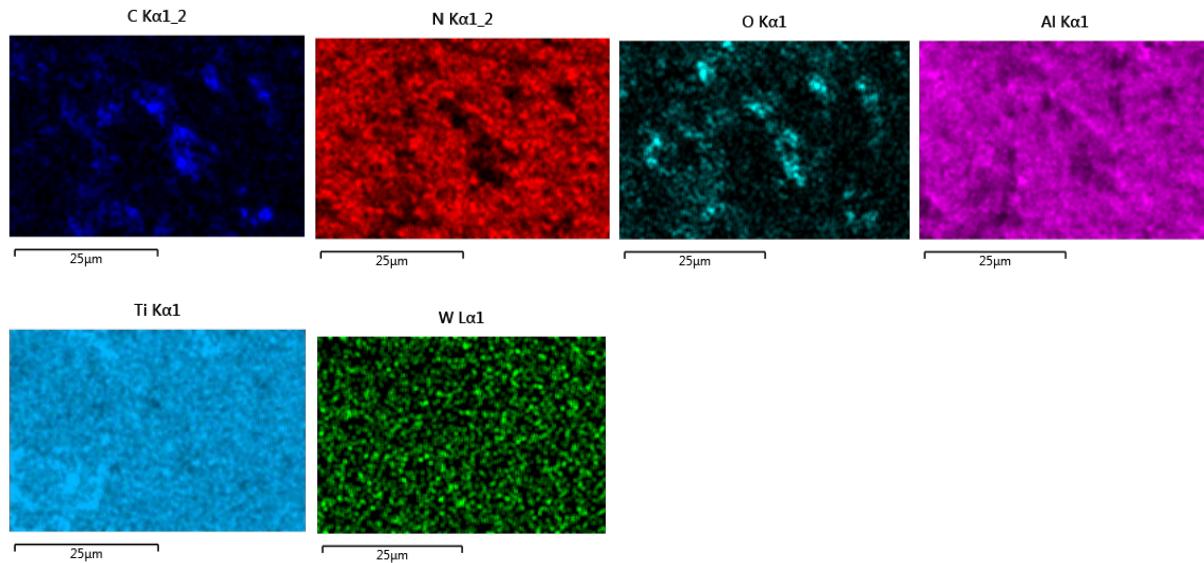
Figure 4-14 : EDS elemental mapping analysis of an unused insert

Figure 4-15 shows the results of EDS analysis of a selected surface of an unused tool. It can be seen that very small amounts of tungsten (W) and cobalt (Co), were detected on the surface. Moreover, quantitative EDS analysis revealed that titanium with (46.7%), nitrogen (N) 23.5%, aluminum (Al) 16.9%, oxygen (O) 9%, and carbon (C) with 3.6% are the tool composition.
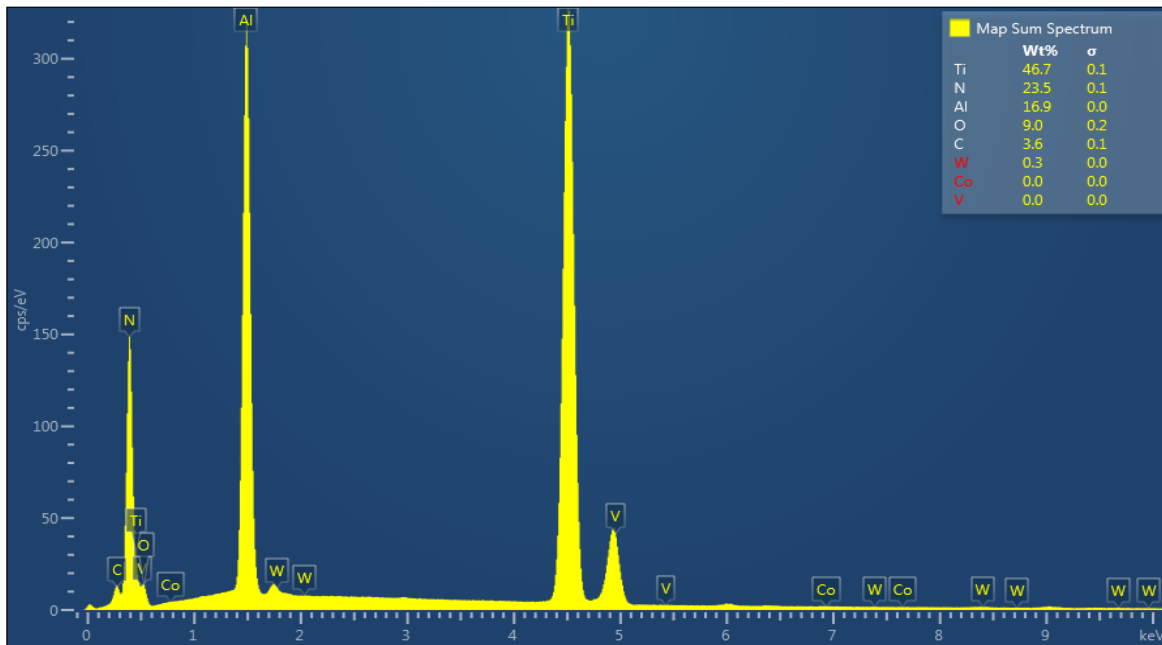
Figure 4-15 : EDS spectra of a selected area on flank face of an unused insert, shown in Figure 4-13 along with the element content table

4.4.1 SEM/EDS analysis of an insert with cutting time 0.5 second

A photo and two SEM micrographs of flank face after 0.5 second of machining are shown in Figure 4-16.

It is suggested that due to TiC particles being pulled out of the work-piece and getting pulled on the machined surface, the scraches and grooves were emmerged at the flank face of the tool. Other possibilty is that since this is a coated tool, the harder coating particles might disintegrate and etch the tool surface.

The EDS elemental mapping (Figure 4-17 (c)) revealed the initial step of wear mechanism where work-piece material on the wear land starts to wear off the cutting edge exposing the substrate beneath.

After 0.5 second of machining (shown in Figure 4-17) there are small amounts of vanadium (V) in V K series and titanium (Ti) in Ti K series on the surface (Zone 2). It should be noted that in an elemental mapping spectrum, brighter concentration represents higher concentration of the element at the location.
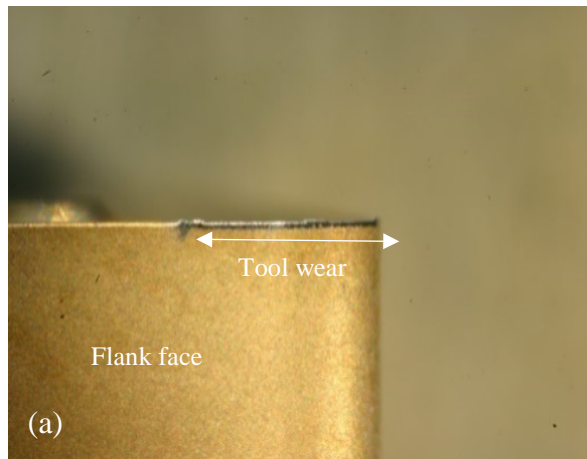
Process parameters:

 Machining time = 0.5 Second

Cutting speed Vc = 50 m/min

Feed rate f = 0.15 mm/rev
Depth of cut a_P = 1.5 mm

Material: Ti-MMC

Cutting tool: Carbide TiAlN/TiN coated
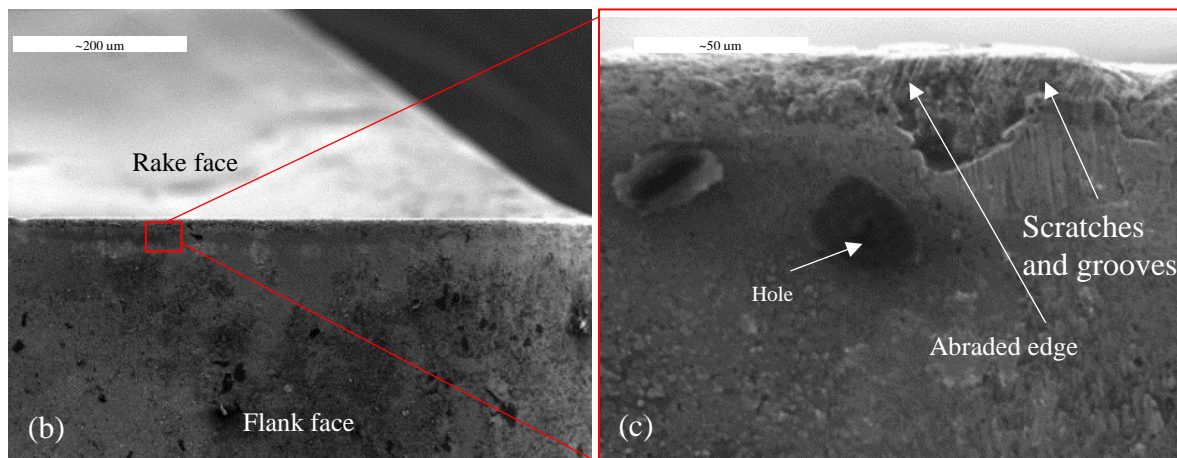
Figure 4-16 : A photo and SEM images of flank face; (a) photo of flank wear and tool wear region (b) SEM micrograph of flank face (c) enlarged micrograph of (b) shows two holes and vertical scratches caused by TiC particles and abrasive wear

Furthermore, the deposition of material can be seen in N K series with a lower concentration of nitrogen at the deposited material. It is suggested that these elements belong to Ti-MMC matrix (Ti-6Al-4V) transferred from the work-piece material.

Also, the orange colored tungsten (W) in W M series and green colored cobalt (Co) in Co K series (brighter color) which were revealed mostly on the edge represent the substrate elements (Zone 1). Furthermore, the region near the cutting edge (Zone 1) implies that the abrasive wear of insert starts near the cutting edge.
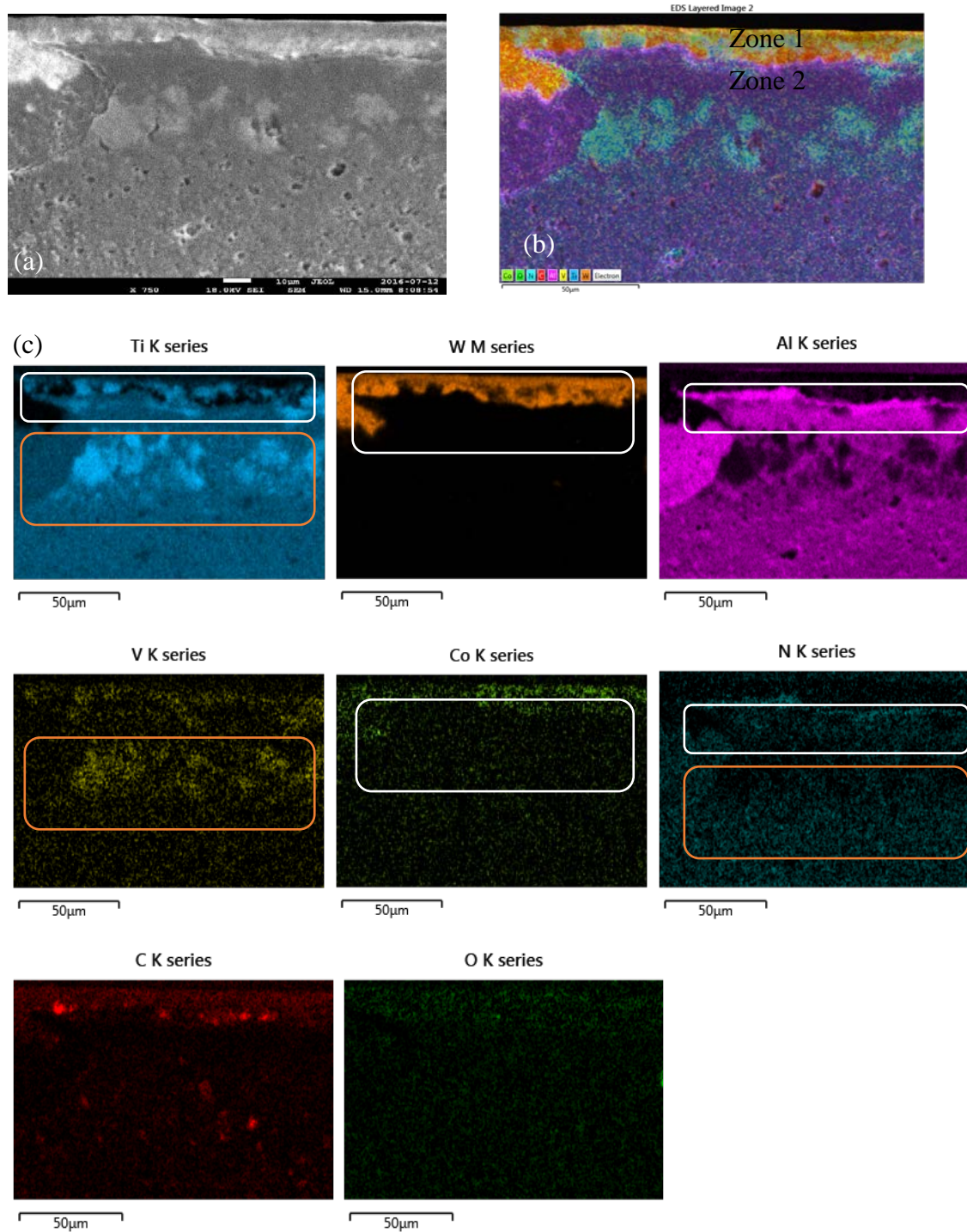
Figure 4-17 : (a) SEM micrograph of an insert with 0.5 second of machining shows two different zones in the surface. (b) An EDS layered image of the composition of the worn out surface (c) EDS mapping analysis of SEM micrograph (a) shows that there are small amounts of vanadium (V) in V K series and titanium (Ti) in Ti K series

The orange colored tungsten (W) in W M series, and green colored Co in Co K series (brighter color) which were revealed mostly on the edge represent the substrate elements as well.

Also, a color change along the width of worn-out edge (shown in Figure 4-17 (a) and zone 1 (b)) might be due to the removal of the coating.

Eventually, in N K series, Al K series and Ti K series a small narrow brighter region can be the TiAlN coated layer of insert revealed due to abrasion wear.

In Figure 4-17 (b) and (c) the variations in elemental composition of the sample are shown. Aluminum (Al), titanium (Ti), nitrogen (N), and tungsten (W) seem to be the main constituents with small amount of oxygen (O) carbon (C), and very small amounts of vanadium (V) and cobalt (Co) were detected.

The corresponding chemical compositions detected by EDS are presented in Figure 4-18.
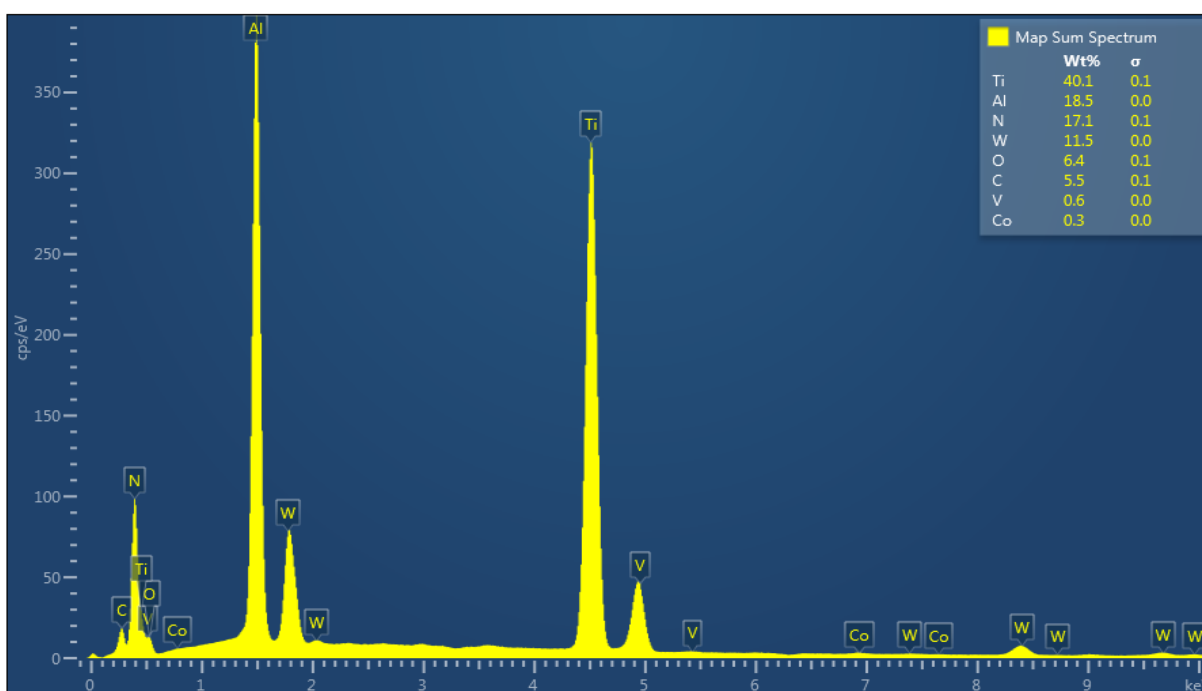
Figure 4-18 : An EDS spectrum of the insert with cutting time 0.5 second along with the element content table

The results show the elements such as: oxygen (O), and nitrogen (N) which typically exist in tool surface and titanium (Ti), carbon (C) and aluminum (Al), frequently exist in both the work-piece and tool material. Also, tungsten (W), cobalt (Co), refer to carbide substrate.

4.4.2 SEM/EDS analysis of an insert with cutting time 1 second

A photo and two SEM micrographs of flank face after 1 second of machining are shown in Figure 4-19.

Process parameters:

Machining time = 1 Second

Cutting speed Vc = 50 m/min

Feed rate f = 0.15 mm/rev
Depth of cut a_p = 1.5 mm

Material: Ti-MMC

Cutting tool: Carbide TiAlN/TiN coated

Figure 4-19 : A photo and SEM micrographs of flank face; (a) a photo of flank face and tool wear region (b) SEM micrograph of flank face; a micro fracture is shown (c) highly magnified flank face shows some holes and scratches probably caused by TiC particles and a smooth adhered layer which has covered the scratches and grooves. Moreover, the original edge of the insert has been chamfered after 1 second of the start of machining

The EDS elemental mapping of the sample are shown in Figure 4-20. It can be seen that a layer of Al starts to be shaped between two layers of Ti. As it was shown earlier in Figure 4-4, the first transition time is around 1second after machining.

In Figure 4-20 (b) and (c) the variations in elemental composition of the sample are shown. Aluminum (Al) and titanium (Ti), seem to be the main constituents with small amount of nitrogen (N), oxygen (O) carbon (C), and vanadium (V). Very small amounts of tungsten (W) were detected.
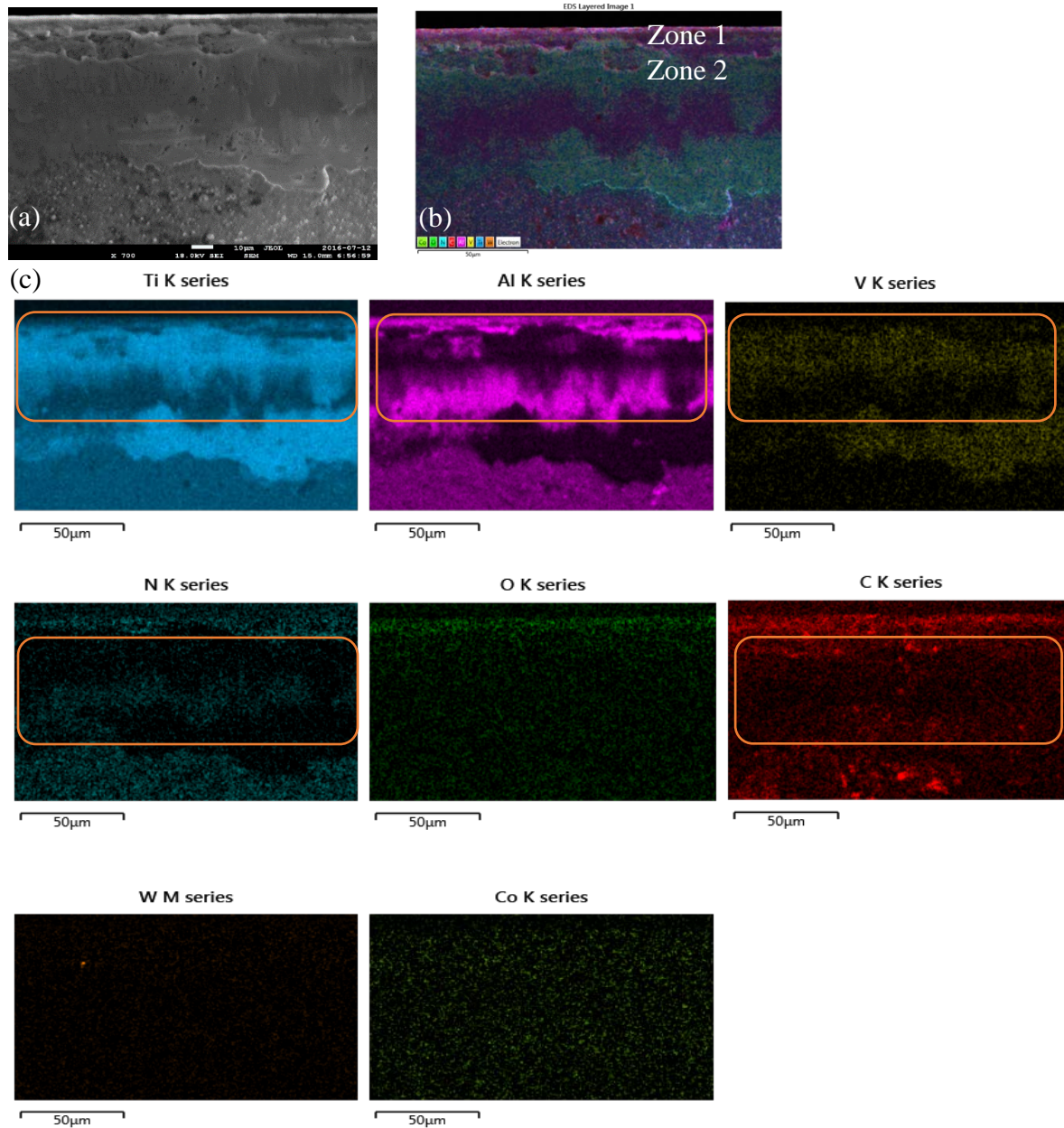
Figure 4-20 : (a) SEM micrograph of an insert after 1 second of machining having a butter spread appearance adhered layer (b) An EDS layered image showing the different compositions of the worn surface showing two different zones in the surface(c) EDS mapping analysis of SEM micrograph (a)

Another different characteristic of flank wear is observed at Zone 1 in Figure 4-20 (b). The abraded edge was covered by an Al-enriched layer.

The presence of Ti and also V (which only exists in the matrix of the work-piece material

Ti-6Al-4V) in the deposited layer (zone 2) implies that these materials were transferred from the work-piece to the tool.

There are not any evidence of tungsten and cobalt which had been revealed in the sample with 0.5 second of machining. The concentration of C in the zone 1 increased as shown in C K series and implies that probably carbon is being chemically-pulled out of the tool (WC/Co insert) due to a chemical-potential.

Other possibility is that since the concentration of carbon in zone 1 (Figure 4-20 (c) C K series) has increased being in the same direction of work-piece rotation and the first region in contact with work-piece, the TiC particles were deposited in this zone.

The corresponding chemical compositions of the worn flank face (Figure 4-20 (a)) detected by EDS are presented in Figure 4-21.

Figure 4-21 : An EDS spectrum of the insert with cutting time 1 second along with the element content table

The correlation between the tool wear progression and cutting force before the first second of machining will be discussed in section 4-5.

4.4.3 SEM/EDS analysis of an insert with cutting time 1.5 seconds

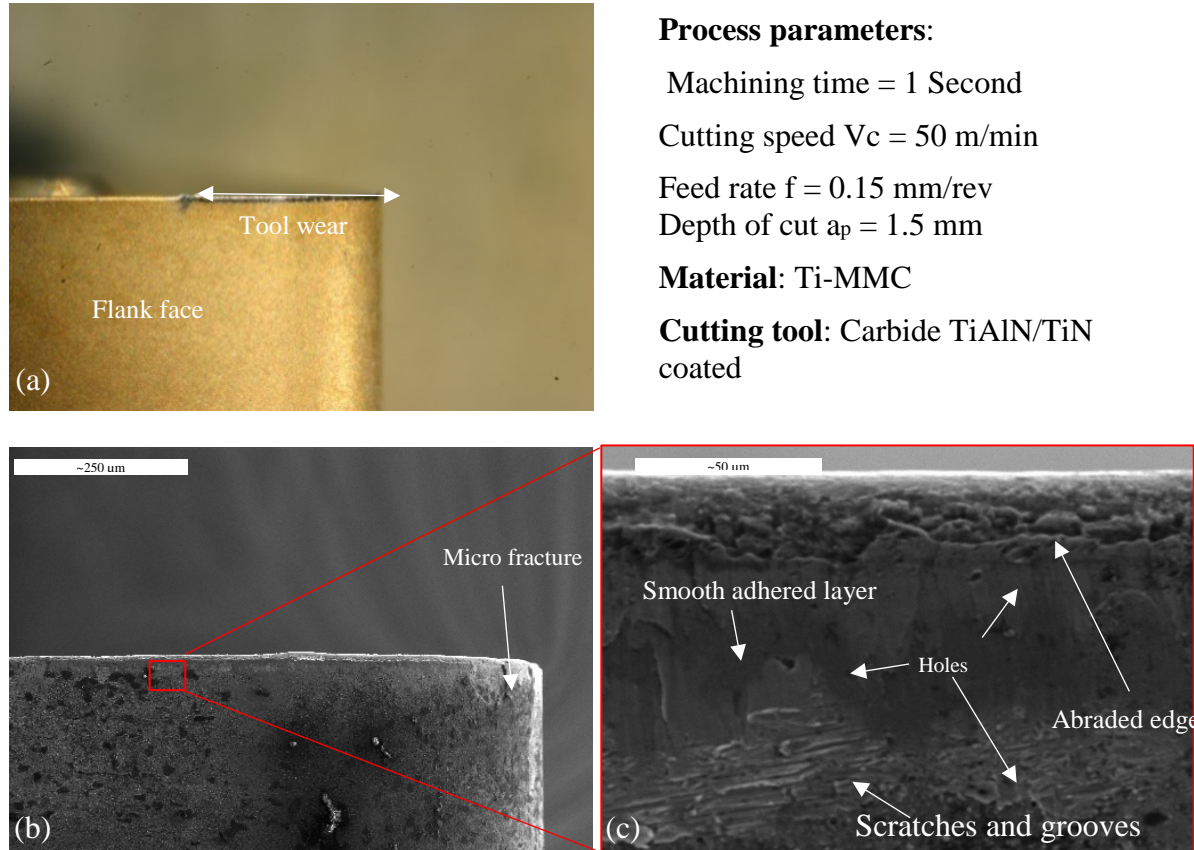A photo and two SEM micrographs of the flank face after 1.5 seconds of machining are shown in Figure 4-22.

The SEM micrographs (Figures 4-22 (b) and (c)) show clearly that the deposited materials smear on the flank face and the thin adhered layer has the appearance of spread butter.

Process parameters:
Machining time = 1.5 Seconds

Cutting speed Vc = 50 m/min

Feed rate f = 0.15 mm/rev

Depth of cut a_p = 1.5 mm

Material: Ti-MMC

Cutting tool: Carbide TiAlN/TiN coated
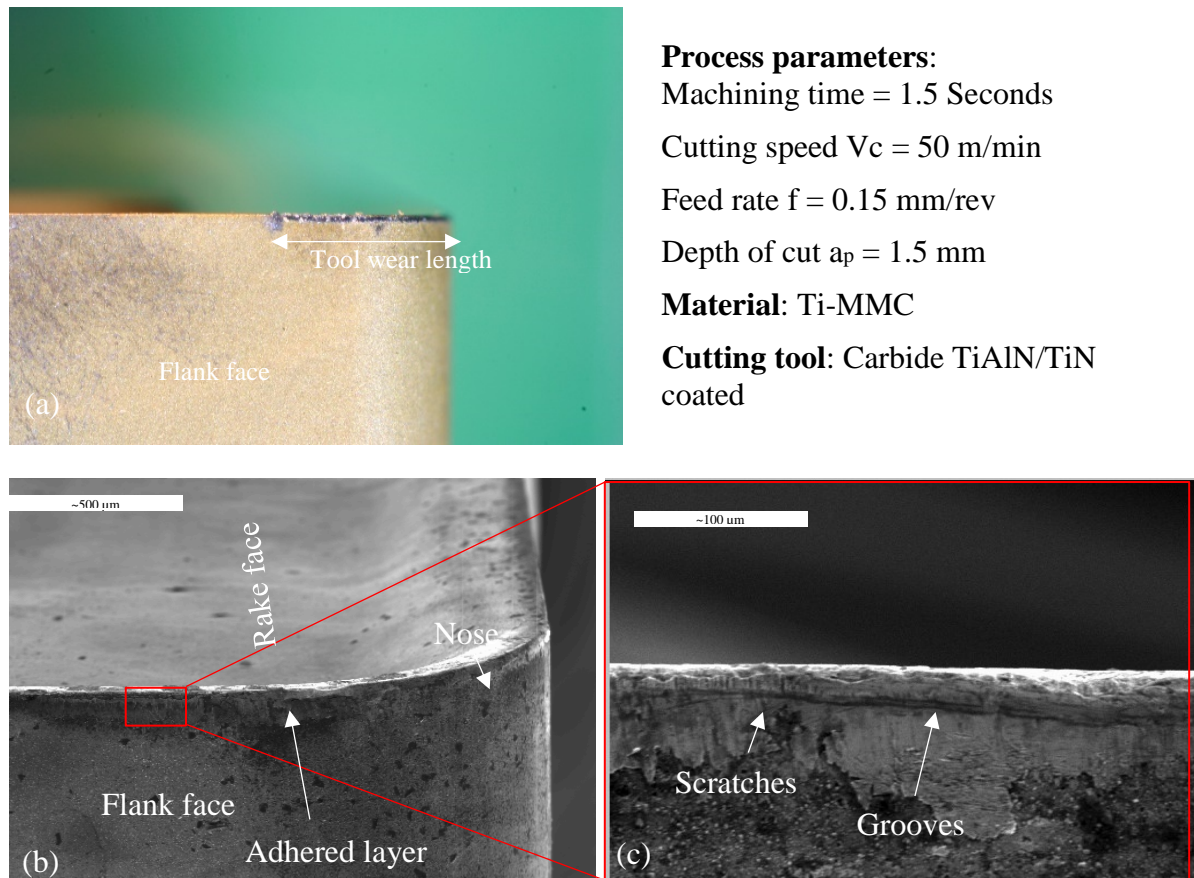
Figure 4-22 : A photo and SEM micrographs of flank face; (a) photo of flank wear and tool wear region (b) SEM micrograph of flank face, and adhered layer observed on flank face near the nose (c) highly magnified flank face shows scratches and grooves caused by TiC particles

In Figure 4-23 (b) and (c) the variations in elemental composition of the sample are shown. Aluminum (Al), titanium (Ti), and nitrogen (N) seem to be the main constituents with small amount of oxygen (O) carbon (C), and vanadium (V). Very small amounts of tungsten (W) and cobalt (Co) were detected.

The elements deposited on the wear zones (Zone 1 and 2), are suggested to be the Ti-6Al-4V transferred from the work-piece material.

Also, the abrasive wear mechanism traces as the carbide substrate materials W and Co (in

Zone 1) were covered with a thin adhered layer.

(a) 1.1 µm

(b) EDS Layered Image 9
Zone 1
Zone 2

(c) Ti K series | Al K series | N K series

O K series | C K series | V K series

W M series | Co K series
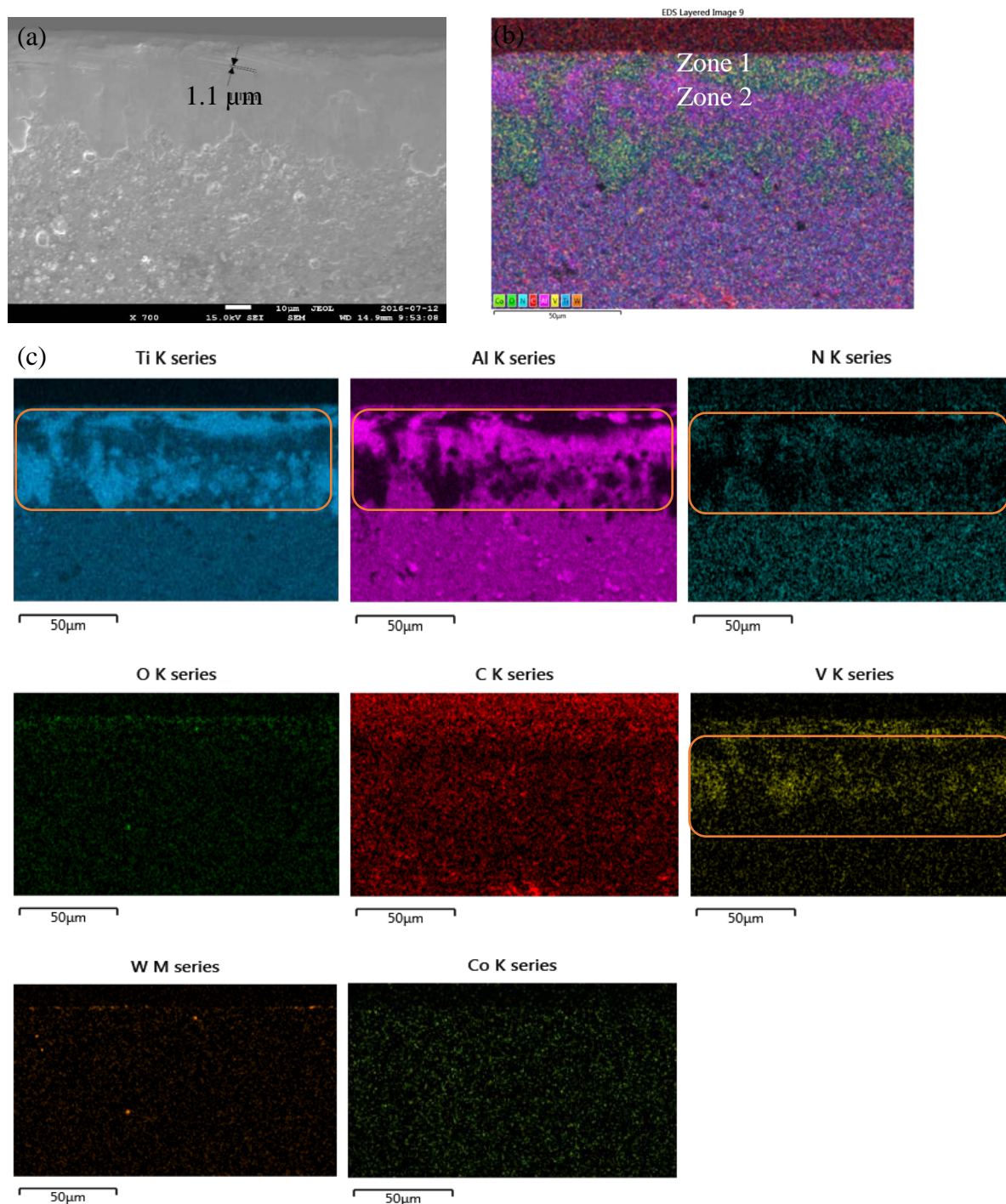
Figure 4-23 : (a) SEM micrograph of the sample at 700 X magnification. A groove diameter was measured and equals to 1.1 µm. (b) An EDS layered image showing the different compositions of the worn surface. (c) EDS mapping analysis of SEM micrograph

The corresponding chemical compositions of the worn flank face (Figure 4-23 (a)) detected by EDS are presented in Figure 4-24.

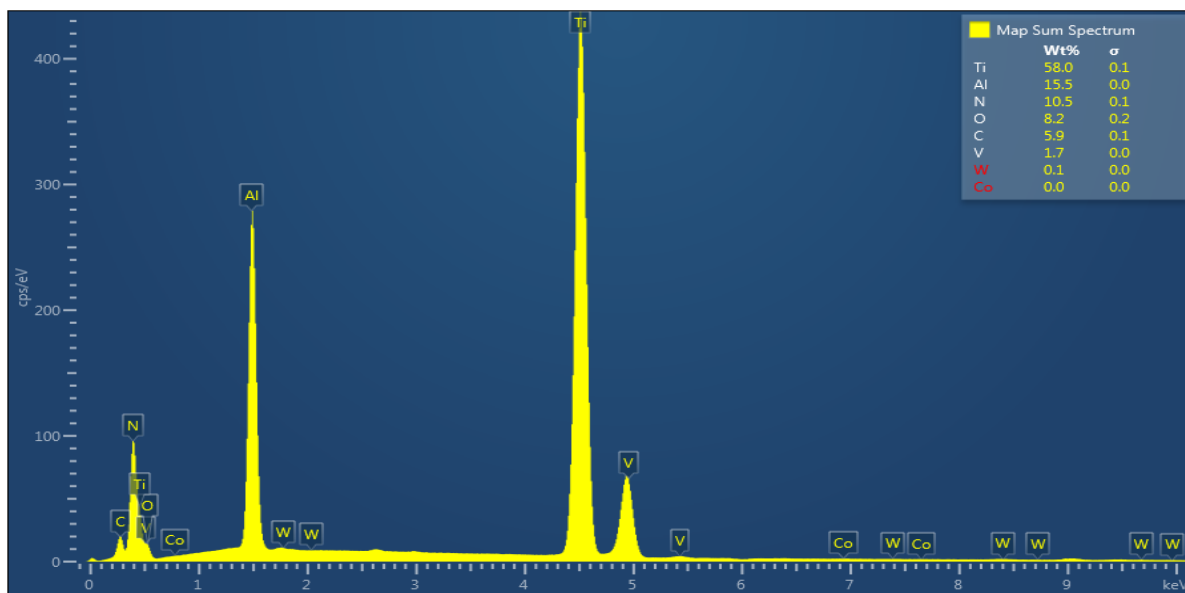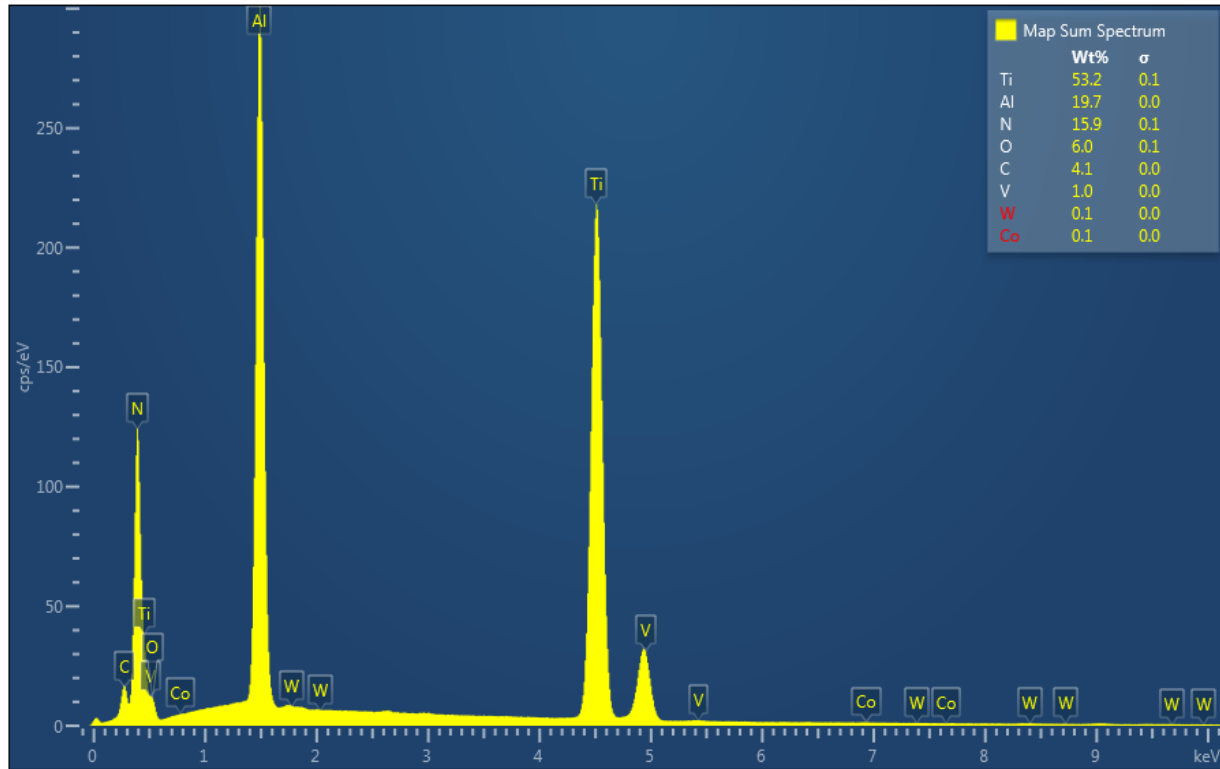Figure 4-24 : An EDS spectrum of the insert with cutting time 1.5 seconds along with the element content table

4.5 Cutting the tool

To find out what exactly happens during the first transition period, an insert that had machined two seconds a cylindrical Ti-MMC at a speed of 50 m/min and feed rate of 0.15 mm/rev was cut off by a diamond cut-off saw, as shown in Figure 4-25 (a) and (b). To have a better understanding, in Figure 4-25 (c) a schematic picture of cut-off surfaces and the worn out area are shown.

Two SEM micrographs of a cut-off sample are shown in Figure 4-26 (a) and (b).

These figures are related to the cross-sectional view of the cut-off surface, the layer containing coated and adhered sub-layers is quite distinct from the other part. Although the sub-layers were not distinctly detected and the thickness of adhered layer could not be measured separately, but the thicknesses of the complete sub-layers containing adhered and coated were measured. The difference between the coating thickness (10.7 µm) and thickness of the adhered and coated layer in the interact region with work- piece is interesting (7.4 µm).

Based on these measurements, it could be suggested that the contact region with work-piece has a smaller thickness than coated layer which means most of the coating is abraded after 2 seconds of machining. In other words, the adhesion of the work-piece material on the tool surface is lower than the removal of material from the insert.
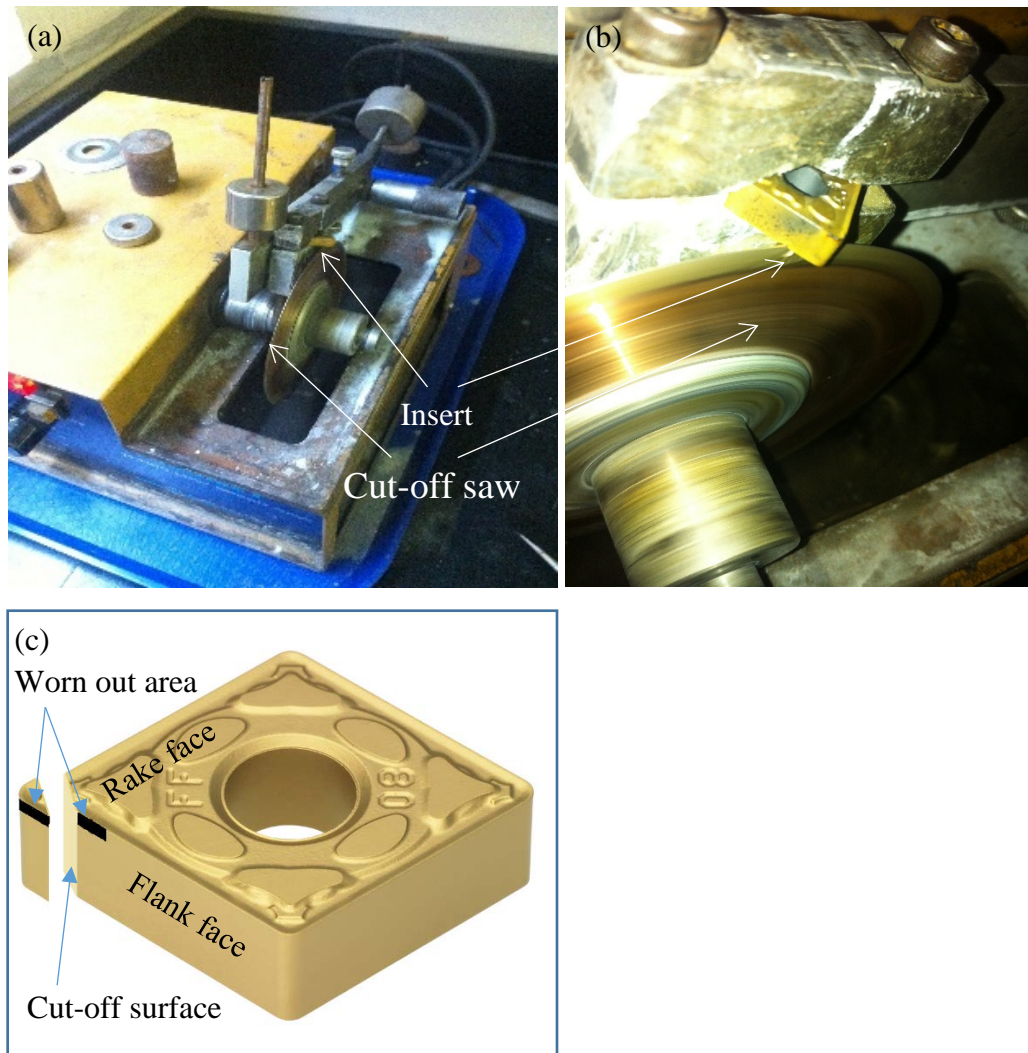
Figure 4-25 : (a) Cutting the tool with a cut-off saw (b) closer picture (c) schematic picture of cut-off tool and the surfaces

To find the chemical composition of the adhered layer and the coating, an EDS elemental mapping analysis was performed (shown in Figure 4-27).
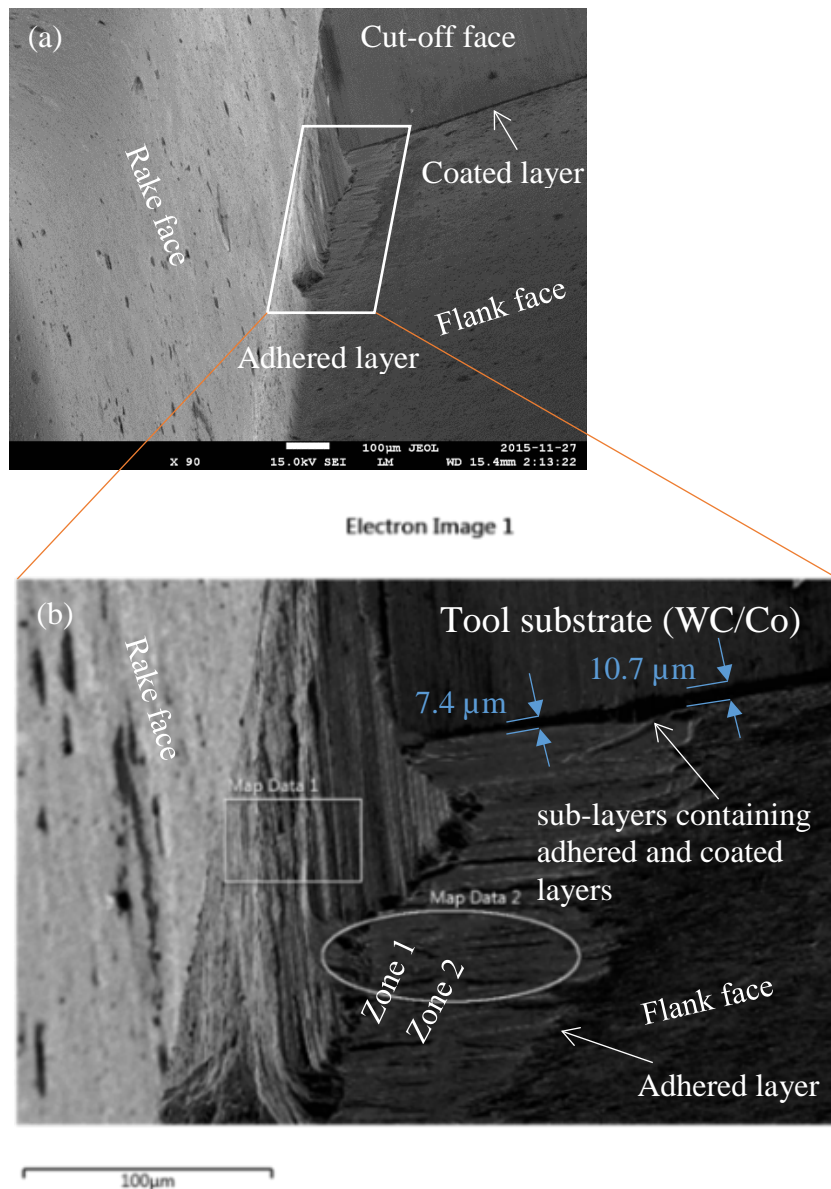
Figure 4-26 : (a) A SEM micrograph of flank and rake face. Sub-layers containing adhered and coated layers were observed (b) another image with higher magnification. The average coating thickness, outside of contact region with work-piece is about 10.7 µm and the inside is 7.4 µm. Also, it can be seen that zone 1 is fully covered by the adhered layer

The brighter color in Figure 4-27 Al kα1 and Ti kα1 which means a higher concentration of this element clearly shows the chemical composition of the layer and the difference between the thickness of the inside and outside of the interact region but does not distinguish the elements of the sub-layers precisely.
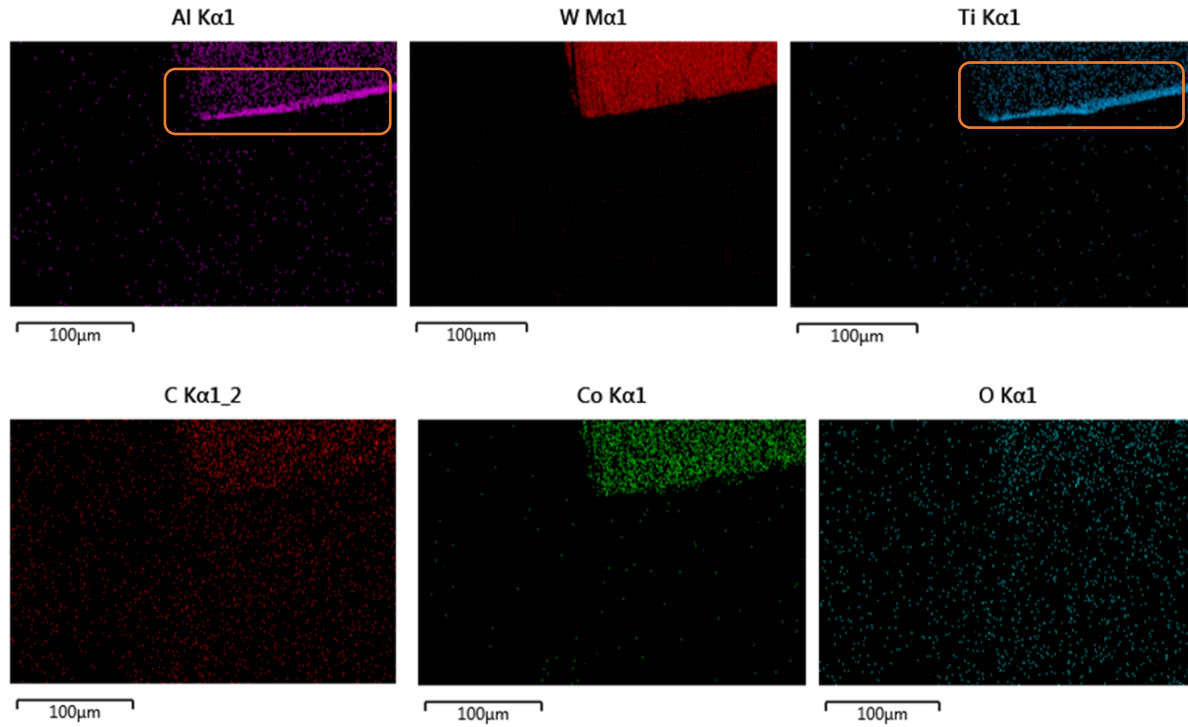
Figure 4-27 : An EDS elemental mapping analysis of the cut-off insert (shown in Figure 4-26 (b))

EDS elemental mapping analysis on the cut area (Figure 4-27) reveals WC/Co substrate of the insert which contains tungsten and cobalt as binder.

Moreover, the small amounts of titanium (Ti) and Aluminum (Al) were detected on the WC/Co substrate may possibly be due to physical contact of the diamond saw with the cut-off surface and pulling out the material from the coated layer toward the substrate.

4.6 Focused ion beam (FIB)

Immediately after applying the FIB technique to remove a cross-sectional part in rake face, the samples were analysed. An SEM micrographs of the rake face of the insert with the mentioned machining process parameters are shown in Figure 4-28.

In comparison with cutting off the insert, the FIB technique removes the materials in a process called sputtering. In this process, materials are removed delicately, without any trace of the remaining material like Ti on the substrate surface that was observed after cutting the tool with a cut-off saw.
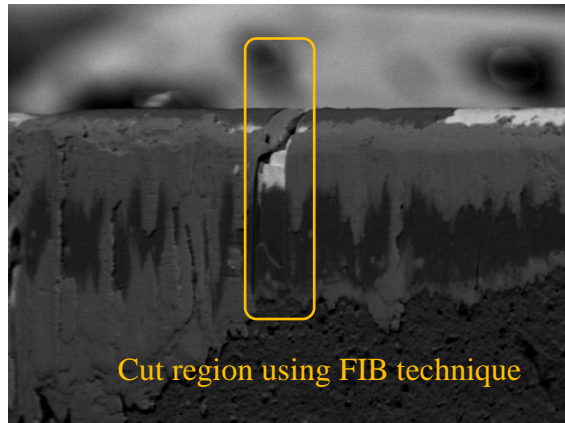
Process parameters:
Machining time = 4 Seconds

Cutting speed Vc = 50 m/min

Feed rate f = 0.15 mm/rev

Depth of cut a_p = 1.5 mm

Material: Ti-MMC

Cutting tool: Carbide TiAlN/TiN coated

Figure 4-28 : The SEM micrographs of flank face of an insert after 4 seconds of machining. The FIB cut region and butter spread appearance of the adhered layer are shown

Three SEM micrographs of the rake face having the cut section are shown in Figure 4-29.
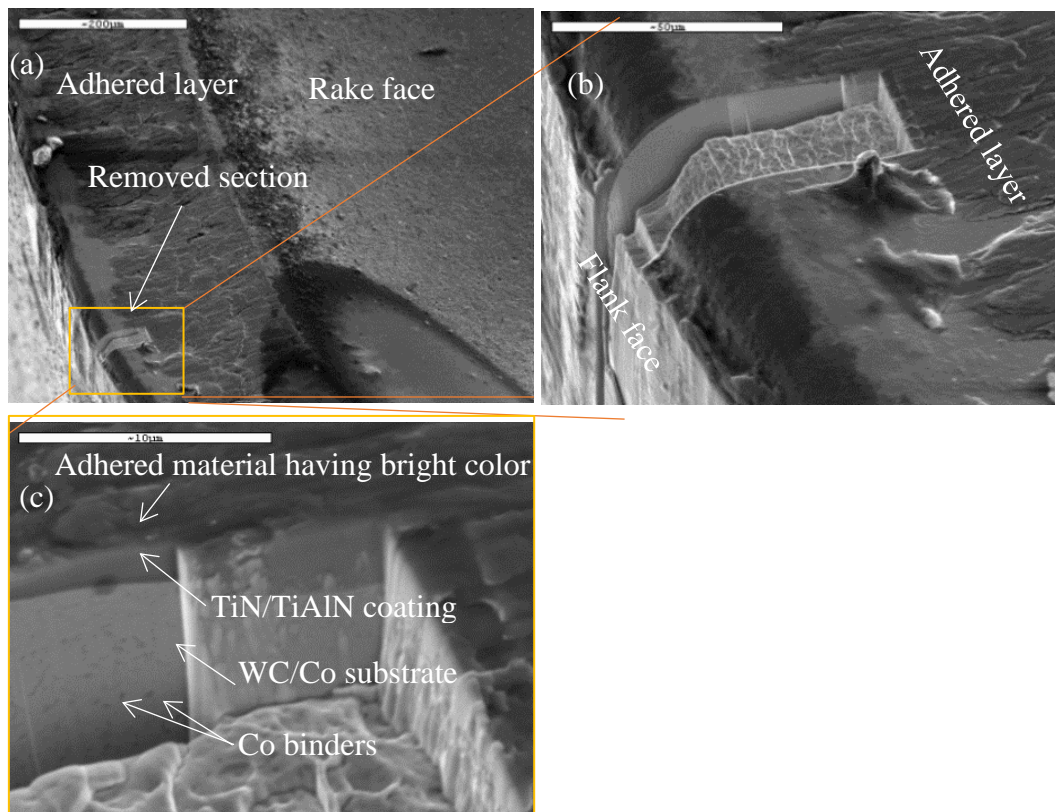
Figure 4-29 : SEM micrographs of rake face; (a) micrograph of rake face having the cut section; (b) higher magnification of SEM micrograph of removed section; (c) highly magnified rake face showing different layers of thin adhered (with brighter color in comparison with the coating) and coated layers. Also, Co binders in the WC/Co substrate are shown

It can be seen in Figure 4-30 that two layers with different color of adhered and coated layers are revealed. Also, Co binders in the WC/Co substrate are clearly distinct.

A typical line scan conducted on the cross-section is shown in Figure 4-30. The graph shows the distribution of various elements across the surface in terms of mass percent.
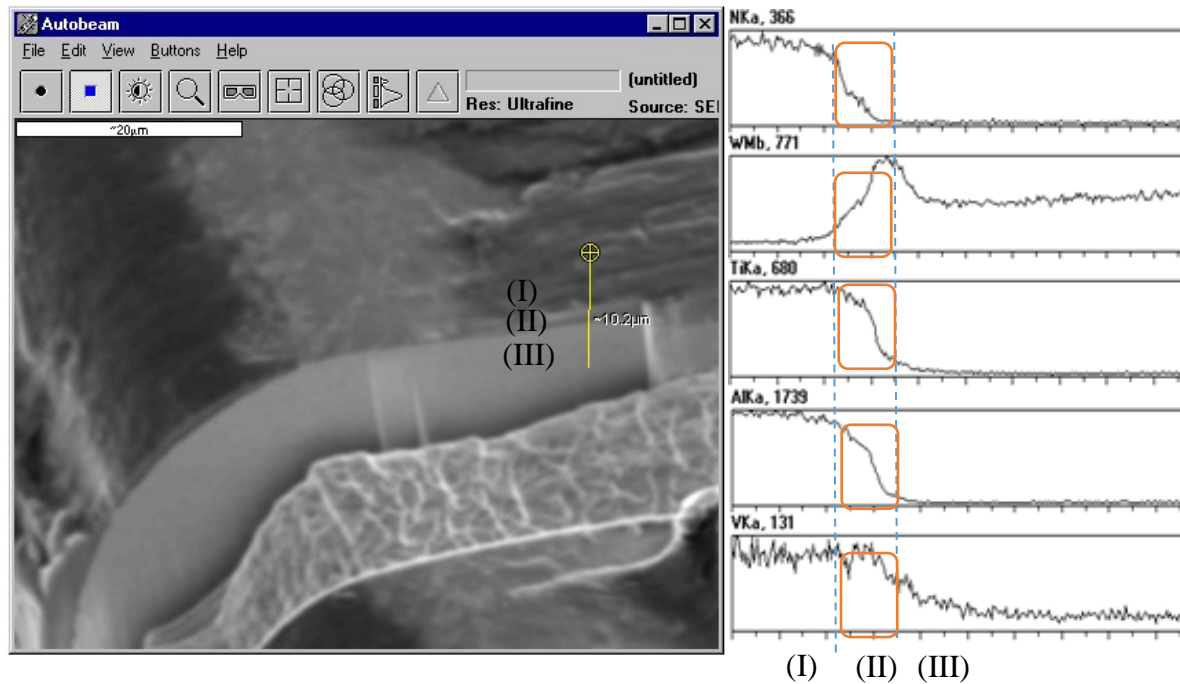
Figure 4-30 : Line scan analysis of FIB sectioned wedge

Line scan analysis shows the mass percent of titanium, nitrogen, and aluminum in the region II have dropped in, inversely proportional to the mass percent of tungsten.

The higher concentration of Ti and N on the region I and W on region II shows the presence of a coating layer on the tool substrate.

The line scan analysis also revealed the presence of vanadium in regions I and II, which is assumed to be a part of the transfer of the work-piece matrix suggesting the material adhesion.

In short, from the outermost layer to the center of the insert, the distribution is: region I with N, Ti, Al, and V and then region II, which the amounts of Al, Ti, and N are decreasing while V appear to be constant and further, region III enriched with W and small amounts of V.

It is interesting to note that W, slightly increases in region II while the amounts of V are constant. It is suggested that there is a mixture of work-piece material components and cutting tool material constituents.

CHAPTER 5   DISCUSSION

The results of experiments, described in the previous chapter are presented and discussed here.

First, XPS analysis of a Ti-MMC sample as work-piece and an unused WC/Co PVD coated with TiAlN/TiN as the insert are compared with their EDS results. Next, the results of EDS on worn-out flank face during the initial moments of machining are presented. Then, the cutting force and its relation to the initial tool wear progression are presented. Finally, based on all previous results the initial wear mechanisms are discussed.

5.1 Comparison of XPS and SEM/EDS analyses

XPS analysis of the Ti-MMC sample shows that the dominant signals are associated with: O, Ti and C, with weaker contributions of N and Al (Table 4-2). Also, the chemical states which were detected through the high resolution scan are: C-C, TiO, TiN_xO_y, TiO_2, C-O, C-N, TiAlV, Al_2O_3, and TiN (Table 4-2).

For the insert sample, the dominant signals detected through the XPS analysis are: C, O, and Ti with weaker contributions of N (Table 3-3). Moreover, the chemical states detected with high resolution scan are: C-C, C-O, C-N, Oxinitride (TiNxOy), O-metal, TiO2, and TiN (Table 4-4).

EDS analysis of Ti-MMC sample revealed that the elements in chemical composition of the sample are: Ti, Al and V that are the constituent components of Ti-6Al-4V and C that probably belongs to TiC Particles Figure 4-12).

For the insert sample, the EDS analysis demonstrated tool elements such as: Ti, N, and Al which typically exist in tool surface and W and Co which exist as the substrate of the insert (Figure 4-15).

As it is well-known, EDS method is able to detect the surface elements in the range of 0.1 µm to 5 µm, whereas XPS is a surface sensitive technique and probes the material to a depth of maximum 5 to 10 nm. Also, in comparison with EDS the sensitivity and accuracy of XPS measurements are higher.

It should be noted that due to possible surface contamination or the concentration of small metal-oxide particles on the surface, XPS would lead to an overestimation in the actual results.

Probably, this is the reason of the difference between XPS analysis result of Ti (10.6 % shown in Table 4-1) and EDS (88.5 % shown in Figure 4-12).

In spite of these limitations, the XPS technique provides a more accurate analysis for states present in a microstructure in comparison with EDS technique.

Ti-MMC sample contains the following elements: C, Al, and Ti and insert sample contains Ti and N, detected by both the EDS and XPS analyses. The presence of chloride in XPS result of Ti-MMC sample (Table 4-1), which possibly corresponds to chloride salts was not detected by EDS analysis (Figure 4-12). It is possible that the sample might be touched by a human body. Moreover, very small amounts of Ca, Zn, and Pb were observed in XPS result might be some debris present as contaminants in the outermost surface atomic layers due to the lack of their presence in EDS result.

The Ti2p and N1s photoelectron spectra of the insert sample (Figure 4-10) confirm the presence of TiN band. These data are in good correlation with SEM results (Figure 4-15) which show high atomic percentages of Ti (46.7%) and N (23.5 %) on the surface. Oxygen has the highest amounts (26.2%) in XPS result of Ti-MMC sample whereas it was not detected by EDS.

The presence of vanadium in Ti-MMC sample was not detected by XPS, whereas Al and Ti in TiAlV bond were detected. Also, the presence of a thin layer of TiO_2 on the surface of Ti-MMX sample detected by XPS was not confirmed by EDS.

Comparison of the EDS and XPS results indicates that the Ti-MMC sample contains Ti, Al, V, and C with a very thin layer of TiO_2 on the surface and Insert sample contains Ti, Al, N, C, W, and Co. Also, TiN is the outermost surface atomic layer.

5.2 Flank wear analysis

The SEM images of the worn-out surfaces of carbide TiAlN/TiN coated inserts were analyzed to identify initial tool wear mechanisms acting in machining of Ti-MMCs. In order to study the change in chemical composition of the inserts during the initial moments of machining, EDS was performed on the flank face in wear zone. Analyses of elemental compositions on flank face wear lands for cutting times 0.2, 0.5, 1, 1.5 and 2.5 seconds are presented in Figure 5-1 and show how compositions vary with cutting time.

The results show that the wear land (horizontal axis) consists of mainly Ti, Al, V, N, C, and O.

The detected amounts of titanium (Ti), which are the highest in the insert composition in atomic percentage, seem to have the most distinct difference over time. First, the amounts increase rapidly after just 0.2 second of machining which indicates a work-piece material deposition. Then the amounts decrease in 0.5 second, increase until 1 second, and finally stabilized after that. In contrast, a significant decrease in the amounts of N is seen after 0.2 second of machining and it increases in 0.5 second, decreases in 1 second and increases slowly after that.

The amounts of aluminum (Al) detected here appear to be negatively correlated with the amounts of titanium (Ti) and seem to have a similar pattern to nitrogen (N) but with a lower variation rate. The amounts of vanadium (V) and titanium (Ti) seem to follow the same variation pattern.

It should be noted that in the sample with cutting time 0.5 second the mass percentage of tungsten (W) increased to 11.5 % and cobalt (Co) to 0.3 % which suggests that the coating is abraded and substrate materials revealed.

The amounts of carbon (C) present on the analysed surfaces seem to slightly increase with cutting time until the first second of machining. It is difficult to explain whether the increase of C occurs from the material beneath since no W or Co was detected after 0.5 second but that is a possibility.

Briefly, periodic variation of Ti, Al, and V implies a continuous process of addition and removal of these elements in the analysed region result in periodic adhesion-abrasion wear.
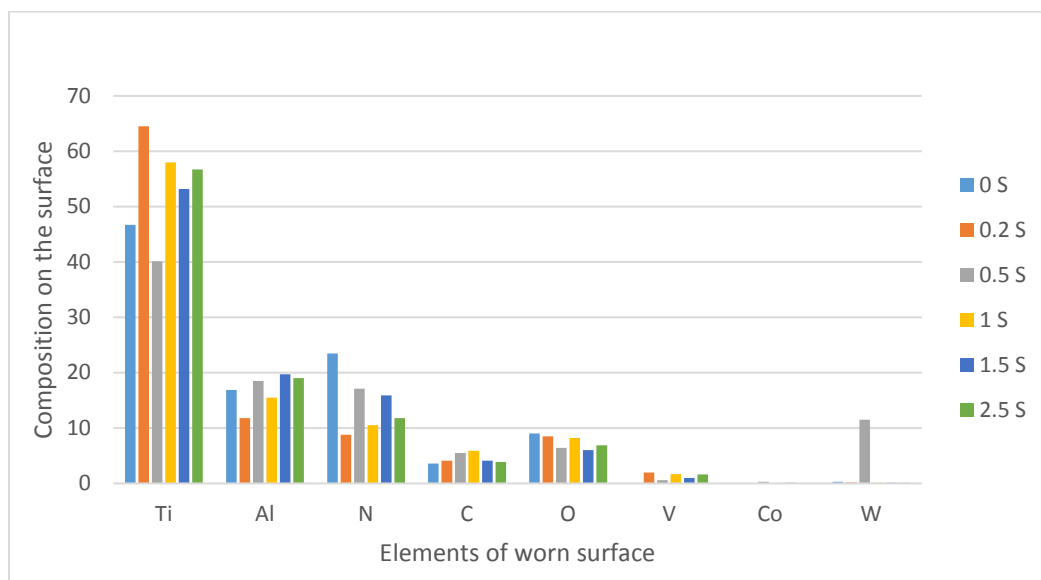
Figure 5-1 : Variation of elemental composition on flank face wear land adhered material

It is worth noting that on comparing EDS analysis results of different specimens, some variations in composition may be found because of the limited area analysed.

5.3 Cutting forces

To study the change in cutting force components containing F_t, F_c, and F_f during the initial moments of machining Ti-MMC the results of measured and plotted forces versus time (Figure 4-6 (a) to (j)) are presented in Figure 5-2.

The force diagrams illustrate that before the first second of machining all force components increase rapidly and variation rates are high (Figure 5-2 region (I)), but after this time these forces have relatively stabilized (Figure 5-2 region (II)). This is the time that the high tool wear rate changes to the steady-state condition (the transition period shown in Figure 4-4).

Comparing the cutting force results (Figure 5-2) with tool wear progression chart (Figure 4-4) clearly reveals the correlation between the transition period and the time of stabilization of the cutting forces (both within the first second of machining).
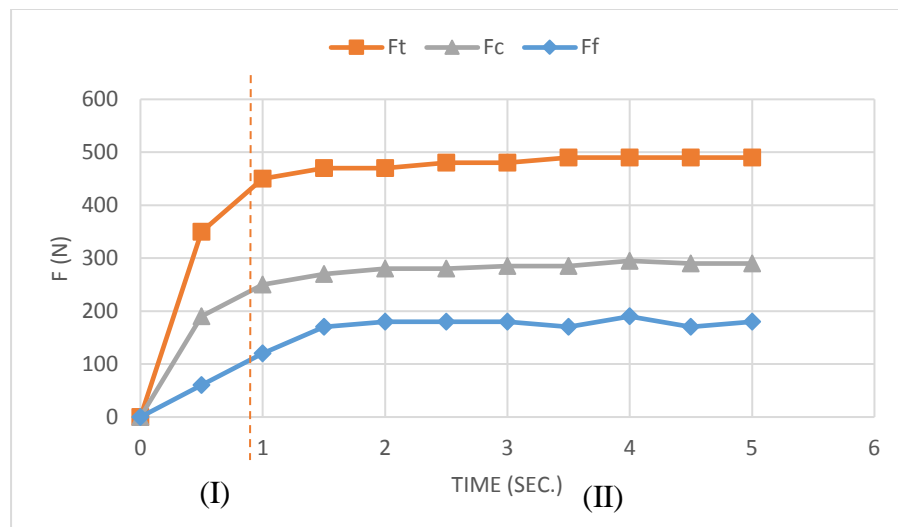
Figure 5-2 : The average amounts of feed forces (Ff), thrust forces (Ft), and cutting forces (Fc) for 10 different tools; each test was done using a brand new insert

In other words, for all cutting force components, steady state was reached within the 1 second and the forces were almost constant until a certain time.

The results presented in Figure 5-2, clearly confirm the stabilization of the forces around the first second of the process (end of the region (I)). Meanwhile, the levels of all three cutting force

components seem to become almost steady after the first second for the tools with higher machining time (region (II)).

Moreover, the large variation in cutting forces could be a reasonable explanation for an early coating loss and abrasion wear on the flank face (shown in SEM micrographs and elemental mapping in Figure 4-17).

Hence, it can be concluded that there is a direct relation between machining forces and tool wear.

From SEM and EDS analysis (Figures 4-19 (c) and 4-20), a formation of a thin and smooth layer at 1 second of machining was detected. It may help to reduce the friction between the tool and work- piece result in stabilizing the cutting forces by covering the grooves and holes.

The idea that the adhered layer provides a certain protection against abrasion could be a good answer to the question of why the amounts of cutting force components and hence tool wear (due to their correlation) increase rapidly in the region I and stabilize at the end of this region.

Performing a protection layer or brace shield which prevents of rapid tool wear and improves tool life agrees with the results of another study done by Troung et al. (2015).

The initial changing in tool geometry might be another answer to stabilizing the forces. As it was shown earlier (Figure 4-19 (b) and (c)), the geometrical form of the cutting edge is changed (sharp edge was chamfered) within the first second of machining and a smooth adhered layer is covered the scratches and the grooves. This could affect the friction between the tool and work-piece.

5.4 Initial tool wear mechanisms

Based on EDS analyses presented accordingly to SEM micrographs (shown in Figures 4-17, 20, and 23) it is suggested that due to the high friction between the insert and work-piece and high cutting forces, material transfer occurs in the contact region.

Concerning the first 0.5 second of machining (Figure 4-17), it is suggested that the flank wear has been progressed with mechanical abrasion by plowing of the hard particles containing TiC or hard coating particles, disintegrating and etching the tool surface.

As shown in Figure 4-17 (c) scratches and grooves (1.1 µm in diameter measured in micrograph 4-23 (a)) on the flank face are shown which might be attributed to the hard particles from the

material of the work-piece (TiC) (2.3 µm in diameter, measured in micrograph 3-11 (a)) or the hard coating particles might disintegrate and etch the tool surface.

According to these analyses, it is reasonable to consider that due to:

- the very low amounts of adhered elements on the flank surface (zone 2 in Figure 4-17 (a)),

- abraded edge, scratches, grooves on the interact region of the insert,

- revealed substrate elements such as tungsten (W) (Figure 4-17 (c) W M series) and its binder cobalt (Co), and

- revealed TiAlN/TiN coated layer (Figure 4-17 (c) Al K series),

the predominant wear mechanism is mostly abrasion. Figures 4-17 (b) and (c) Ti K series, clearly shows the presence of very low amounts of adhered layer on the flank surface and provides support to this wear behavior.

Hence, it could be a good suggestion that the deposited TiAlN/TiN coating is continuously removed by abrasive action of hard TiC particles randomly dispersed on the work-piece.

Furthermore, the EDS analysis revealed that the produced layer contains Ti, Al, and V (shown in Figure 5-1), which suggest a strong adhesive wear mode when using TiAlN/TiN coated carbide tools in the machining of Ti-MMCs.

By cutting off the worn out region in the flank face of an insert after 2 seconds of machining perpendicular to the cutting edge by a diamond cut-off saw, it was observed in SEM micrograph and the elemental mapping of the flank face (Figures 4-26 and 27) that the adhered layer is more consistent in the worn out region and becomes thinner towards the cutting edge.

EDS line scan analysis on the cross-section cut of an insert after 4 seconds of machining using FIB technique revealed the presence of Ti, Al, and V in the adhered layer and also W and Co in the substrate. Also, EDS analysis of the adhered layer provide a mixture between work-piece material components and cutting tool material constituents.

In summary:

The abrasion process starts with the deposition or sticking of work-piece material onto the coating as shown in Figure 4-17 (b) and highlighted in Figure 4-17 (c).

After 1 second of machining it was found that a butter spread like layer is revealed (shown in Figure 4-20), which suggests an adhesive wear mode because of the cyclic nature of the sticking and separating phenomenon of adhered materials.

After 2 seconds of the machining process, the lower thickness of the wear region in comparison with the original coating thickness implies that the TiAlN/TiN coating is removed and a thin adhered layer (Figure 4-20) is formed on the insert surface. This could be due to the sliding interactions and high friction between work-piece and tool materials result in some elements be separated from the wear region and some new materials be deposited on the contact surface.

Furthermore, the abraded edge was covered by an Al-enriched layer. The presence of Ti and also V (which only exists in the matrix of the work-piece material Ti-6Al-4V) in the deposited layer (zone 2 in Figure 4-20 (b)) indicates that these materials were transferred from the work-piece. There are not any evidence of tungsten and cobalt which had been revealed in the sample with 0.5 second of machining.

CHAPTER 6   CONCLUSION AND RECOMMENDATIONS

This study presents information on the initial tool wear and wear mechanisms on the experimental turning of Ti- MMCs with carbide TiAlN/TiN coated inserts.

First part of the research deals with the experimental tests, tool wear progression charts, first transition period, the cutting force and its relation with the tool wear mechanism during the first moments of machining.

In the second part, it was focused on the analysis of the initial tool wear mechanisms. In this step, in order to have a better understanding of initial tool wear behavior and to characterize the microstructure features of the wear region, some XPS, SEM/EDS analysis were conducted.

To reveal the sub-layers, made the adhered layer on the tool flank face, FIB technique was employed.

6.1 Observations

- An adhered layer having the butter spread appearance was observed at the initial moments of machining.

- Formation of built-up edge, plastic deformation, chipping or carbon discoloration were not observed during the initial moments of machining.

6.2 Conclusions

The general conclusions based on this experimental and analytical research are listed below:

- It was attempted to find the best regression in tool wear progression charts to obtain the precise transition time between different states of tool wear. In all three times of the machining tests, by drawing the trend line with a linear regression, the transition point is within a second of machining. Also, the second transition period is after about the 83rd second of machining.

- As shown in cutting force diagrams of the first 5 seconds of machining, after 1 second of machining all cutting force components, especially tangential force which plays the most important role in machining, are fairly stable.

- After comparing the transition time in the tool wear charts with the forces diagram, it can be stated that due to their full synchronization, there is a direct relation between the transition time in cutting force components and tool wear progression.

- In all SEM images, adhered materials and abrasion grooves are clearly demonstrated. It is considered that the abrasion was attributed to the hard particles from the material of the work-piece (TiC) since the average of the grooves diameter (1.1 µm) and TiC particles diameter (2.3 µm) are close to each other.

- The findings of the present study well demonstrated an adhered layer which comes from work-piece materials. It contains Ti, Al, V, and C, found on the tool surfaces (on the worn part) inside the contact region. Afterwards, a new aluminum and titanium film cover the worn surface and then is scratched away by plowing of the hard particles containing TiC or hard coating particles disintegrating and etching the tool surface, and these cyclic processes result in the progressive wear of the tool.

  Hence, it could be proposed that abrasion is the predominant wear mechanism before 0.5 second of machining. In the first moments of machining, the abrasive particles scratch the contact region, aluminum and titanium also start to fill the grooves and holes caused by the hard particles and make the brace shield. This could be result in adhesion wear as a dominant mechanism in the primary period of machining Ti-MMCs.

- Concerning insert XPS and SEM/EDS results, it is suggested that between 0.5 and 1 second of machining, an adhered layer containing aluminum, titanium and vanadium probably act as a protective layer against the tool wear. It could be proposed that due to the formation of this layer, the amounts of the cutting force components and the tool wear rate decrease rapidly.

- The amounts of oxygen do not show a major changing which suggests that the oxidation could not be as a secondary wear mechanism during the initial moments of the machining.

6.3 Research contributions

To the best of my knowledge this was the first time that:

- an insert was cut off by a diamond cut-off saw to study on the tool wear region. It was revealed that the contact region on the tool flank face with work-piece has a smaller thickness than the original coating which means that most part of the coating is abraded after 2 seconds of machining.

- FIB technique was applied to cut the adhered layer on the tool wear region to find out what elements or sub-layers are under the layer that perform during the machining of T-MMCs.

- initial tool wear mechanisms of carbide TiAlN/TiN coated inserts in turning of Ti-MMCs were deeply analysed. There is not any literature review or academic article available regarding the initial tool wear mechanism during turning of Ti-MMCs.

6.4 Recommendations

- A complementary study of tool life optimization with the different cutting conditions introduced in this study is recommended.

- Performing more investigations into initial tool wear and its influences on surface roughness, which is as important as the tool life, is suggested.

- The interactions between initial wear mechanisms can be exclusively studied.

BIBLIOGRAPHY

Aramesh, M. et al. (2015). Machinability of titanium metal matrix composites (Ti-MMCs).

Ask, M., Lausmaa, J., & Kasemo, B. (1989). Preparation and surface spectroscopic characterization of oxide films on Ti-6Al-4V. Applied surface science, 35(3), 283-301.

Astakhov, V. P. (2006). Tribology of metal cutting (Vol. 52): Elsevier.

Astakhov, V. P. (2012). Tribology of cutting tools. 1-66.

Astakhov, V. P., & Davim, P. (2006). Tools (Geometry and Material) and Tool Wear.

Atnafu, T., & Yimer, S. (2013). Calcium Chloride Recovery in soda ash production by solvay's process.

Aurich, J. C., Zimmermann, M., Schindler, S., & Steinmann, P. (2015). Effect of the cutting condition and the reinforcement phase on the thermal load of the work-piece when dry turning aluminum metal matrix composites. The international journal of advanced manufacturing technology, 1-18.

Basavarajappa, S., Chandramohan, G., Rao, K. N., Radhakrishanan, R., & Krishnaraj, V. (2006). Turning of particulate metal matrix composites—review and discussion. Proceedings of the institution of mechanical engineers, Part B: Journal of engineering manufacture, 220(7), 1189-1204.

Bejjani, R., Collin, M., Thersleff, T., & Odelros, S. (2016). Multi-scale study of initial tool wear on textured alumina coating, and the effect of inclusions in low-alloyed steel. Tribology International.

Bejjani, R. et al. (2012). Machinability and modeling of cutting mechanism for titanium metal matrix composites (Ph.D), École polytechnique de Montreal.

Brun, M., Lee, M., & Gorsler, F. (1985). Wear characteristics of various hard materials for machining SiC-reinforced aluminum alloy. Wear, 21-29.

C. Veiga, J. P. D., A.J.R. Loureiro. (2013). Review on machinability of titanium alloys: the process perspective.

Childs, T. (2000). Metal machining: theory and applications: Butterworth-Heinemann.

Chou, Y. K., & Evans, C. J. (1997). Tool wear mechanism in continuous cutting of hardened tool steels. Wear, 212(1), 59-65.

Coupal, J. (2012). Metal matrix composite pushrods and pistons. Disponible: http://www.alsic.com/_blog/Structures_and_Armor/post/ Metal_Matrix_Composite _Pushrods/.

Da Silva, R. B., Machado, Á. R., Ezugwu, E. O., Bonney, J., & Sales, W. F. (2013). Tool life and wear mechanisms in high speed machining of Ti–6Al–4V alloy with PCD tools under various coolant pressures. Journal of Materials processing technology, 213(8), 1459-1464.

Davim, J. P. (2008). Machining fundamentals and recent advances (J. P. Davim Ed.).

Davim, J. P. (2014). Machining of titanium alloys (J. P. Davim Ed.).

Dimla, D. E. (2000). Sensor signals for tool-wear monitoring in metal cutting operations-a review of methods. International journal of machine tools and manufacture, 40(8), 1073-1098.

Dobrzański, L. A., Gołombek, K., Mikuła, J., & Pakuła, D. (2006). Improvement of tool materials by deposition of gradient and multilayers coatings. Journal of achievements in materials and manufacturing engineering, 19(2), 86-91.

Ernest, R. (1995). Friction and wear of materials. John Willey & Sons, Inc. New York, 44-238.

Ezugwu, E. O., & Wang, Z. M. (1997). Titanium alloys and their machinability—a review. Journal of materials processing technology, 68(3), 262-274.

Gerez, J. M., Sanchez-Carrilero, M., Salguero, J., Batista, M., & Marcos, M. (2009, November). A SEM and EDS based study of the microstructural modifications of turning inserts in the dry machining of Ti6Al4V alloy. In third manufacturing engineering society international conferences (Vol. 1181, No. 1, pp. 567-574). AIP Publishing.

Hartung, P. D., Kramer, B., & Von Turkovich, B. (1982). Tool wear in titanium machining. CIRP Annals-Manufacturing Technology, 31(1), 75-80.

Hosseini, A., & Kishawy, H. A. (2014). Cutting tool materials and tool wear machining of titanium alloys (pp. 31-56): Springer.

Hua, J., & Shivpuri, R. (2005). A cobalt diffusion based model for predicting crater wear of carbide tools in machining titanium alloys. Journal of engineering materials and technology, 127(1), 136-144.

Ingolf, k. (1998). Pin-on-disc test. from http://www.ist.fraunhofer.de/en/services/analysis_and_quality_assurance/friction_and_wear_measurement/tribometer.html.

Isakov, E. (2004). Engineering formulas for metalcutting: presented in customary US and metric units of measure: Industrial Press Inc.

ISO.3685. (1993). International Organization for Standardization.Tool-life testing with single-point turning tools.

Jain, P., Soni, S., & Baredar, P. (2014). Review on machining of aluminium metal matrix composites. Material science research India, 11(2), 114-120.

Kainer, K. U. (2006). Basics of Metal matrix composites. 1-54.

Kannan, S., Kishawy, H. A., & Balazinski, M. (2013). Analysis of two-and three-body abrasive wear during machining of aluminium-based metal matrix composite. International Journal of Materials and Product Technology, 46(1), 81-94.

Kim, W., & Kwon, P. (2002). Phase transformation and its effect on flank wear in machining steels. Journal of manufacturing science and engineering, 124(3), 659-666.

Kishawy, H. A., Kannan, S., & Balazinski, M. (2005). Analytical modeling of tool wear progression during turning particulate reinforced metal matrix composites. CIRP Annals-Manufacturing Technology, 54(1), 55-58.

Kramer, B., & Suh, N. (1980). Tool wear by solution: a quantitative understanding. Journal of engineering for industry, 102(4), 303-309.

Kuttolamadom, M. (2012). Prediction of the wear & evolution of cutting tools in a carbide/Ti-6Al-4V machining tribosystem by volumetric tool wear characterization & modeling.

Kwon, P. (2000). Predictive models for flank wear on coated inserts. Journal of tribology, 122(1), 340-347.

L.Bin. (2012). A review of tool wear estimation using theoretical analysis and numerical simulation technologies. International journal of refractory metals and hard materials, 35, 143-151.

Manna, A., & Bhattacharayya, B. (2003). A study on machinability of Al/SiC-MMC. Journal of materials processing technology, 140(1), 711-716.

Marco, J. F. et al. Surf. interface anal. 27, 71-75 (1999)

Martin, P. M. (2009). Handbook of deposition technologies for films and coatings: science, applications and technology: William Andrew.

MC-21-Inc. Motorcycle disc brake rotor. from http://www.mc21inc.com/powersports.html.

Miracle, D. B., Donaldson, S. L., Henry, S. D., Moosbrugger, C., Anton, G. J., Sanders, B. R., Muldoon, K. (2001). ASM handbook (Vol. 21): ASM international materials park, OH, USA.

Moreno, L. H., Ciacedo, J. C., Martinez, F., Bejarano, G., Battaille, T. S., & Prieto, P. (2010). Wear evaluation of WC inserts coated with TiN/TiAlN multi/nanolayers. Journal of the brazilian society of mechanical sciences and engineering, 32(2), 114-118.

Moulder, John F. et al. Handbook of X-ray photoelectron spectroscopy. Eden Prairie, Minnesota: Perkin-Elmer Corporation, Physical electronics division, (1992).

Murray, J. (1986). The Mg− Ti (magnesium-titanium) system. Bulletin of alloy phase diagrams, 7(3), 245-248.

Neale, M., & Gee, M. (2001). A guide to wear problems and testing for industry. William Andrew.

Nikhilesh, C., & Chawla, K. K. (2006). Metal matrix composites.

Niknam, S. A., Khettabi, R., & Songmene, V. (2014). Machinability and machining of titanium alloys: A review machining of titanium alloys (pp. 1-30): Springer.

NIST XPS database http://srdata.nist.gov/xps/main_search_menu.aspx.

Olortegui-Yume, J. A., & Kwon, P. Y. (2007). Tool wear mechanisms in machining. International journal of machining and machinability of materials, 2(3/4), 469.

Peters, M., Kumpfert, J., Ward, C. H., & Leyens, C. (2003). Titanium alloys for aerospace applications. Advanced engineering materials, 5(6), 419-427.

Pramanik, A., & Littlefair, G. (2015). Machining of titanium alloy (Ti-6Al-4V)-Theory to application. Machining science and technology, 19(1), 1-49.

Pramanik, A., Zhang, L. C., & Arsecularatne, J. A. (2008). Machining of metal matrix composites: Effect of ceramic particles on residual stress, surface roughness and chip formation. International journal of machine tools and manufacture, 48(15), 1613-1625.

Rabinovich, G. S., Kovalev, A. I., Aguirre, M. H., Beake, B. D., Yamamoto, K., Veldhuis, S. C., & Rashkovskiy, A. Y. (2009). Design and performance of AlTiN and TiAlCrN PVD coatings for machining of hard to cut materials. Surface and coatings technology, 204(4), 489-496.

Rabinowicz, E. (1977). The dependence of the adhesive wear coefficient on the surface energy of adhesion. Wear of materials- 1977, 36-40.

Ravindra, H. V., Srinivasa, Y. G., & Krishnamurthy, R. (1993). Modelling of tool wear based on cutting forces in turning. wear, 169(1), 25-32.

Sharif, S., E. Abd Rahim, & Sasahara, H. (2012). Machinability of titanium alloys in drilling. ISBN: 978-953-51-0354-7, InTech, available from: http://www.intechopen.com/books/titanium-alloystowards-achieving-enhanced-properties-for-diversified-applications/drilling-of-titanium-alloys.

Shaw, M. (2005). Metal cutting principles, (2nd edition ed.), New York: Press Inc.

Smith, G. T. (2008). Cutting tool technology: industrial handbook: Springer Science & Business Media.

Soboyejo, W. O., & Srivatsan, T. (2006). Advanced structural materials: properties, design optimization, and applications: CRC Press.

Stephenson, D., & Agapiou, J. (2006). Metal cutting operations. Metal cutting theory and practice, Second ed., Taylor and Francis Group, Boca Raton, FL, 17-70.

Stephenson, D. A., & Agapiou, J. S. (2005). Metal cutting theory and practice (Vol. 68): CRC press.

Torres, Y., Tarrago, J., Coureaux, D., Tarrés, E., Roebuck, B., Chan, P. , Viswanadham, R. (2014). Fracture and fatigue of rock bit cemented carbides: Mechanics and mechanisms of crack growth resistance under monotonic and cyclic loading. International journal of refractory metals and hard materials, 45, 179-188.

Trent, E. M., & Wright, P. K. (2000). Metal cutting. Butterworth-Heinemann.

Troung, D. X et al. (2015). Chaos theory applied to analyze tool wear during machining Ti-MMCs.

Upadhyaya, G. S. (1998). Cemented tungsten carbides: production, properties and testing. William Andrew.

Upadhyaya, G. S. (2001). Materials science of cemented carbides—an overview. Materials & Design, 22(6), 483-489.

Variola, F., Yi, J. H., Richert, L., Wuest, J. D., Rosei, F., & Nanci, A. (2008). Tailoring the surface properties of Ti-6Al-4V by controlled chemical oxidation. Biomaterials, 29(10), 1285-1298.

Yousheng, L., & Jianxin, D. (2008). Wear mechanism of cemented carbide tool in high speed machining titanium alloy. Tribology, 28(5), 444-447.

Wong, T., Kim, W., & Kwon, P. (2004). Experimental support for a model-based prediction of tool wear. Wear, 257(7), 790-798.

Zackrisson, J., & Andrén, H. O. (1999). Effect of carbon content on the microstructure and mechanical properties of (Ti, W, Ta, Mo)(C, N)–(Co, Ni) cermets. International journal of refractory metals and hard materials, 17(4), 265-273.

Zlatin, N., & Field, M. (1973). Procedures and precautions in machining titanium alloys. In titanium science and technology (pp. 489-504). Springer US.